NASA CONTRACTOR REPORT

NASA CR-2199

NASA CR-2199

FINITE DEFORMATION OF ELASTO-PLASTIC SOLIDS

by J. R. Osias

Prepared by
CARNEGIE-MELLON UNIVERSITY
Pittsburgh, Pa. 15213
for Langley Research Center

NATIONAL AERONAUTICS AND SPACE ADMINISTRATION • WASHINGTON, D. C. • MARCH 1973

Page Intentionally Left Blank

ERRATA

NASA Contractor Report CR-2199

FINITE DEFORMATION OF ELASTO-PLASTIC SOLIDS

By J. R. Osias
March 1973

Please note that pages 55, 56, and 57 were inadvertently placed in the wrong order.

Issue date: March 15, 1973

Page Intentionally Left Blank

1. Report No.	2. Government Accession No.	3. Recipient's Catalog No.
NASA CR-2199		

4. Title and Subtitle	5. Report Date
FINITE DEFORMATION OF ELASTO-PLASTIC SOLIDS	March 1973
	6. Performing Organization Code

7. Author(s)	8. Performing Organization Report No.
J. R. Osias	SM-72-22
	10. Work Unit No.

9. Performing Organization Name and Address	11. Contract or Grant No.
Carnegie-Mellon University Pittsburgh, Pennsylvania 15213	NGL-39-002-023
	13. Type of Report and Period Covered
12. Sponsoring Agency Name and Address	Contractor Report
National Aeronautics and Space Administration Washington, DC 20546	14. Sponsoring Agency Code

15. Supplementary Notes

16. Abstract

A theoretical basis is established for analysis of finite deformation of metals. The observation that finite deformation of such elasto-plastic materials may be viewed as a process rather than an event leads to derivation of a complete initial-and boundary-value problem distinguished by its quasi-linear nature. This feature of the formulation motivates adoption of an incremental approach to numerical problem solving. Numerical solution capability is established for problems of plane stress and plane strain. The validity of the theory and numerical analysis is demonstrated by consideration of a number of problems of homogeneous finite deformation for which analytic solutions are available.

Subsequently the analysis is employed for the investigation of necking in flat metal tensile bars. The results of this investigation provide the first full numerical solutions for tensile necking in plane stress and plane strain. In addition a basis is provided for assessment of the validity of stress-strain relations inferred from tensile test data.

17. Key Words (Suggested by Author(s))	18. Distribution Statement
Finite Deformation Plasticity Numerical Analysis Tensile Test	Unclassified

19. Security Classif. (of this report)	20. Security Classif. (of this page)	21. No. of Pages	22. Price*
Unclassified	Unclassified	174	$3.00

*For sale by the National Technical Information Service, Springfield, Virginia 22151

TABLE OF CONTENTS

FIGURES

INTRODUCTION

Tensile testing of nominally prismatic round and flat bars has long provided a basis for evaluation of the properties of metals. The primary data from such tests, load, extension and minimum deformed cross-sectional area may be used to infer stress-strain relations taken to be characteristic of the material tested. Inference of such material property relations is appropriate so long as the deformation and associated stress field may be assumed uniform over the cross-section in some region or gage length of the tensile bar.

For ductile metals the assumption of uniformity of the deformation and stress field clearly breaks down for extensions in excess of some material dependent critical value. Once the extension exceeds this value the axial load decreases and subsequent prescribed overall specimen extension is observed to concentrate in a highly strained local neck. Within this necked region inhomogeneous deformation and a complex multi-axial stress field must exist. The phenomenon is referred to as tensile instability.

Evaluation of the validity of stress-strain relations inferred from post-instability tensile test data as well as study of tensile failure by fracture and/or rupture requires detailed knowledge of the stress and strain fields existing in a necking tensile bar. This need has motivated extensive experimental investigations, most

notably by Bridgeman [1] and Nadai [2], as well as a variety of approximate analyses incorporating idealized models of material behavior. Typically these analyses neglect either elastic deformation or work hardening, or both.

The absence of a complete theory suitable for analysis of problems of general finite deformation of elasto-plastic continua, such as necking in metal tensile bars, has provided the motivation for development of such a formulation.

Analysis of finite deformation of elasto-plastic materials requires explicit consideration of nonlinear effects arising from both inelastic material behavior and deformation magnitude. While the recent literature contains many examples of analyses incorporating either material or geometric nonlinearity, few attempts have been made at solution of the combined problem.* Excellent surveys of these efforts are provided by Marcal [4] and Stricklin et. al. [5]. These previous developments typically employ finite element techniques based upon energy principles and are primarily intended for analysis of problems involving large deflections of plates and shells in which local strains are small. The application of these analyses to the tensile instability problem is of questionable

*Oden [3] provides extensive development of theory and solution techniques for finite deformation of hyperelastic materials. The approaches employed, while incorporating both material and geometric nonlinearity, do not admit application to the elasto-plastic case.

value since the necking process involves large displacements, strains and rotations distributed over a continuum of arbitrary shape. The kinematic assumptions underlying analyses of plates and shells are of limited validity under these conditions. Solution of a general elasto-plastic continuum problem requires a formulation appropriate for analysis of deformations of any magnitude irrespective of the configuration of the deforming solid.

The adoption of what is herein termed *the rate viewpoint** toward the mechanics of finite deformation of an elasto-plastic solid has led to the development of a complete theoretical formulation of the problem. Rather than seeking equations governing the total deformation attention is restricted to the time rates of the independent variables, stress rate and velocity. Equations are derived governing the time dependent velocity field in a deforming elasto-plastic solid.

The formulation differs from previous developments in two fundamental respects.

*A similar viewpoint is taken by Cowper and Onat [6] in establishing admissible solutions for tensile necking in plane strain but they do not attempt full solution for deformation and stress histories.

1. The entire development proceeds in an Eulerian or spatial reference frame rather than the Lagrangian, or material, frame usually employed in nonlinear analyses of plates and shells.
2. Constitutive equations for finite elasto-plastic deformation are obtained by generalizing those of the infinitesimal theory in the spatial rather than material frame. The fundamental features of the infinitesimal theory are preserved without introducing problem dependent deviations associated with the use of material frame stress tensors.

A complete initial- and boundary-value problem is posed in which finite elasto-plastic deformation is viewed as a time dependent process. The formulation reduces to well established results in the limit of infinitesimal deformation.

The governing equations of the finite problem are distinguished by their quasi-linear nature. This feature, which follows directly from adoption of the rate viewpoint in an Eulerian frame, enables the use of an incremental technique for accurate and efficient numerical solution of finite deformation problems. Finite element solution capability may be developed directly from the governing differential equations.

Numerical procedures have been developed for analysis of finite

deformation under conditions of plane stress or plane strain. The capabilities of these procedures have been investigated by considering a number of problems of homogeneous finite deformation for which analytic solutions are available. Comparison of numerical and analytic results for these problems indicates that accurate numerical solutions can be obtained for problems involving dimensional changes of an order of magnitude and rotations of forty-five degrees.

The numerical analysis has been employed in an investigation of symmetric necking in flat tensile bars of elasto-plastic material. Solutions are obtained for the limiting cases of plane stress and plane strain extension of bars containing a small initial geometric imperfection. Full histories of neck geometry and internal stress and deformation fields are obtained. The development of inhomogeneous internal fields as the necking process proceeds is clearly demonstrated, as is elastic unloading of previously yielded material in regions outside the neck. The solutions also provide a vehicle for assessment of the validity of stress-strain relations inferred from tensile data over the full range of a test from initial yield through the development of a significant neck.

I. THEORETICAL DEVELOPMENT

The Rate Viewpoint

The equations describing finite deformation of elasto-plastic solids may be derived in what is termed a rate form. That is, attention is focused not upon field quantities such as stress and strain but rather upon their rates of change with respect to time. The approach is conceptually analogous to that employed by Swedlow [7] for infinitesimal deformation. Even with this analogy, however, analyses of infinitesimal and finite deformation are operationally distinct.

In analysis of infinitesimal deformation stress and strain tensors as well as all governing equations are referred to a single configuration of the body. Either deformed or undeformed states may be employed as they are by assumption indistinguishable from one another. Thus time derivatives of field quantities reflect only changes in component magnitudes with respect to an invariant frame of reference. Should the deformation be regarded as finite, however, deformed and undeformed configurations must be distinguished. Time derivatives of field quantities such as stress and strain must reflect changes in the fundamental reference frame provided by the deforming configuration of the body.

The present theory incorporates equations of elasto-plastic behavior and stress equilibrium which reflect the foregoing implica-

tions of finite deformation. The equations are assembled to define a complete initial -and boundary-value problem for the time dependent velocity field in a deforming body.

The development of the constitutive and equilibrium equations is predicated upon the character of certain tensorial measures of stress and strain and their time rates of change. In the next few sections these quantities are defined and discussed. Subsequently the field equations are derived, boundary and initial conditions developed and the full velocity problem is assembled.

I.1 Fundamental Concepts

General concepts of nonlinear continuum theory are developed below to the extent necessary to support the ensuing analysis. More extensive discussions* may be found in Eringen [8] and Truesdell and Toupin [9].

Descriptions of continuum deformation and loading are developed in a fixed or laboratory reference frame. Deformation, deformation rate, stress and stress rate tensors are defined. All definitions are subject to the constraint of material objectivity, or spatial invariance, which requires that the analysis be independent of rigid motion of a deforming continuum.

Continuum Motion: Consider a three dimensional body whose undeformed reference configuration is B_o with boundary ∂B_o. The deformed configuration of the body is B with boundary ∂B. Material points in the reference state are located by coordinates X^I in an orthogonal curvilinear coordinate system. In the deformed state these points are located by coordinates x^i in the same system.

Thus the time dependent deformation may be given as the mapping**

*Much of the discussion in this section has been abstracted from the texts cited.

**General tensor notation is employed. Repeated indices in subscript-superscript pairs imply summation over 1,2,3. A comma denotes partial and a semi-colon covariant differentiation.

from B_o to B in Figure (1).

$$x^i = x^i(X^K, t) \tag{1}$$

The nature of the motion (1) is limited only by the constraint of material continuity:

$$J = |x^i_{,K}| > 0 \tag{2}$$

In the special case where the mapping of B_o to B given by (1) is such that angle and distance are everywhere preserved the motion is termed rigid. In this case (1) admits the representation

$$x^i = Q^i{}_K X^K + b^i \tag{3}$$

In (3) the tensor $Q^i{}_K$ is orthogonal, (4)*, and both $Q^i{}_K$ and b^i are functions of time.**

$$Q^i{}_K Q^{TK}{}_j = g^i{}_j \tag{4}$$

Reference Frames and Time Derivatives: We may define a velocity field v^i for the motion (1) by noting that the X^K are constant and differentiating (1) with respect to time.

*In (4) overscript T denotes transpose. The mixed metric tensor $g^i{}_j$ is equivalent to the Kronecker delta δ^i_j.

**In cartesian coordinates $Q^K{}_i$ is a rotation and b^i a translation. In general coordinates no simple physical interpretation is possible.

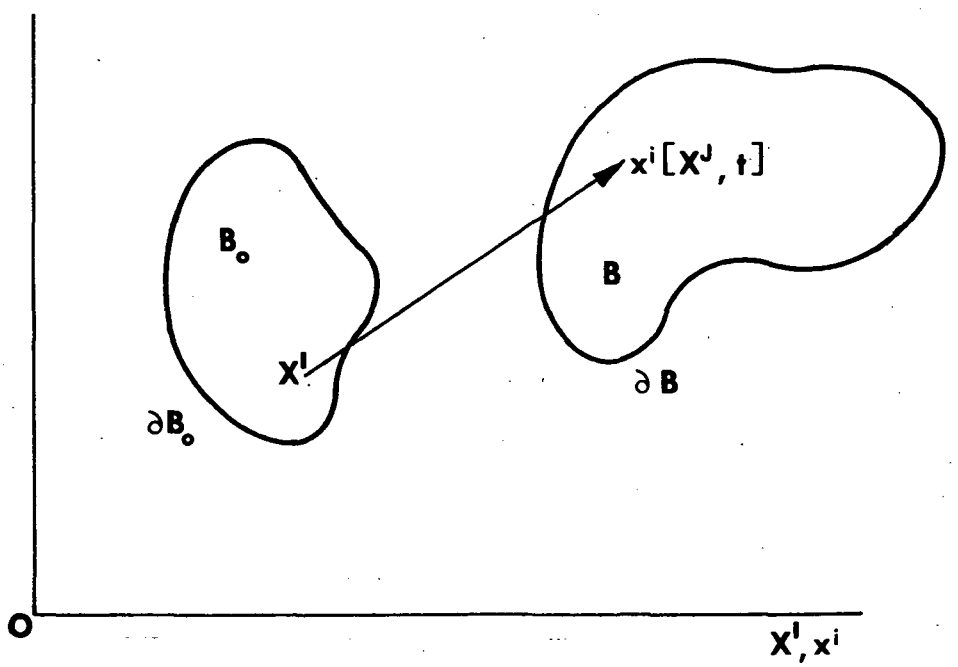

Figure 1 Deformation Mapping

$$v^i \equiv \partial x^i/\partial t = v^i[x^i(X^K,t),t] = v^i(X^K,t) \tag{5}$$

Note that the coordinate dependence of v^i may be given in terms of either x^i or X^K.

The choice of coordinate dependence in (5) is characteristic of all tensor field quantities employed in finite deformation analysis. Analysis employing the X^K is termed material or Lagrangian while that employing the x^i is termed spatial or Eulerian. The present theory is developed in Eulerian form.

In differentiating Eulerian field variables with respect to time, the time dependence of the x^i must be fully taken into account. Thus if $\phi(x^i,t)$ is a tensor field of any order its time derivative $\dot{\phi}$ is

$$\dot{\phi}(x^i,t) = \partial\phi/\partial t + \phi_{,i}v^i \tag{6}$$

The derivative (6) is the total or material derivative of ϕ. Unless specific exception is noted it is the only type of time derivative employed in the present theoretical development.

Material Objectivity: Any theory attempting to describe physical phenomena must be independent of the observer of an event. This constraint is known as objectivity. A familiar example of its significance is the restriction of Newtonian mechanics to inertial reference frames.

In continuum analysis objectivity is most conveniently expressed as the requirement that any theory be independent of rigid motion. The constraint may be expressed operationally by considering tensor fields referred to deforming bodies whose motions differ by a rigid component. Objectivity requires that components of such tensors be related by the transformation relating the two motions.

Consider, for example, the velocity fields corresponding to two such motions, y^i and $\bar{y}^i$, which are termed objectively equivalent. From (3)

$$y^i = Q^i{}_j \bar{y}^j + b^i \tag{7}$$

Differentiating (7) with respect to time we find:

$$v^i = \dot{Q}^i{}_j \bar{y}^j + Q^i{}_j \bar{v}^j + \dot{b}^i \tag{8a}$$

However the tensor transformation of $\bar{v}^i$ from $\bar{y}^i$ to y^i defines components $\bar{\bar{v}}^i$ given by

$$\bar{\bar{v}}^i = (\partial y^i / \partial \bar{y}^j)\, \bar{v}^j = Q^i{}_j\, \bar{v}^j \tag{8b}$$

Thus velocity components referred to y^i and $\bar{y}^i$ are not related by a tensor transformation. We therefore conclude, not unexpectedly, that velocity is not an objective tensor.

Necessary conditions for objectivity may be developed for tensor fields and functions of any order. Employing the two motions

y^i and $\bar{y}^i$ defined above, the following objectivity constraints are found for vectors q^i, second order tensors t^{ij} and second order tensor functions $f^{ij}(t_{kl})$. Recalling that the transformation $Q^i{}_j$ is a function of time we require the following to hold for all times.

Vectors:

$$q^i = Q^i{}_j \, \bar{q}^j \tag{9}$$

Tensors:

$$t^{ij} = Q^i{}_k \, Q^j{}_l \, \bar{t}^{kl} \tag{10}$$

Tensor Functions:*

$$f^{ij}(t_{kl}) = Q^i{}_p \, Q^j{}_q \, \bar{f}^{pq}(Q^r{}_k \, Q^s{}_l \, t_{rs}) \tag{11}$$

Strain and Strain Rate: The initial and deformed lengths of a differential material line segment are given by dS and ds respectively.

$$dS^2 = dX^I \, dX^J \, G_{IJ} \tag{12}$$

$$ds^2 = dx^i \, dx^j \, g_{ij} \tag{13}$$

where g_{ij} and G_{IJ} are the metric tensors of the deformed and undeformed coordinates. The change in length may be

*Tensor functions satisfying constraints of the form (11) are termed hemitropic functions of their arguments.

represented as

$$ds^2 - dS^2 = dx^i dx^j g_{ij} - dX^I dX^J G_{IJ} \tag{14}$$

The differentials dx^i and dX^I are related by the deformation mapping (1)

$$dX^I = X^I{}_{,i} dx^i \tag{15}$$

Therefore (14) may be written entirely in terms of the deformed coordinates x^i

$$ds^2 - dS^2 = (g_{ij} - X^I{}_{,i} X^J{}_{,j} G_{IJ}) dx^i dx^j \tag{16}$$

The local deformation may therefore be described by the Almansi strain tensor ε_{ij}.

$$\varepsilon_{ij} \equiv (1/2)(g_{ij} - X^I{}_{,i} X^J{}_{,j} G_{IJ}) \tag{17}$$

Similarly the local rate of deformation may be characterized by considering the time derivative of ds^2 in (13).

$$d(ds^2)/dt = 2\, d_{ij} dx^i dx^j \tag{18}$$

$$d_{ij} \equiv (1/2)(v_{i;j} + v_{j;i}) \tag{19}$$

The Euler deformation rate d_{ij} provides a complete, objective representation of the local non-rigid component of the velocity field. It is of particular consequence in the present analysis by virtue of its linear dependence on the velocity gradient. In the presence of local rotation the angular velocity ω^k of its principal axes is found

from the skew-symmetric velocity gradient, or spin tensor, ω_{ij}

$$\omega^k = \varepsilon^{kij}\omega_{ij} \tag{20}$$

$$\omega_{ij} \equiv (1/2)(v_{i;j}-v_{j;i}) \tag{21}$$

where ε^{kij} is the permutation operator.

Almansi strain and the deformation rate are related as:

$$d_{ij} = \chi^I{}_{,i}\chi^J{}_{,j}\ \frac{d}{dt}\left(x^m{}_{,I}x^n{}_{,J}\varepsilon_{mn}\right) \tag{22}$$

Stress and Stress Rate: The Cauchy stress tensor σ^{ij} referred to the deformed configuration is the i^{th} component of traction on a surface normal to the j^{th} coordinate direction. The symmetric, objective Cauchy stress provides a complete description of the loading state at a point in a deformed body. Components of traction t^i on planes of arbitrary orientation having normal vector components ν_i are found as linear combinations of the σ^{ij}

$$t^i = \sigma^{ij}\nu_j \tag{23}$$

The time rate of traction $\dot{t}_i$ is found by differentiating (23), noting that the normal vector is itself time dependent.

$$\dot{t}^i = (\dot{\sigma}^{ij}-\sigma^{pi}v^j{}_{;p})\nu_j \tag{24}$$

The stress rate $\dot{\sigma}_{ij}$ in (24) is not objective.
We must therefore seek an alternative objective characterization of

the time rate of stress for use in the constitutive equations of elasto-plastic flow.

The objectivity constraint (10) is necessary but not sufficient to define a unique objective stress rate. Such tensors have been developed by a number of investigators including Jaumann [10], Truesdell [11], and Oldroyd [12]. As suggested by Prager [13] for use in analysis of elasto-plastic flow the present analysis employs the Jaumann rate.

Consider a stress S^{ij} referred to the principal axes of the deformation rate (19). The rotation of these axes at a point in a deforming body is given by the spin ω_{ij} of (21). The relative orientation of the rotating coordinates and a fixed frame is given by an orthogonal mapping $Q^i{}_j$, defined by

$$\omega^i{}_j = Q^i{}_p \dot{Q}^p{}_j \tag{25}$$

The stresses S^{ij} and σ^{ij} are at all times related by

$$S^{ij} = Q^i{}_p Q^j{}_q \sigma^{pq} \tag{26}$$

The time derivative of S^{ij} is objective. Differentiating (26) and transforming the result back to a fixed reference yields the symmetric objective Jaumann stress rate $\hat{\sigma}^{ij}$

$$\hat{\sigma}^{ij} \equiv Q^i{}_p Q^j{}_q \dot{S}^{pq} \tag{27}$$

$$\hat{\sigma}^{ij} = \dot{\sigma}^{ij} + \sigma^i{}_m \omega^{mj} - \sigma_m{}^j \omega^{im} \tag{28}$$

The Jaumann stress rate provides a measure of the time rate of stress as seen by an observer participating in rotation of a deforming continuum at every point.

A Jaumann rate may be constructed as above for any tensorial quantity. If the quantity is intrinsically objective the Jaumann rate and material derivative (6) are equivalent.

I.2 Constitutive Theory

General Character of the Theory

A constitutive formulation is derived for elasto-plastic flow of metals undergoing finite deformation. The theory is derived as a generalization of an elasto-plastic flow theory appropriate for analysis of infinitesimal deformation (See Fung [14]). Its application is restricted to analysis of homogeneous isotropic metals undergoing quasi-static isothermal deformation.

The character of the finite deformation constitutive formulation is dictated by the adoption of three fundamental characteristics of the infinitesimal theory.

1. The flow mode, elastic or elasto-plastic, is dictated by the behavior of a scalar loading function f which is dependent upon current stress state and deformation history.

$$\begin{aligned} f = 0 \;;\; \dot{f} = 0 \quad &: \text{the cases of loading, elasto-plastic flow, and neutral loading, elastic flow, may be identified.} \\ f < 0 \quad &: \text{elastic flow or unloading} \end{aligned} \tag{29}$$

2. The deformation rate is *a priori* assumed to be separable into elastic and plastic components whose dependence upon stress is independently defined.

3. The constitutive equations take the form of first order differential equations relating time rates of stress and deformation.

The generalization to the finite case employs consistent interpretation of the time derivatives of stress and deformation appearing in the constitutive differential equations. The resulting formulation obeys the constraint of material objectivity. Deformation magnitude is limited only by an assumption that recoverable, elastic, deformation is infinitesimal.

In the following sections elastic and plastic flow modes are separately defined and then assembled to provide governing equations relating Jaumann stress rate and total deformation rate.

Elastic Flow Mode: Following Green and Naghdi [15] an elastic strain component is defined as the difference between total and permanent deformation. Explicit representation of this recoverable strain component* $\varepsilon_{ij}^{(e)}$ in terms of problem kinematics is neither sought nor necessary. It is defined only as the time integral of $d_{ij}^{(e)}$, the elastic component of the deformation rate tensor.

Stress and elastic strain are assumed to be related through a positive definite strain energy density function $W^{(e)}$. The energy density is defined such that

$$\sigma^{ij} = \partial W^{(e)} / \partial \varepsilon_{ij}^{(e)} \tag{30}$$

*$^{(e)}$ is not an index.

Since the strain energy is positive definite and the elastic strain is infinitesimal we may approximate $W^{(e)}$ as a quadratic function of $\varepsilon_{ij}{}^{(e)}$. It may then be inferred* from (30) that the stress and elastic strain are related as

$$\sigma^{ij} = E^{ijkl}\varepsilon_{kl}{}^{(e)} \tag{31}$$

Taking a Jaumann time derivative of (31) and inverting the result, yields an objective relation between the elastic deformation rate and the Jaumann stress rate.

$$d_{ij}{}^{(e)} = M_{ijkl}\,\hat{\sigma}^{kl} \tag{32}$$

For an isotropic material the constitutive compliance tensor M_{ijkl} has the simplest isotropic form for a fourth order tensor.

$$M_{ijkl} = \frac{1}{2\mu}\left[1/2(g_{ik}g_{jl} + g_{il}g_{jk}) - \frac{\nu}{1+\nu}\,g_{ij}g_{kl}\right] \tag{33}$$

The constants μ and ν in (32) are the shear modulus and Poisson's ratio of classical linear elasticity.

Plastic Flow Mode: Equations governing infinitesimal plastic flow of work hardening materials may be inferred from a hypothesis

*This portion of the development follows that employed in Green's method for development of the generalized Hooke's law of classical linear elasticity. (See Eringen [8], chapter 5.)

first enunciated by Drucker [16]. It is postulated that plastic flow produced by application and removal of a self-equilibrated stress field is restricted by the rate* inequality.

$$\overset{\cdot}{\sigma}^{ij}\overset{\cdot}{\varepsilon}_{ij}^{(p)} > 0 \tag{34}$$

Three characteristics of plastic flow theory are implied by (34).**

1. The loading function, f = const., is a convex closed figure in stress space.
2. The plastic strain rate is normal to f = const.
3. Plastic strain rate and stress rate are linearly related.

Development of a similar formulation for finite deformation is impeded by the absence of a unique choice of an objective stress rate tensor for use in a generalized form of (34). In the present theory the Jaumann rate is chosen for its conceptual simplicity and obvious physical interpretation. The implications of Drucker's hypothesis are postulated as operational characteristics of the finite theory.

The loading function is taken to be of the form

$$f = \phi(\sigma^{ij}) - K(W^{(p)}) \tag{35}$$

*For infinitesimal deformation these rates may be taken as partial time derivatives, for which objectivity is an unnecessary constraint since the deformed and undeformed states are indistinguishable.

**Demonstration of these consequences of Drucker's hypothesis is also provided by Naghdi (17).

In (35) ϕ is the yield surface and K is a work hardening parameter determined solely by prior plastic work, $W^{(p)}$.

Yield surface dependence upon current stress state is restricted to the invariants of the deviatoric stresses. Plastic flow independence of hydrostatic stress, and material isotropy are thereby guaranteed. This restriction also eliminates the Bauschinger effect since the yield surface will expand isotropically in stress space. Hence ϕ in (35) is written

$$\begin{aligned} \phi &= \phi(J_2, J_3) \\ \text{where} \quad J_2 &= (1/2)s^i{}_j s^j{}_i \\ J_3 &= (1/3)s^i{}_j s^j{}_k s^k{}_i \\ s^i{}_j &= \sigma^i{}_j - (1/3)\sigma^k{}_k g^i{}_j \end{aligned} \tag{36}$$

The plastic component of the deformation rate is taken to be normal to the loading function.

$$d_{ij}^{(p)} = \Lambda \, \partial f / \partial \sigma^{ij} \tag{37}$$

The proportionality constant Λ in (37) may be found from a consistency condition for plastic flow given in (29) as

$$\dot{f} = 0 \tag{38}$$

Taking the Jaumann time derivative of (35) obtains

$$\dot{f} = \dot{\phi} - \dot{K} = (\partial\phi/\partial\sigma^{ij})\ \hat{\sigma}^{ij} - K'\dot{W}^{(p)} = 0 \tag{39}$$

$$K' \equiv dK/dW^{(p)} \tag{40}$$

The Jaumann rate appears explicitly in (39) only for stress since material derivatives of all other quantities present are objective. The rate of plastic work $\dot{W}^{(p)}$ in (39) may be expressed as

$$\dot{W}^{(p)} = \sigma^{ij} d_{ij}^{(p)} \tag{41}$$

Substituting (41) and (37) into (39) one may solve for Λ in (37). The resulting expression for the plastic deformation rate is

$$d_{ij}^{(p)} = \left[\frac{(\partial\phi/\partial\sigma^{ij})\ (\partial\phi/\partial\sigma^{kl})}{K'(\partial\phi/\partial\sigma^{rs})\sigma^{rs}} \right] \hat{\sigma}^{kl} \tag{42}$$

in which a linear relation between plastic deformation rate and Jaumann stress rate is apparent.

Plastic flow is fully defined by (42). Practical use of this result requires a choice of an explicit form for the yield surface ϕ and definition of the work hardening function K. To complete the formulation we employ a construction proposed by Swedlow [7] for the infinitesimal case.

Dimensional consistency in (42) is established by assuming ϕ

to have the dimensions of stress. It is therefore plausible and convenient to consider it as an equivalent stress* τ_{eq}. We then may define an equivalent plastic strain rate $d_{eq}^{(p)}$ conjugate to τ_{eq} in the sense that

$$\tau_{eq}\, d_{eq} = \dot{W}^{(p)} = \sigma_{ij} d_{ij}^{(p)} \tag{43}$$

Substituting for $d_{ij}^{(p)}$ in (43) leads after some manipulation to the equivalence

$$K' = (1/\tau_{eq})(\dot{\tau}_{eq}/d_{eq}^{(p)}) \tag{44}$$

This expression for K' provides means for its determination from experimental data. Defining a total equivalent plastic strain $\varepsilon_{eq}^{(p)}$ as the integral of $d_{eq}^{(p)}$, (44) may be written

$$K' = 2\mu_{eq}^{(p)}/\tau_{eq} \tag{45}$$

where we have defined an equivalent plastic modulus $\mu_{eq}^{(p)}$ dependent solely on the equivalent stress.

$$\mu_{eq}^{(p)}[\tau_{eq}] \equiv (1/2)\, d\tau_{eq}/d\varepsilon_{eq}^{(p)} \tag{46}$$

Derivation of the plastic modulus from uniaxial tensile test data is described in detail in Appendix I.

*eq not indices

Introducing the equivalent stress and modulus in the flow equations (42) yields

$$d_{ij}^{(p)} = \frac{\tau_{eq}}{2\mu_{eq}^{(p)}} \left[\frac{(\partial\tau_{eq}/\partial\sigma^{ij})(\partial\tau_{eq}/\partial\sigma^{kl})}{(\partial\tau_{eq}/\partial\sigma^{rs})\sigma^{rs}} \right] \hat{\sigma}^{kl} \tag{47}$$

For convenient reference (47) is written as

$$d_{ij}^{(p)} = N_{ijkl}\, \hat{\sigma}^{kl} \tag{48}$$

N_{ijkl} is hemitropic function of the deviatoric stresses. The full flow equation is objective.

Elasto-Plastic Flow: The total deformation rate is simply the sum of its elastic and plastic components. Assembling equations (32) and (48)

$$d_{ij} = d_{ij}^{(e)} + d_{ij}^{(p)} = [M_{ijkl} + N_{ijkl}]\, \hat{\sigma}^{kl} \tag{49}$$

It is convenient to rewrite (49) as

$$2\mu d_{ij} = B_{ijkl}\, \hat{\sigma}^{kl}$$

$$B_{ijkl} \equiv (1/2)[g_{ik}g_{jl}+g_{il}g_{jk}] - \frac{\nu}{1+\nu}\, g_{ij}g_{kl} \tag{50}$$

$$+ (\mu/\mu_{eq}^{(p)})\tau_{eq} \left[\frac{(\partial\tau_{eq}/\partial\sigma^{ij})(\partial\tau_{eq}/\partial\sigma^{kl})}{(\partial\tau_{eq}/\partial\sigma^{rs})\,\sigma^{rs}} \right]$$

In (50) μ is the shear modulus of linear elasticity.

$$\mu = E/[2(1+\nu)] \tag{51}$$

The flow mode is controlled in (50) by the modulus ratio $\mu/\mu_{eq}^{(p)}$. For elastic loading and unloading the plastic modulus becomes infinite and (50) reduces to the elastic equations (32).

Perfect plasticity is specifically excluded from the formulation. Hence

$$\mu_{eq}^{(p)} \neq 0 \tag{52}$$

and (51) may be inverted.

$$\hat{\sigma}^{ij} = p^{ijkl}\, d_{kl} \tag{53}$$

In (53)

$$p^{ijkl} \equiv \mu[(g_{ik}g_{jl}+g_{il}g_{jk} + \frac{\nu}{1-2\nu}\ (g_{ij}g_{kl})] - 2\mu\gamma^2 \left[\frac{(\partial\tau_{eq}/\partial\sigma^{ij})(\partial\tau_{eq}/\partial\sigma^{kl})}{1+\gamma^2(\partial\tau_{eq}/\partial\sigma^{mn})(\partial\tau_{eq}/\partial\sigma^{rs})g^{mr}g^{ns}} \right] \tag{54}$$

$$\gamma^2 \equiv \tau_{eq}(\mu/\mu_{eq}^{(p)}) \,/\, [(\partial\tau_{eq}/\partial\sigma^{rs})\sigma^{rs}] \tag{55}$$

The tensor p^{ijkl} is a hemitropic function of the deviatoric stresses. It possess the symmetries

$$p^{ijkl} = p^{jikl} = p^{klji} \tag{56}$$

and cannot be decomposed into elastic and plastic components. The inverse constitutive equations (53) are objective. The equations are expanded for planar flow in Apendix II.

Examination of the constitutive equations reveals two critical features of finite elasto-plastic flow.

1. The constitutive equations cannot be integrated to define relations between total stresses and strains except under very restricted conditions.* The stresses must be proportional *and* the deformation must be homogeneous.
2. The total strain, found as the time integral** of d_{ij}, cannot in general be decomposed into elastic and plastic components. The elastic and plastic deformation rate components are defined with respect to the instantaneous configuration of a body. This configuration reflects the previous history of both elastic and plastic flow. Hence the total deformation reflects problem dependent coupling of elastic and plastic behavior.

These facets of finite elasto-plastic deformation provide the motivation for the rate viewpoint adopted for the entire analysis.

*The usual distinction between incremental and deformation theories of plasticity (Fung [14], p. 476]) is identified but must be extended to exclude local rotation.

**See (22).

I.3 Equilibrium Theory

The Concept of Rate Equilibrium

The rate nature of the constitutive equations for elasto-plastic materials dictates that their deformation be viewed as a time dependent flow process. Hence requirements of mechanical equilibrium must be applied not only to instantaneous states of a deforming body but also to the flow itself.

Equilibrium equations governing total stresses and their rates of change are developed below. The derivation of the total stress equations provides a model for establishment of appropriate rate equations.

The flow is taken as quasi-static thereby allowing inertial effects to be neglected. Body forces are also excluded.

Total Stress Equilibrium: The net load applied to a body B in static mechanical equilibrium must be zero. The net load is found as the integral of surface traction (23) over ∂B the boundary of B.

$$\int_{\partial B} t^i ds = \int_{\partial B} \sigma^{ij} \nu_j ds = 0 \tag{57}$$

Applying the divergence theorem* to (57) yields the volume integral over the body

$$\int_B \sigma^{ij}{}_{;j} \, dV = 0 \tag{58}$$

Since B is arbitrary, field equilibrium equations

$$\sigma^{ij}{}_{;j} = 0 \quad \text{in } B \tag{59}$$

may be inferred from (58).

Equations (59) are the familiar stress equations of equilibrium in terms of Cauchy stress σ^{ij}. These objective equations are valid irrespective of material constitutive behavior and deformation magnitude.

*Sufficient smoothness of σ^{ij} in B is assumed.

Stress Rate Equilibrium: Rate mechanical equilibrium of a deforming body requires that the time rate of net applied load be zero. The net load rate is given by the material derivative of (57). Existing stresses are assumed to satisfy (59).

$$\frac{d}{dt}\int_{\partial B} t^i ds = \int_{\partial B} (\dot{t}^i + \sigma^{ij} v^p{}_{;p} \nu_j) ds = 0 \qquad (60)$$

$\dot{t}^i$ in (60) is given by (24). The additional term derives from the time dependence of ∂B.

Applying the divergence theorem* to (60) yields

$$\int_B (\dot{\sigma}^{ij}{}_{;j} - \sigma^{pi}{}_{;j}\, v^j{}_{;p})\, dV = 0 \qquad (61)$$

Again noting that B is arbitrary we infer field equations

$$\dot{\sigma}^{ij}{}_{;j} - \sigma^{pi}{}_{;j}\, v^j{}_{;p} = 0 \quad \text{in } B \qquad (62)$$

Satisfaction of (62) guarantees that given an equilibrated stress field equilibrium will be maintained in the presence of time varying loading. The equations are objective.

*Sufficient smoothness of σ^{ij}, $\dot{\sigma}^{ij}$, v_i is assumed.

The stress rate equilibrium equations (62) have been derived by a number of previous investigators. Similarly to the total stress equations (59) they govern the stress field irrespective of deformation magnitude and material behavior. In the case of linear elasticity it may be argued (Hill [18]) that the first term in (62) dominates the second by the approximate order of magnitude ratio (E/σ^{ij}). Thus for elastic deformation of metals under moderate stress ($\sigma^{ij} \ll E$) the rate equation may be approximated as

$$\dot{\sigma}^{ij}{}_{;j} = 0 \tag{63}$$

Since the total deformation is infinitesimal the time integrated equilibrium error introduced by dropping the additional term will be small.

For elasto-plastic deformation, however, Rice [19] notes that the dominance of the first term is diminished by the reduction in material stiffness, $(\mu_{eq}{}^{p}/\mu) \ll 1$. The approximate form (63) may still be employed for infinitesimal deformation but the equilibrium error will be larger, of more concern, and problem dependent. In the present analysis for finite elasto-plastic deformation the complete stress rate equilibrium equations must be employed.

I.4 Governing Equations of Finite Elasto-Plastic Flow

The Initial-and Boundary-Value Problem for Velocity

The elements of a complete theory of finite elasto-plastic flow are now in hand. Assembly of the constitutive and equilibrium equations provides governing equations for the velocity field in a deforming body. Initial and boundary conditions admissible to these equations may be defined. The formulation reduces to previously established results for infinitesimal deformation.

In principle the governing equations may be integrated over space and time yielding solutions for complete stress and deformation histories. In practice such integration is possible in closed form only in a limited number of simple cases. However, the quasi-linear nature of the velocity equations facilitates efficient numerical solution. The potential for obtaining such solutions for complex problems is a primary motivation for the present theoretical development.

The Velocity Equilibrium Equations: The velocity field in a deforming body is chosen as the primary dependent variable thus guaranteeing flow compatibility. Equations governing this velocity field are found by assembling the constitutive and stress rate equilibrium equations. For convenient reference the equations are reiterated below.

Constitutive Equations:

$$\hat{\sigma}^{ij} = p^{ijkl} d_{kl} \tag{64}$$

Rate Equilibrium Equations:

$$\dot{\sigma}^{ij}{}_{;j} - \sigma^{pi}{}_{;j} v^{j}{}_{;p} = 0 \tag{65}$$

Writing the Jaumann stress rate in terms of the material rate $\dot{\sigma}^{ij}$ the constitutive equations may be combined with the equilibrium equations to obtain:

$$(p^{ijkl} d_{kl} - \sigma^{i}{}_{m}\omega^{mj} + \sigma_{m}{}^{j}\omega^{im})_{;j} - \sigma^{pi}{}_{;j} v^{j}{}_{;p} = 0 \tag{66}$$

Using the definitions of the deformation rate (19) and spin (21) tensors (66) may be written entirely in terms of velocity.

$$\begin{aligned}(1/2)[g^{i}{}_{n}(g^{tk}g^{l}{}_{m} - g^{t}{}_{m}g^{lk}) - g^{li}g^{k}{}_{m}g^{t}{}_{n} - g^{ti}g^{k}{}_{n}g^{l}{}_{m}][\sigma^{mm} v_{t;l}]_{;i} \\ + [p^{klij} v_{j;l}]_{;i} + \sigma^{kp} v^{l}{}_{;pl} = 0\end{aligned} \tag{67}$$

This result, the velocity equilibrium equations, governs the instantaneous spatial dependence of the velocity field. Presuming knowledge of the stress field, these differential equations are linear at an instant of time. Furthermore they provide a quasi-linear model for the entire deformation process. Their solution involves simultaneous, but decoupled, integrations with respect to space and time.

Immediate integration of the velocity equilibrium equations with respect to time would provide equations governing the total deformation. However such integration is possible only for homogeneous deformation under proportional loading, the same restrictions which limit such integration of the constitutive equations. Thus the rate viewpoint initially adopted proves to be a viable approach not limited in application to specific classes of loading and deformation.

Complete Problem Definition: Complete definition of the finite elasto-plastic deformation problem includes the governing equations (67), specification of material properties, and prescription of initial and boundary conditions for the dependent variables.

Material Properties: The elastic constants defined by (33) must be known. Work hardening plastic flow character of the material is defined by the equivalent plastic modulus prescribed as a function of equivalent stress τ_{eq}. Any history of prior plastic deformation is reflected in this function.

Initial Conditions: The initial configuration, B_o, must be defined. Initial stress and velocity will normally be taken as null fields. However certain non-zero initial fields are admissible; the stress must be in equilibrium and the velocity single valued.

Boundary Conditions: Admissible boundary conditions include prescription of both traction rate* and velocity on the boundary ∂B of the deforming solid. Traction rate and velocity vectors prescribed at the same point on ∂B must be orthogonal. Three classes of problems may be identified.

1. fundamental problems in which either traction rate or velocity are prescribed on the entirety of ∂B,
2. mixed problems in which traction rate and velocity are prescribed on distinct portions of ∂B, and
3. mixed-mixed problems in which traction rate and velocity are prescribed on the same portions of ∂B and are limited by the orthogonality constraint cited above.

*Traction rate $\dot{t}^i$ is prescribed either explicitly, as in the case of pressure loading, or implicitly from knowledge of the total load rate, $\dot{T}^i$, applied to a finite portion, ∂B_T, of ∂B. In the explicit case from (24)

$$\dot{t}^i = (\dot{\sigma}^{ij} - \sigma^{pi} v^j{}_{;p}) \nu_j$$

Implicitly the traction rate is given by $\dot{T}^i$ through (60)

$$\dot{T}^i = \int_{\partial B_T} (\dot{t}^i + \sigma^{ij} v^p{}_{;p} \nu_j) ds$$

The Limit of Infinitesimal Deformation: The velocity equilibrium equations (67) are valid irrespective of deformation magnitude. Reduction of these equations to forms previously established for infinitesimal deformation derives from the assumption that the stress-velocity gradient coupling terms make negligible contribution to the nature of the total deformation. The distinction between deformed and undeformed coordinates becomes unnecessary. Under these assumptions (67) becomes

$$[P^{klij}v_{j;l}]_{;i} = 0 \tag{68}$$

These are the governing equations of infinitesimal elasto-plastic flow developed by Swedlow [7].

In the absence of plastic flow P^{klij} in (68) reduces to the constant linear elastic form E^{klij} in (31). The velocity equilibrium equations may then be immediately integrated with respect to time. The resulting equations (69) are the Navier equations for displacement u_i of classical linear elasticity.

$$\{[1/(1-2\nu)]g^{ij}g^{k}_{\ p} + g^{i}_{\ p}g^{jk}\}\, u_{i;jk} = 0 \tag{69}$$

II. STRATEGY FOR PROBLEM SOLVING

The solution to a problem of finite deformation must include complete histories of the deformation mapping $x^i(X^K,t)$ and the stress field $\sigma^{ij}(x^k,t)$. Construction of this solution for the elasto-plastic case requires simultaneous integration of:

1. the velocity equilibrium equations (67) to determine the velocity field in the time varying domain B,
2. the velocity field with respect to time in order to determine B, and
3. the constitutive equations (64) with respect to time, thus determining the stress field $\sigma^{ij}(x^k,t)$ in B.

As has been previously noted analytic solutions may be found only for homogeneous deformation under proportional loading. Numerical solution is unavoidable for more general problems.

Solution for the dependent variables as continuous functions of time requires an iterative approach. A variety of techniques might be employed including, for example, relaxation or predictor-corrector methods. While such iterative solution is feasible an enormous amount of computing might be anticipated with no guarantee of numerical stability.

A more economic approach is suggested by the quasi-linearity

of the problem. Rather than seeking a continuous solution for the time varying configuration and stress field we restrict our attention to the behavior of these quantities at a finite number of times during the deformation. The total deformation is approximated as a sequence of incremental deformations.

Adoption of the incremental viewpoint toward problem solving allows spatial and time integration to proceed sequentially rather than simultaneously. Spatial integration of the instantaneously linear velocity equilibrium equations provides the velocity field in B at time t. Subsequent integration of the velocity field and constitutive equations over a time increment δt yields the configuration and stress field at a new time $t + \delta t$. A new spatial problem for the velocity at $t + \delta t$ may then be defined. The computational efficiency of the incremental approach is immediately apparent. A complete problem is solved by a sequence of linear analyses. No iteration is required.*

The availability of the complete theoretical rate formulation provides a distinct advantage for the incremental numerical solution procedure. Problem solving capability is not tied to particular numerical techniques.

*A single exception exists. If elastic unloading occurs during an increment the plastic modulus becomes infinite and the analysis for that increment must be repeated. The iteration is, however, closed in the sense that it need be continued only until the local modulus value is consistent with the behavior of the point in question.

Irrespective of the numerical procedures chosen solution accuracy is controllable. The incremental model assumes that the velocity equilibrium equations written at an instant during the deformation provide an acceptable approximation over a finite time step. Note, however, that the coefficients in these equations are stress dependent and the configuration of the deforming solid defines their domain of integration. Hence the degree of approximation is dependent upon the variation in stress and configuration during a time step. The analyst retains control over the error in modeling a problem through his choice of time step size and is assured of convergence to a precise representation as the step size tends to zero. Thus increased time step size provides a less accurate solution at reduced expense and vice-versa, a measure of control not available in iterative solutions.

The incremental approach to problem solving provides a vehicle for realization of the full potential of the rate formulation for finite deformation of elasto-plastic solids. No inherent restrictions exist upon loading type, geometry or deformation magnitude. The utility of the analysis is limited only by the availability of requisite material property data.

III. NUMERICAL SOLUTION PROCEDURE

Overview

The incremental approach is adopted for numerical solution of the finite elasto-plastic deformation problem. A finite element technique is employed to reduce spatial integration of the field problem of Section I.4 to algebraic form. The overall procedure for analysis of a deformation increment is summarized below and developed in detail in subsequent sections. The procedures described are valid for analysis in three spatial dimensions in any coordinate system.

The deforming solid is partitioned into an array of contiguous sub-regions or finite elements. Behavior of the complete solid is modeled by coupling these elements at a finite number of common points or nodes. Within each element spatial dependence of field variables is approximated in terms of nodal values which become the principal unknowns of the numerical problem.

Linear algebraic equations governing the nodal velocities at the beginning of a time step are developed by applying the Galerkin method* [20] to the velocity equilibrium equations.

*Note that for finite elasto-plastic flow energy principles are not available as a basis for finite element solutions. Hence an approach based solely on the governing differential equations is required. This point is further discussed in Section III.1.

These equations, termed the rate stiffness equations are of the form*

$$T^{\alpha} = K^{\alpha\beta} V^{\beta} \quad (\alpha,\beta=1,\ldots,M) \tag{70}$$

where T^{α} and V^{β} are nodal loading rates and velocities, respectively. The range M is the total number of degrees of freedom associated with the finite element model. The rate stiffness $K^{\alpha\beta}$ in (70) depends upon the instantaneous configuration, prior plastic deformation, and the existing equilibrated stress field. Boundary conditions of the problem must prescribe precisely half of the 2M variables, load rates and velocities.

Solution of the rate stiffness equations for the unknown nodal quantities provides the basis for evaluation of a deformation increment. Nodal coordinates and loads as well as stress and strain fields in the elements are found by integration with respect to time. Values of these quantities at the beginning of the increment provide initial values for this integration. A new problem for the nodal velocities, may then be defined and the incremental procedure repeated.

*Greek superscripts indicate matrix character. Repeated Greek superscripts are to be summed over an indicated range.

A single exception to the above procedure exists. Elastic unloading is signalled by a decrease in the equivalent stress in a region previously deforming plastically. When this occurs the rate stiffness must be recomputed to reflect elastic behavior in elements comprising that region at that time, and the incremental solution repeated.

The incremental method described above has been implemented for analysis of planar deformation in plane stress or plane strain. Equations governing numerical solution of planar problems are given in Appendix III.

III.1 Spatial Integration: The Galerkin Method

The use of finite elements for spatial integration of the velocity equilibrium equations is contingent on the availability of a method for transforming these equations to an algebraic form involving a finite number of dependent variables. Discretization procedures developed for analysis of infinitesimal deformation, Zienkiewicz [21], provide a model for the present finite case.

Reduction to a finite number of variables is accomplished by approximation of element field variables in terms of their nodal values. These nodal values are taken as the dependent variables of the numerical problem. Algebraic equations governing these variables must be derived from the governing differential equations.

In analysis of infinitesimal deformation advantage is taken of the symmetric nature of the governing equations, e.g. the Navier equations of linear elasticity. Problems governed by such equations admit alternative statement as the variation of quadratic functionals. The variational problem may be extremal, e.g. minimum potential energy, or stationary, e.g. the Reissner [22] principle. The functional is written in terms of the finite element field variable approximation, integrated over each element and the variation taken with respect to the nodal

variables. The resulting linear algebraic equations are then solved for the nodal quantites. This entire procedure is known as the Ritz method.

Application of the Ritz method to the present case of finite elasto-plastic deformation requires that the velocity equilibrium equations be symmetric. Writing these equations in terms of a linear differential operator L^i, however,

$$L^i \{v_j\} = 0 \qquad \text{in } B \tag{71}$$

and the boundary conditions as

$$f^i(v_j) = 0 \qquad \text{on } \partial B \tag{72}$$

we find

$$\int_B [L^i\{v_j\}]w_i \, dV \neq \int_B [L^i\{w_j\}] \, v_i \, dV \tag{73}$$

In (73) v_j and w_j are independent, single-valued velocity fields satisfying (72). Symmetry requires that (73) be an equality. Thus the Ritz method is not applicable in the present case. An alternative integral method is required which, while admitting the use of a finite element field variable approximation, does not restrict the nature of the governing differential equations.

The present numerical solution procedure employs the Galerkin method which is applied directly to the governing differential equations and is appropriate irrespective of their character. Rate stiffness equations are developed for single elements and assembled to define master equations for a complete problem.

The velocity field v_i in an element B_m is approximated* by $\tilde{v}_i$

$$v_i \tilde{=} \tilde{v}_i = \Gamma^{\alpha\beta} V^{\beta} \overset{T}{\phi}{}_i^{\alpha}(x^k) \quad \alpha,\beta=1,\ldots,N \tag{74}$$

where V^{β} are nodal velocities, $\Gamma^{\alpha\beta}$ is dependent upon the nodal coordinates, $\phi_i^{\alpha}(x^k)$ is a vector of functions of x^k and N is the number of degrees of freedom associated with the element. The ϕ_i^{α} in (74) are prescribed functions of x^k providing an approximate representation of the spatial variation of v_i in B_m. The matrix $\Gamma^{\alpha\beta}$ is defined by requiring that evaluation of $\tilde{v}_i$ at the nodal positions yield V^{β}.

The Galerkin method** is based on the observation that if the ϕ_i^{α} in (74) are considered independent then requiring $\tilde{v}_i$ to satisfy (71) as N tends to infinity implies orthogonality of

*Combined matrix tensor notation is employed. Greek superscripts denote matrix character and Latin indices denote tensor components. Thus the elements of ϕ_i^{α} are first order tensor components. The overscript T denotes a matrix transpose.

**This discussion is intended to communicate the essence of the technique. Rigorous discussions may be found in Kantorovich and Krylov [20] and Rektorys [23].

each of ϕ_i^α (α=1,...,N) to $L^i\{v_j\}$ in B_m. Thus

$$\int_{B_m} [L^i\{v_j\}]\, \phi_i^\alpha \, dV = 0 \qquad \alpha=1,\ldots,N \tag{75}$$

The orthogonality conditions (75) provide N linear algebraic equations for the unknown V^β of (74). Expansion of (75) for finite N yields the rate stiffness equations (76) for the element B_m. The range of all Greek superscripts is N.

$$\int_{\partial B_m} \{(\partial t_i/\partial t)\, {}^T\Gamma^{\eta\beta}\phi^{\beta i} - t_j {}^T\Gamma^{\eta\beta}[\phi^{\beta i}\, {}^T\phi^{\delta p}{}_{;p} - \phi^{\beta l}\, {}^T\phi^{\delta i}{}_{;l}]\}\, \Gamma^{\delta\alpha} V^\alpha \, dV \tag{76}$$

$$= K^{\eta\alpha} V^\alpha$$

$$\begin{aligned} K^{\eta\alpha} = \int_{B_m} \{ & {}^T\Gamma^{\eta\beta}[\phi^\beta_{ij}\, P^{ijkl}\, {}^T\phi^\delta_{kl} \\ & - 2\phi^\beta_{ij}\, \sigma^j{}_m\, {}^T\phi^{\delta im} \\ & + \phi^\beta_{j;i}\, \sigma^{ip}\, {}^T\phi^{\delta j}{}_{;p} \\ & + \phi^\beta_{i;p}\, \sigma^{ip}\, {}^T\phi^{\delta j}{}_{;j}]\Gamma^{\delta\alpha}\} \, dV \end{aligned} \tag{77}$$

and

$$\phi_{ij} = (1/2)\,(\phi_{i;j} + \phi_{j;i}) \tag{78}$$

The surface integral in (76) corresponds to the time rate of load (See Section I.4) on the element boundary and may be taken to define a vector of nodal load rates T^{α}. Hence (76) is written

$$T^{\eta} = K^{\eta\alpha}V^{\alpha} \qquad \eta,\alpha=1,\ldots,N \tag{79}$$

The rate stiffness matrix $K^{\eta\alpha}$ is full; depends upon the element configuration through the nodal coordinates in $r^{\alpha\beta}$ and upon the existing equilibrated stress state. In general the rate stiffness matrix is not symmetric.

Having written (79) for each element, master rate stiffness equations are written for the entire body by summing the load rate components at each node. Thus follow the equations

$$T^{\alpha} = K^{\alpha\beta}V^{\beta} \qquad \alpha,\beta=1,\ldots,M \tag{80}$$

where the range M is the total number of degrees of freedom associated with the assemblage of finite elements used to model a complete body. The stiffness matrix $K^{\alpha\beta}$ is M x M, sparse and not symmetric. Banded coefficient structure may be achieved in $K^{\alpha\beta}$ by appropriate construction of the finite element map.

Solution of the linear algebraic system (80) requires specification of M of the 2M variables, T^{α} and V^{α}. At internal nodes equilibrium requires T^{α} to be zero. At boundary nodes

either T^{α} or V^{α} may be prescribed* subject to the same orthogonality restriction governing the boundary conditions of the original field problem of Section I.4. Solution of the equations may procede by any convenient technique and yields full knowledge of the velocity field in B and loading rate on ∂B as characterized by their nodal values.

*Boundary loading is prescribed either as rate of total load T at nodal positions or through the traction rate $\dot{t}_i$ on ∂B. In the latter case the rate stiffness equations are employed in the form (76) and the requisite surface integrations performed numerically.

III.2 Time Integration

The solution of the rate stiffness equations at time t_o provides a basis for evaluation of ensuing changes in deformation and loading occurring during a small but finite time step δt. Time dependent variables are expanded in Taylor series about t_o, truncated to linear form and evaluated at $t_o+\delta t$. The procedure allows evaluation of the deformation, nodal coordinates and element strains, and loading, nodal forces and element stresses, at $t_o+\delta t$, the end of the time step. Requisite time derivatives are provided by the rate stiffness equation solution at t_o.

The procedures of this section provide sufficient data, nodal coordinates and element stresses, for evaluation of the rate stiffness $K^{\alpha\beta}$ at $t_o+\delta t$, the beginning of the next time step. Although more sophisticated time integration schemes might be employed, including higher order Taylor series representations, the linear technique proves adequate in practice.

Nodal Coordinates: The time dependent nodal coordinates are expanded as

$$x^{\alpha}(t) = x^{\alpha}(t_o) + [\dot{x}^{\alpha}(t_o)]\delta t + \ldots \qquad (81)$$

Hence the nodal coordinates $\tilde{x}^\alpha$ at the end of a deformation increment may be approximated at $(t_o+\delta t)$ as

$$\tilde{x}^\alpha = \overset{\circ}{x}{}^\alpha + V^\alpha \, \delta t \tag{82}$$

where $\overset{\circ}{x}{}^\alpha$ are the nodal coordinates at t_o and V^α are the nodal velocities. Total nodal displacements U^α are subsequently defined by

$$U^\alpha \equiv x^\alpha - X^\alpha \tag{83}$$

where X^α are the nodal coordinates of the original (t=0) undeformed configuration.

Element Strains: The element deformation mapping function (1) at $(t_o+\delta t)$ is written

$$\tilde{x}^i{}_{\delta}{}^I{}_i = X^I + U^I \tag{84}$$

where the total displacement field U^I is taken as a function of the undeformed field coordinates X^I.

The element total displacement field is approximated in terms of nodal quantities in the same manner as was the velocity field in the development of the rate stiffness equations in Section III.1

$$U^I(X^K) \cong \Gamma^{\alpha\beta} \, U^\beta \, \overset{T}{\phi}{}^{\alpha I}(X^K) \tag{85}$$

Substituting (85) into (84) the element deformation gradient is written

$$\tilde{x}^i{}_{,I} = g^i{}_I + g^i{}_J \Gamma^{\alpha\beta} U^\beta \overset{T}{\phi}{}^{\alpha J}{}_{,I} \tag{86}$$

Inverse deformation gradients $\partial X^I/\partial x^i$ are defined by observing that

$$(\partial \tilde{x}^i/\partial X^I)\ (\partial X^I/\partial \tilde{x}^j) = g^i{}_j \tag{87}$$

A variety of strain measures may be computed from the total deformation gradients (86). Almansi strain, for example, is given by

$$\varepsilon_{ij} = (1/2)[g_{ij} - (\partial X^I/\partial \tilde{x}^i)\ (\partial X^J/\partial \tilde{x}^j)\ G_{IJ}] \tag{88}$$

It should be recalled that the strain is not separable into elastic and plastic portions.

Nodal Loads: The time dependent nodal loads may be expanded as

$$F^\alpha(t) = F^\alpha(t_o) + [\dot{F}^\alpha(t_o)]\ \delta t + \ldots \tag{89}$$

Truncating this series to linear form the nodal loads at the end of a time step are approximated as

$$F^\alpha(t_o+\delta t) = F^\alpha(t_o) + T^\alpha\ \delta t \tag{90}$$

where T^α are the nodal load rates of (80).

Element Stresses: Evaluation of the element stress field requires distinguishing between Cauchy stress σ^{ij} referred to the instantaneous configuration of an element and a Kirchhoff stress S^{ij} referred to the configuration at t_o. Both σ^{ij} and S^{ij} are time dependent and are equal at t_o. Denoting the Cauchy stress at t_o as $\overset{\circ}{\sigma}{}^{ij}$ we define the Kirchhoff stress such that

$$\lim_{t \to t_o} [S^{ij}(\overset{\circ}{x}{}^k, t)] = \sigma^{ij}(\overset{\circ}{x}{}^k, t_o) = \overset{\circ}{\sigma}{}^{ij}(\overset{\circ}{x}{}^k) \tag{91}$$

where $\overset{\circ}{x}{}^k$ are the element field coordinates at t_o. At $t_o + \delta t$ the two stress fields are related by

$$\sigma^{ij}(\tilde{x}^k, t_o + t) = (1/J)\,(\partial \tilde{x}^i / \partial \overset{\circ}{x}{}^k)(\partial \tilde{x}^j / \partial \overset{\circ}{x}{}^l) S^{kl}(\overset{\circ}{x}{}^r, t_o + \delta t) \tag{92}$$

where $J = |\partial \tilde{x}^i / \partial \overset{\circ}{x}{}^j|$. Hence the final Cauchy stress may be found from the final Kirchhoff stress using the transformation (92).

S^{ij} is approximated at $(t_o + t)$ by the truncated Taylor series

$$S^{ij}(t_o + \delta t) \cong \overset{\circ}{\sigma}{}^{ij} + \dot{S}^{ij} \delta t \tag{93}$$

The Kirchhoff stress rate $\dot{S}^{ij}$ in (93) is computed from the Jaumann stress rate $\hat{\sigma}^{ij}$ at t_o.

$$\dot{S}^{ij} = \hat{\sigma}^{ij} + \overset{\circ}{\sigma}{}^{ij} d^{k}_{k} - \overset{\circ}{\sigma}{}^{jp} d^{i}_{p} - \overset{\circ}{\sigma}{}^{ip} d^{j}_{p} \tag{94}$$

where from (53)

$$\hat{\sigma}^{ij} = P^{ijkl} d_{kl}$$

and the deformation rate d_{ij} is computed from the element velocity field approximation (74).

Computation of σ^{ij} using (92) is facilitated by approximating the element incremental deformation mapping $\tilde{x}^{i}(\overset{\circ}{x}{}^{j})$ in the same manner as the total deformation of (86). Thus

$$\tilde{x}^{i} = \overset{\circ}{x}{}^{i} + u^{i}(\overset{\circ}{x}{}^{k}) \tag{95}$$

The incremental displacement field u^{i} is represented in terms of incremental nodal displacements u^{β} as

$$u^{i}(\overset{\circ}{x}{}^{k}) = \Gamma^{\alpha\beta} u^{\beta} \overset{T}{\phi}{}^{\alpha i}(\overset{\circ}{x}{}^{k}) \tag{96}$$

where the incremental nodal displacements are determined from (82)

$$u^{\beta} = V^{\beta}\, \delta t \tag{97}$$

III.3 The Limit of Infinitesimal Deformation

It has been noted in Section I.4, that the velocity equilibrium equations reduce to well established results in the limit of infinitesimal deformation. It is therefore reasonable to expect similar limiting behavior of the algebraic equations governing finite element solutions. This expectation is reinforced by noting (Kantorovich and Krylov [20]) that application of the Galerkin method to symmetric differential equations, such as those governing the infinitesimal case, yields precisely the algebraic equations derived from a Ritz approximation.

For infinitesimal deformation stress-velocity gradient coupling is assumed negligible and deformed and undeformed element configurations are taken to be indistinguishable. The rate stiffness equations (76) become

$$T^{\eta} = K^{\eta\beta} V^{\beta} \tag{98}$$

where

$$K^{\eta\alpha} = \int_{B_m} \{ {}^{T}\Gamma^{\eta\beta} \phi^{\beta}_{ij} \; P^{ijkl} \; {}^{T}_{\phi^{\delta}_{kl}} \Gamma^{\delta\alpha} \} \, dV \tag{99}$$

The stiffness matrix $K^{\eta\alpha}$ is symmetric and positive definite and is recognized as that governing infinitesimal deformation, see, for example, Zienkiewicz [21] p. 16.

For elasto-plastic flow T^{α}, V^{α} in (98) are interpreted as increments of nodal load and displacement. Total strain (assumed $<<1$) and stress are found as simple sums of incremental results since the reference frame transformations of Section III.2 become identity operations. In the case of elastic behavior (98) integrates directly to provide linear relations between total nodal loads and displacements.

IV. EVALUATION OF SOLUTION CAPABILITY

IV.1 The FIPDEF Program

The procedures of Section III have been implemented to provide incremental solution capability for problems of planar finite deformation. The computer program, FIPDEF (FInite Plastic DEFormation), performs analysis of elastic and elasto-plastic materials deforming under conditions of plane stress or plane strain. Elastic unloading and subsequent reverse plastic loading are automatically treated.

The program employs triangular finite elements defined by nodes at their vertices. The velocity field is approximated within each element by assuming linear spatial variation. Rate stiffness equations for these elements are developed in Appendix III. General program logic is shown in Figure (2). The FIPDEF program is written in Fortran IV and is operational on the Univac 1108 system at Carnegie-Mellon University.

Problem definition includes the initial finite element map geometry, material properties and incremental histories of nodal boundary conditions. Material behavior is described by the elastic constants, a proportional limit value of octahedral stress and pointwise specification of an octahedral stress-octahedral plastic strain curve.*

*See Appendix I.

Figure 2

GENERAL STRUCTURE OF THE FIPDEF PROGRAM

1. Read and check input.
2. Set initial elastic material properties.
3. Generate rate stiffness matrix for the N^{th} time step. ($1 \leq N \leq NINC$)
4. Solve for nodal velocities and load rates for step N.
5. Evaluate element stresses at the end of step N.
6. Check all elements for load reversal.
   a. if reversal has occurred in any element(s); modify element material properties accordingly and return to 3. to repeat the N^{th} step.
   b. if loading continues in all elements evaluate their material properties for step N+1.
7. Evaluate nodal loads and coordinates and element strains at the end of step N.
8. Output
9. If N < NINC: go to 3 for step N+1.
10. If N = NINC: STOP.

IV.2 Verification Analysis

Evaluation of the finite deformation analysis capability provided by the FIPDEF program is difficult since comparison with analytic solutions is possible for a limited number of problems. In particular analytic solutions may be obtained only for homogeneous deformation under proportional loading. Despite their conceptual simplicity, however, such problems retain considerable nonlinearity and therefore provide an acceptable, albeit limited, basis for assessment of numerical results.

Furthermore, since the deformation of individual finite elements employed in FIPDEF analysis is restricted to homogeneous form, the behavior of these elements may be completely evaluated. Verification of the accuracy of individual element response is significant for two reasons.

1. It demonstrates the viability of both the rate theory and the incremental approach for solution of finite deformation problems.
2. Accurate prediction of individual element behavior is a necessary condition for accurate solution of inhomogeneous deformation problems requiring the use of element arrays.

It should be recognized that the use of element arrays to solve inhomogeneous problems may of itself introduce error in numerical solutions. Quantitative assessment of this discretization error is not possible on the basis of the homogeneous deformation problems for which analytic solutions are available. Some indication of the potential significance of this type of error can be inferred from the numerical solutions of planar necking problems which are presented and evaluated in Section V.

FIPDEF and analytic results are compared below for three classes of homogeneous finite deformation problems: extension, simple shear and simultaneous extension and rigid rotation. These three types of problems span the range of possible finite deformations. The non-rigid portion of any continuum motion may be viewed as the simultaneous occurrence of dimensional changes, such as those associated with finite extension, and combined shearing and rotation of the form found in simple shear. The third problem, extension and rotation, provides a means for verifying the objective character of the analysis since the solution must be tensorially independent of rotation.

Complete solutions for the verification problems are developed in Appendix IV. Salient features of these solutions are discussed below and compared with the results of numerical

analysis. It is demonstrated that accurate, objective numerical solutions can be obtained for deformations involving dimensional changes of a full order of magnitude and rotations of up to 45 degrees. These upper limits do not reflect deterioration of the numerical results but rather the judgement that most deformations of practical interest will be within these bounds.

IV. 3 Finite Extension

The unit cube of Figure (3a) is deformed into a bar, Figure (3b), by prescribing its horizontal or x dimension as a function of time. The deformation at any time is fully described by the coordinate stretch ratios

$$\lambda_x \equiv \ell_x/\ell_o$$

$$\lambda_y \equiv \ell_y/\ell_o \qquad (100)$$

$$\lambda_z \equiv \ell_z/\ell_o$$

in which ℓ_o is the original unit dimension. No shearing deformation occurs.

The deformation is produced by uniaxial loading ($\sigma_x \neq 0$, $\sigma_y = 0$) and may procede under conditions of plane stress or plane strain. In plane stress we require

$$\sigma_z = 0$$

while in plane strain

$$\lambda_z = 1$$

In either case the applied load is found as

$$P_x = \sigma_x A_x \qquad (101)$$

Figure 3 Kinematics of Homogeneous Extension

A.

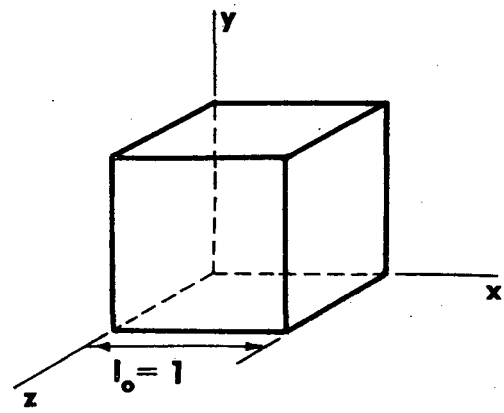

B.

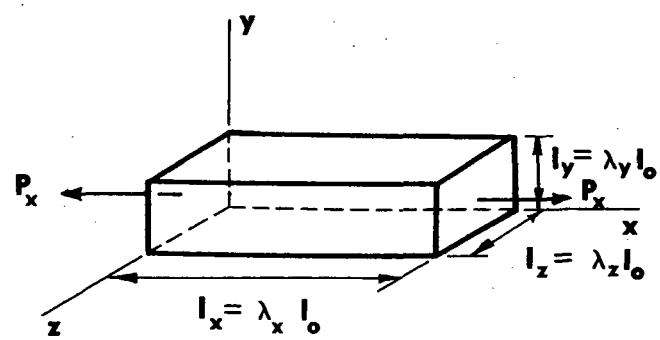

C.

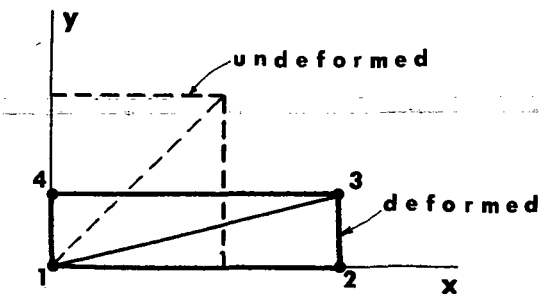

where

$$\sigma_x = \sigma_x(\epsilon_x) \tag{102}$$

$$\epsilon_x = \ell_n \lambda_x$$

and the cross-sectional area A_x is found from

$$A_x = A_x(\lambda_x) = \lambda_y \lambda_z \tag{103}$$

In plane strain we have the additional result

$$\sigma_z = \sigma_z(\lambda_x) \tag{104}$$

Full solutions for load, stresses and area are developed in Appendix IV for plane stress and plane strain extension of elastic and elasto-plastic materials.

For purposes of verification analysis elastic materials are defined as those governed by (32) irrespective of deformation magnitude. To facilitate analytic solution elasto-plastic problems employ the bilinear material property representation of Figure (4).* While the validity of material property models restricts engineering application of the FIPDEF program, it does not affect evaluation of solution accuracy. The only concern here is consistent definition of verification problems to be solved numerically and analytically.

*The effective stress and plastic strain of Figure (4) are directly related to the "equivalent" quantities of Section I.2 (see Appendix I).

Figure 4 Bilinear Elasto-Plastic Properties

A. $\sigma_{ef} < \sigma_Y \equiv$ **Yield Stress: Elastic Flow**

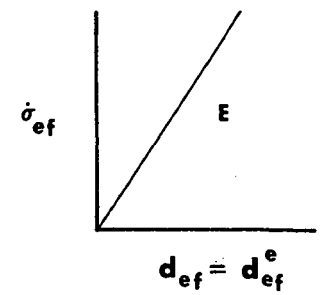

B. $\sigma_{ef} \geq \sigma_Y$: **Elasto-plastic Flow**

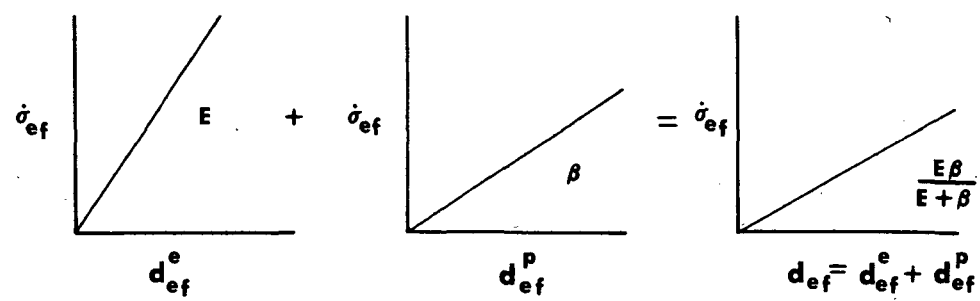

C. Integrating:

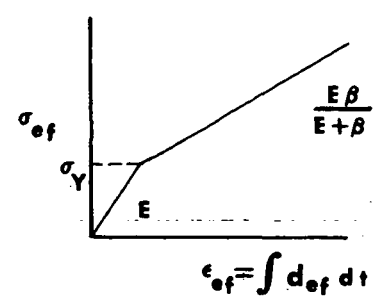

FIPDEF and analytic solutions have been compared for problems of plane stress and plane strain extension for elastic and elasto-plastic materials. All FIPDEF analyses employ the two element model of Figure (3c). The deformation was prescribed in terms of incremental x displacements of the appropriate nodes in this model. With one exception all displacement increments were one percent of the original unit dimension of the cube. For elasto-plastic problems plastic flow was first established by prescription of a number of very small ($<<.01$) incremental displacements. The increment sizes were arbitrarily chosen. Detailed study of increment size effects was not undertaken.

Agreement between analytic and numerical results was excellent in all cases. Applied load, stress and deformed cross-sectional area were predicted within one percent of the analytic results.

Figure (5) is a plot of P_x, σ_x, and A_x as functions of λ_x for an elastic material in plane stress. It illustrates a distinguishing characteristic of all problems of finite extension. The applied load-stretch relation is multiple valued;* a maximum load P_c is attained at a critical, property dependent, stretch λ_c.

*The effect is observable in the data from any tensile test. Discussion of its physical significance is undertaken in Section V.

Figure 5 Finite Elastic Simple Extension

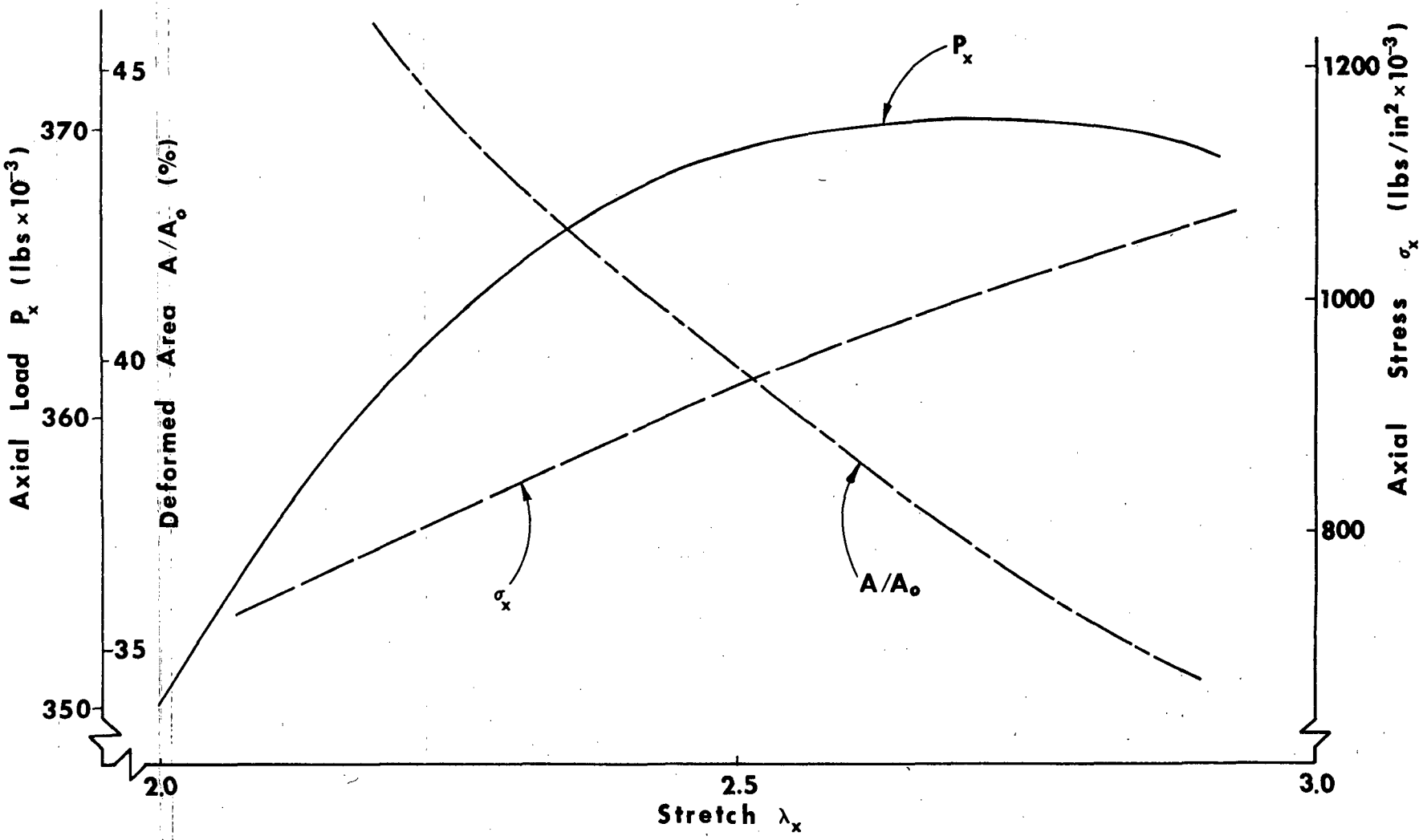

The maximum load and critical stretch may be analytically predicted by solving the equation

$$d(P_x)/d(\lambda_x) = (d\sigma_x/d\lambda_x)A_x + \sigma_x(dA_x/d\lambda_x) = 0 \qquad (105)$$

The plausibility of the maximum load phenomena is evident in (105) since, for the materials considered, $(dA_x/d\lambda_x) < 0$. Analytic expressions for P_c and λ_c are given in Table (IV-1), Appendix IV.

Numerical comparison of FIPDEF predictions and analytic results are given in Tables (1) and (2) for elastic and elasto-plastic problems respectively. Critical stretch, maximum load and critical axial stress are predicted within one percent. All results are dependent upon elastic and plastic properties. Sensitivity to the elastic Poisson ration is shown in Tables (1) and (2) to illustrate the resolution which is attainable.

Load-stretch results for plane stress and plane strain extension of elastic and elasto-plastic materials are given in Figures (6) and (7) respectively. The results are normalized on the critical values P_c and λ_c. FIPDEF results and analytic predictions coincide over the full range of deformation considered.

Table 1

Homogeneous Extension of Elastic* Bodies

Comparison of FIPDEF and Analytic Results

at Maximum Load

Poisson's Ratio	P_c (lbs x 10^{-5})		λ_c		σ_c (lb/in^2 x 10^{-6})	
	FIPDEF	Analysis	FIPDEF	Analysis	FIPDEF	Analysis
Plane Stress:						
0.3	6.15	6.13	5.27	5.30	1.67	1.67
0.4	4.62	4.60	3.48	3.49	1.25	1.25
0.5	3.70	3.68	2.71	2.72	1.00	1.00
Plane Strain:						
0.3	9.46	9.43	10.16	10.29	2.57	2.56
0.4	6.59	6.57	4.46	4.48	1.79	1.79
0.5**	4.93	4.91	2.71	2.72	1.34	1.34

*Note: $E = 10^6$ lb/in^2 in all cases.

**Poisson's ratio of 0.5 is inadmissible in plane strain analysis (See Appendix II). Since it corresponds to elastic incompressibility the present analyses were performed using a high ratio of bulk modulus to Young's modulus $\kappa/E = 10^3$, which approximates such material.

Table 2

Homogeneous Extension of Elasto-Plastic* Bodies

Comparison of FIPDEF and Analytic Results

at Maximum Load

Poisson's Ratio	P_c (lbs x 10^{-4})		λ_c		σ_c (lb/in^2 x 10^{-3})	
Plane Stress:						
0.3	7.78	7.72	1.27	1.27	94.74	94.20
0.4	7.65	7.58	1.25	1.24	93.29	92.56
0.5	7.52	7.44	1.23	1.22	91.45	90.91
Plane Strain:						
0.3	9.29	9.17	1.44	1.43	127.6	127.1
0.4	9.20	9.09	1.42	1.41	125.1	124.0
0.5**	9.03	8.92	1.36	1.36	121.7	121.0

*Note: $E = 10^6$ lb/in^2
$\beta = d\sigma/d\varepsilon^{(p)} = 10^5$ lb/in^2 for $\sigma \geq \sigma_y$
$\sigma_y = 8 \times 10^4$ lb/in^2

**Poisson's ratio of 0.5 is inadmissible in plane strain analysis (See Appendix II). Since it corresponds to elastic incompressibility the present analyses were performed using a high ratio of bulk modulus to Young's modulus $\kappa/E = 10^3$, which approximates such material.

Figure 6 Load-Stretch Response:
Finite Elastic Extension

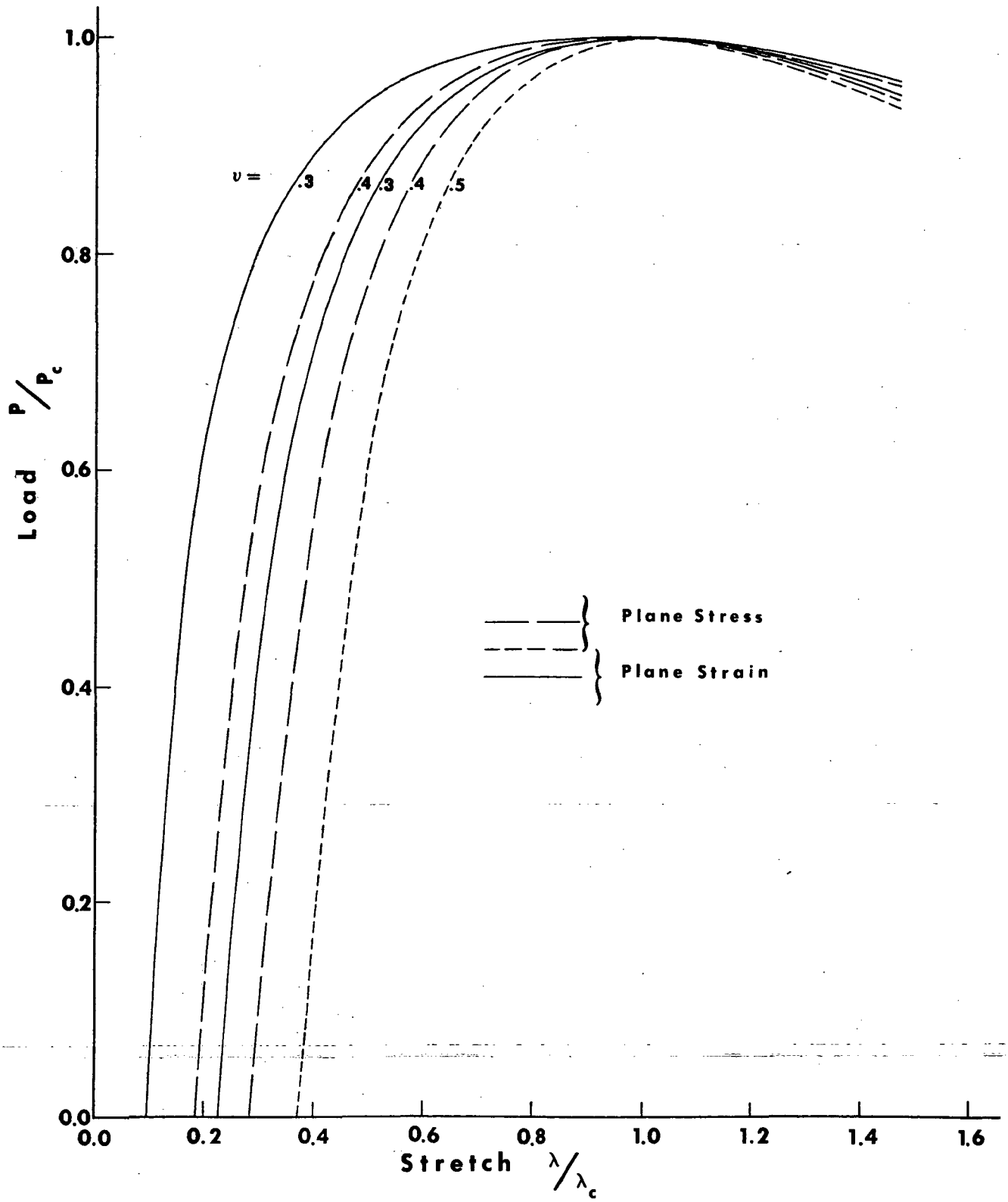

Figure 7 Load-Stretch Response:
Finite Elasto-Plastic Extension

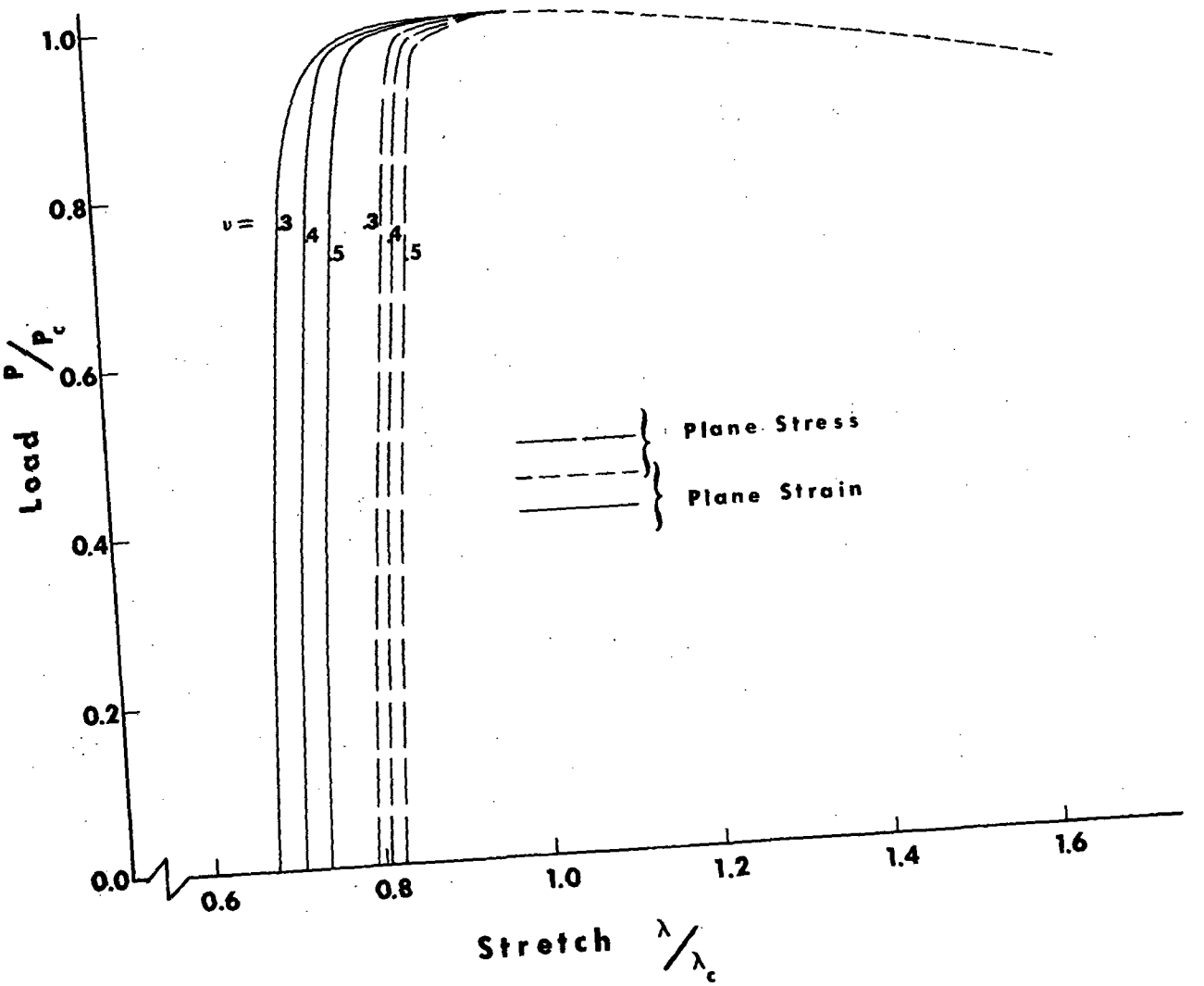

IV.4 Simple Shear

Consider a uniform elastic continuum deforming according to the prescribed velocity field

$$v_x = 2ky$$
$$v_y = v_z = 0 \tag{106}$$

The resulting deformation is homogeneous simple shear in x-y planes of the material. Thus a unit cube of material, Figure (8a), becomes an oblique prism of unit depth, Figure (8b). The deformation is completely described by the shear angle γ in Figure (8b).

$$\gamma = \tan^{-1} \tau$$
$$\tau = 2kt \tag{107}$$

The solution for the time dependent stress field resulting from this deformation is developed in Appendix IV. The non-zero stress components are

$$\sigma_{xy} = \mu \sin \tau$$
$$\sigma_x = \mu (1-\cos \tau) \tag{108}$$
$$\sigma_y = \mu (\cos \tau - 1)$$

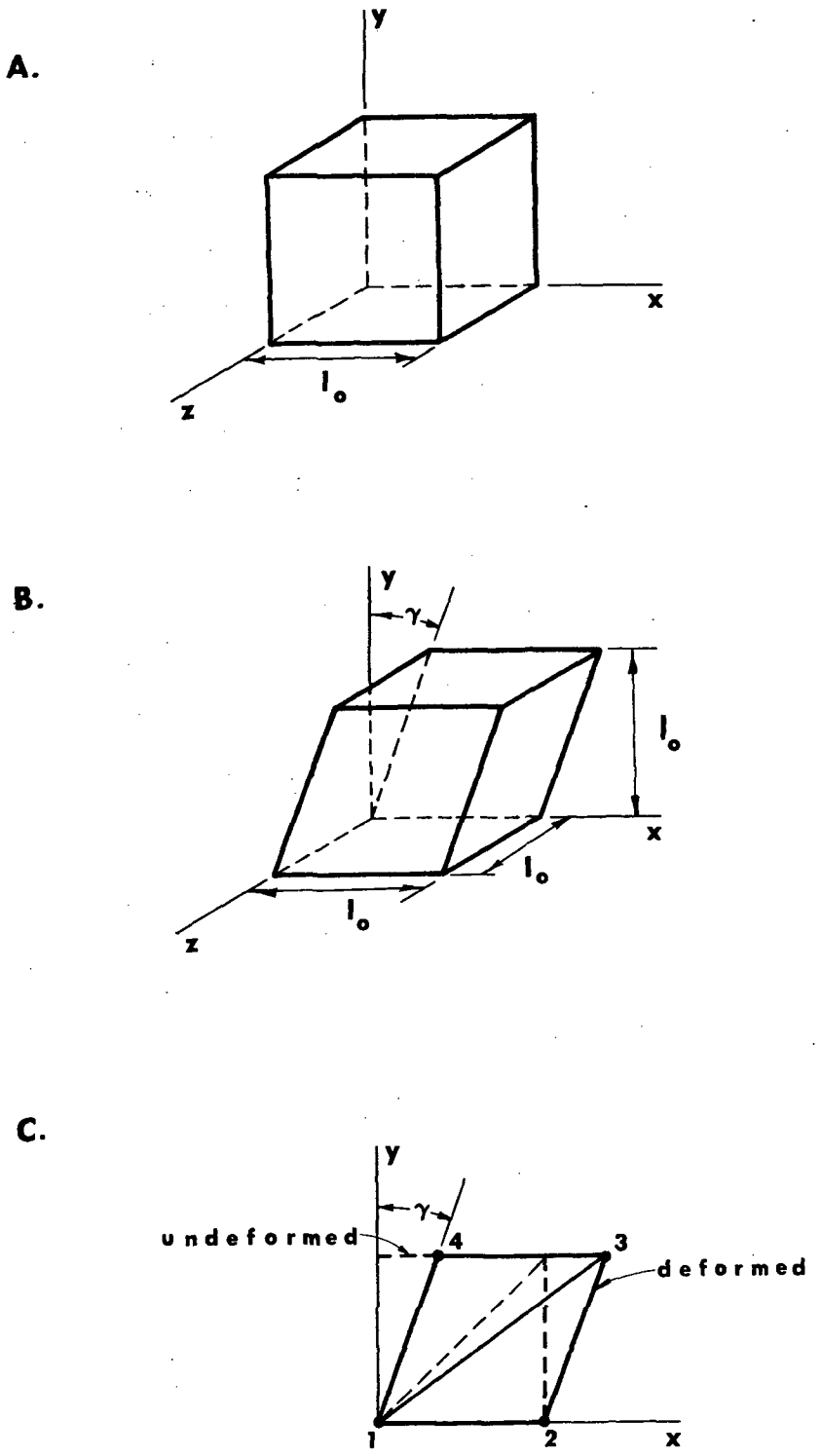

Figure 8 Kinematics of Finite Simple Shear

FIPDEF analysis was performed in both plane stress and plane strain employing the two element model of Figure (8c). Simple shearing deformation was developed by prescribing incremental x displacements of the upper nodes of the element map. All other displacements are null. For the unit dimension model these incremental displacements correspond to increments of τ in (107). The increment size was 0.01.

Analytic and FIPDEF stress results are compared in Figure (9). Shear stress is predicted within one percent and normal stress within five percent over the deformation range $0 \leq \tau \leq 0.7$. Results from plane stress and plane strain analyses are identical.

Figure 9 Stress Response:
Finite Simple Shear

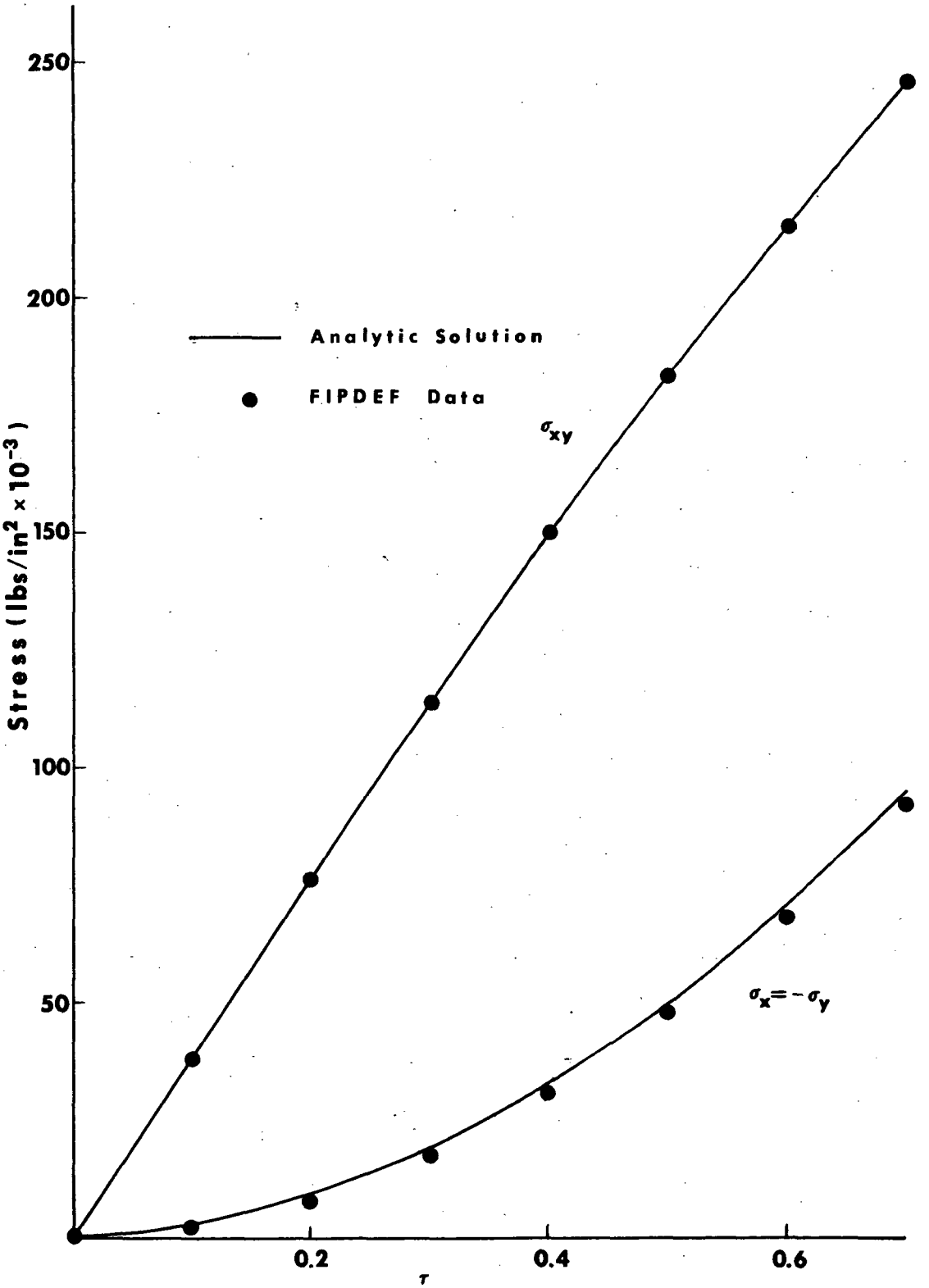

IV.5 Simultaneous Extension and Rotation

Consider the problem of simultaneous rotation and unidirectional extension of a bar of elastic material. As shown in Figures (10 a,b), the x' dimension of the bar is prescribed as a function of time while its y' and z' dimensions are maintained at their original unit values. The bar simultaneous undergoes a rigid rotation $\theta(t)$. This motion may be described in two objectively equivalent ways. In the primed, rotating coordinate frame only the extension process is observed. In the unprimed, fixed frame both extension and rotation must be taken into account.

Components of stress and surface traction corresponding to the above homogeneous deformation are readily found by analyzing the problem in the rotating reference frame of Figure (10). This solution is developed in Appendix IV. It predicts non-zero normal stresses ($\sigma_{x'}$, $\sigma_{y'}$, $\sigma_{z'}$) and normal tractions ($t_{x'}$, $t_{y'}$) on x' and y' coordinate planes respectively.

FIPDEF analysis, however, proceeds in a fixed non-rotating reference frame. Solutions developed in such a reference frame must be independent of rigid rotation, i.e., the analysis must be objective. Hence the FIPDEF solution must be related to the rotating frame solution by the objectivity conditions of Section I.1. Denoting the results of fixed frame analysis by

Figure 10 Kinematics of Combined Extension and Rotation

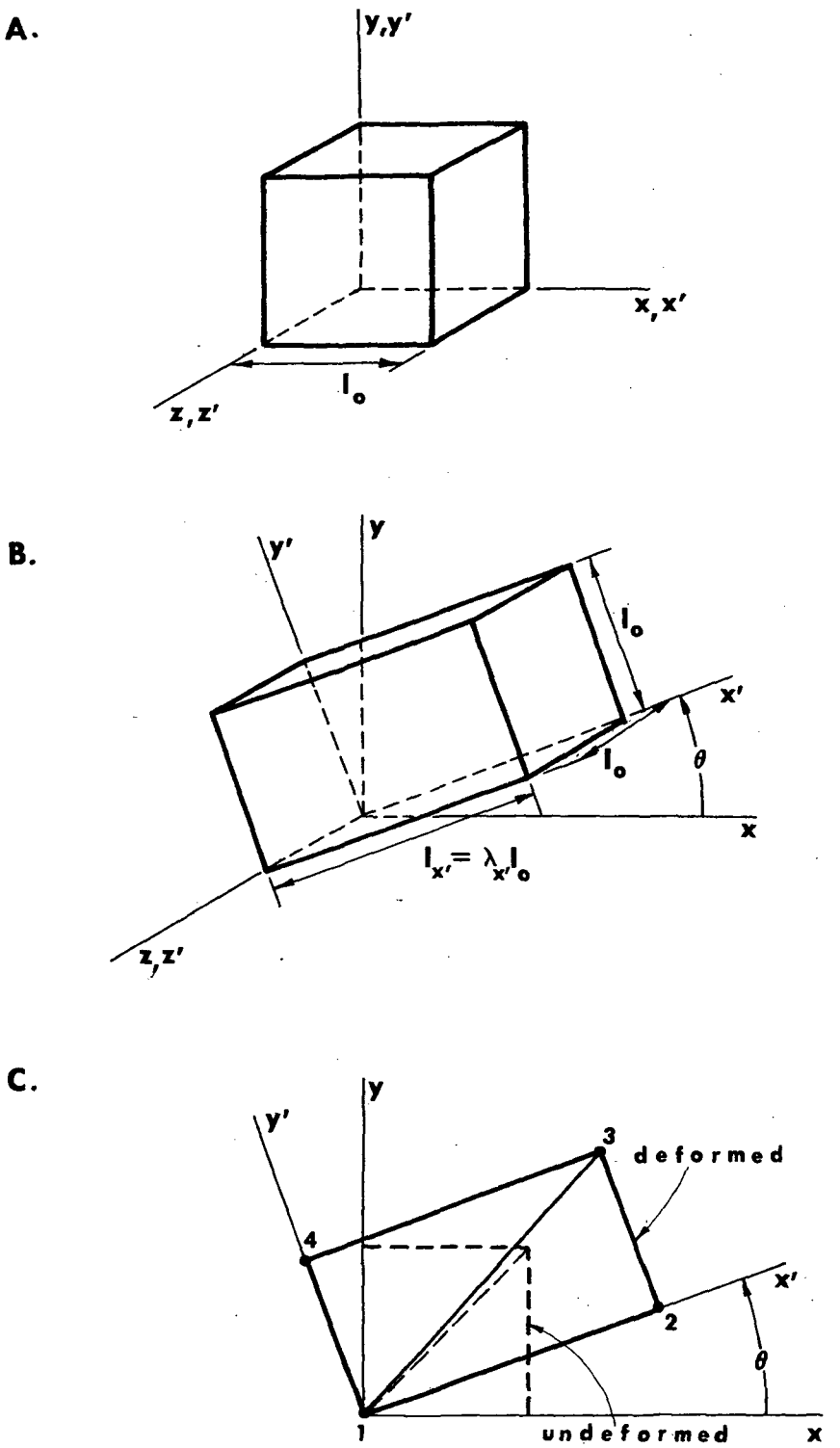

unprimed quantities we require that the stresses be related as

$$\begin{aligned} \sigma_x &= \sigma_{x'} \cos^2\theta + \sigma_{y'} \sin^2\theta \\ \sigma_y &= \sigma_{x'} \sin^2\theta + \sigma_{y'} \cos^2\theta \\ \sigma_z &= \sigma_{z'} \\ \sigma_{xy} &= (\sigma_{x'} - \sigma_{y'}) \cos\theta \sin\theta \end{aligned} \tag{109}$$

and the in-plane nodal forces as

$$\begin{aligned} F_x^{(N)} &= F_{x'}^{(N)} \cos\theta - F_{y'}^{(N)} \sin\theta \\ F_y^{(N)} &= F_{x'}^{(N)} \sin\theta + F_{y'}^{(N)} \cos\theta \end{aligned} \tag{110}$$

In (109,110) θ is the time dependent orientation of the extending bar. In (110) $F_x^{(N)}$ is the x component of total load at the N^{th} node of a finite element model. $F_{x'}^{(N)}$ is analogously defined in the x' system but corresponds to the surface tractions of the rotating frame solution.

The elastic extension-rotation problem was analyzed using the two element model of Figure (10c). Incremental displacements were prescribed at all nodes such that the body underwent simultaneous increments of extension and rigid rotation about node 1 in that figure. Extension increments were one percent of

the original unit length. Rotation increments were 0.005 radians. The final stretch ratio, $\lambda_{x'}$, was 2.6 and the final orientation angle was 0.8 radians.

Results obtained agreed with equations (109) and (110) within one percent over the full range of deformation considered. FIPDEF stress results are plotted in Figure (11) as functions of $\lambda_{x'}$ and θ. Representative nodal force results are given in Figure (12).

On the basis of these results, as well as those of similar analyses for plane stress, it is concluded that affects of finite rotation are properly treated in the FIPDEF program. The objective character of the underlying rate theory is preserved.

Figure 11 Stress Components:
Combined Extension and Rotation

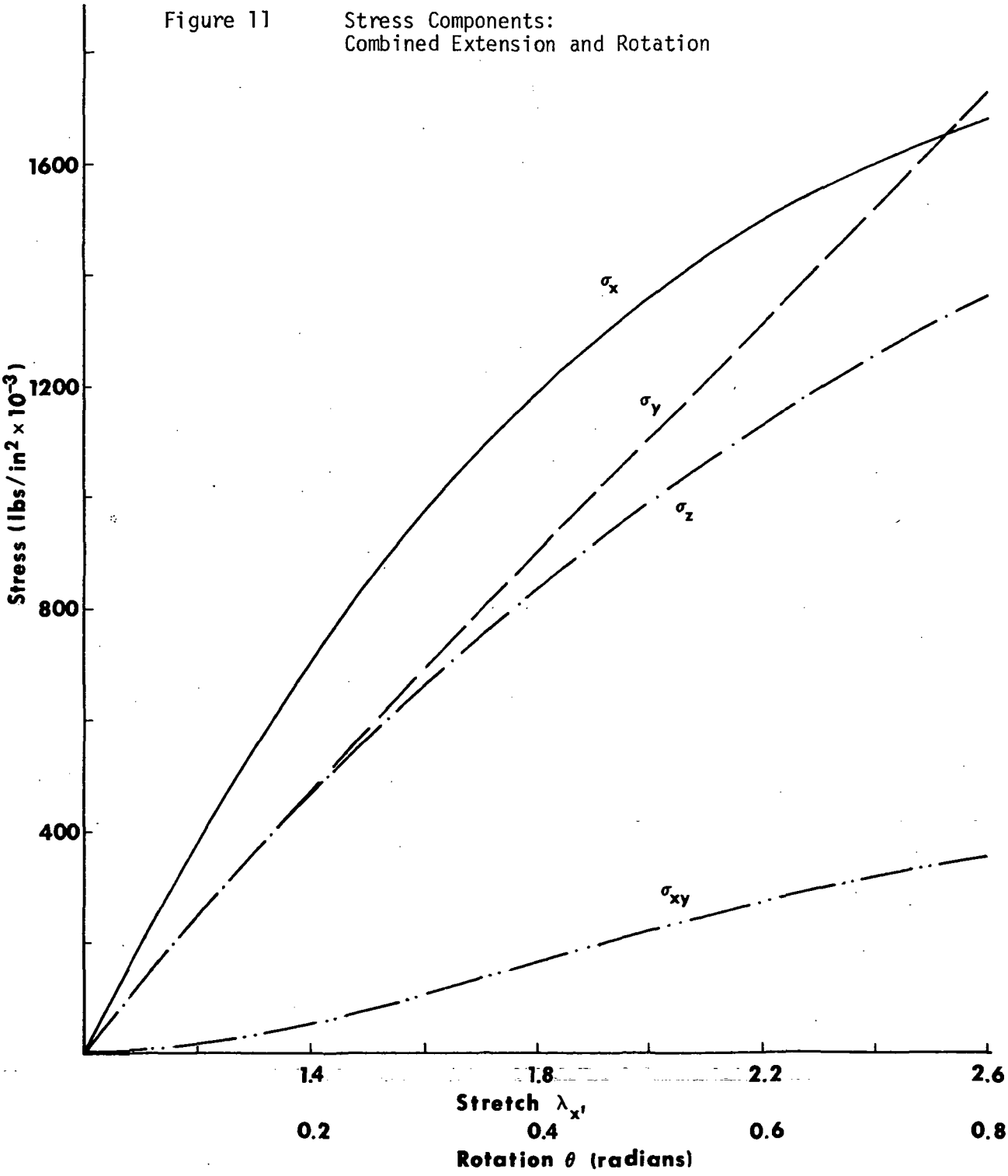

Figure 12 Nodal Forces:
Combined Extension and Rotation

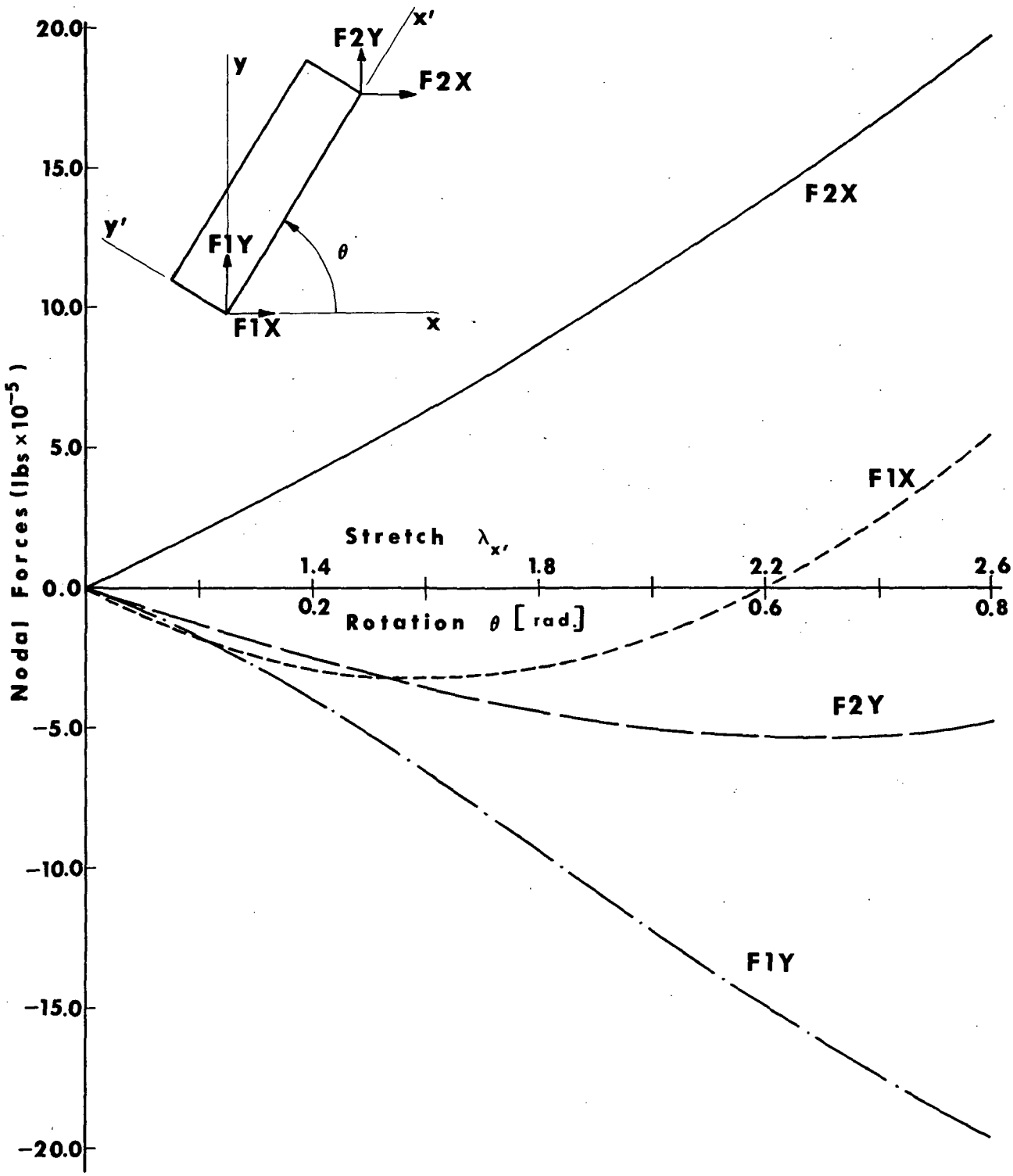

V. NECKING IN FLAT TENSILE BARS

The numerical solution capability which has been developed for problems of two dimensional finite deformation of elasto-plastic materials provides a basis for the investigation of necking in flat tensile bars. The physical aspects of the problem as well as a number of significant previous analyses are discussed below. Subsequently the numerical problem is described and results of analyses under conditions of plane stress and plane strain are presented and discussed. The results provide some insight into the mechanics of the necking process as well as a basis for quantitative evaluation of the utility of stress-strain relations inferred from post-instability tensile test data.

V.1 The Physical Problem

Consider a flat metal bar, Figure (13), initially of length ℓ_o, width w_o and thickness t_o. In a tensile test the bar is quasi-statically extended in the y direction by prescribing its deformed length ($\ell > \ell_o$) as a function of time while the lateral surfaces of the bar remain traction free. The present discussion is limited to tensile testing of metals at room temperature under atmospheric pressure.

Under the above conditions the bar will initially undergo a process of homogeneous extension requiring a monotonically increasing applied load.* For extensions in excess of some critical value the applied load is observed to decrease with increasing extension and subsequently a highly strained local necked region develops in the bar. Extensions corresponding to maximum load and necking initiation are found to vary with the material and to a lesser degree with initial bar geometry. As overall bar length continues to increase plastic straining continues in the necked region while previously yielded material in the remainder of the bar unloads elastically. For convenience we define the onset of necking as that point at which elastic unloading first occurs.

*The upper and lower yield point phenomenon characteristic of mild steel is excluded from this discussion.

Figure 13 Flat Tensile Bar: Initial Geometry

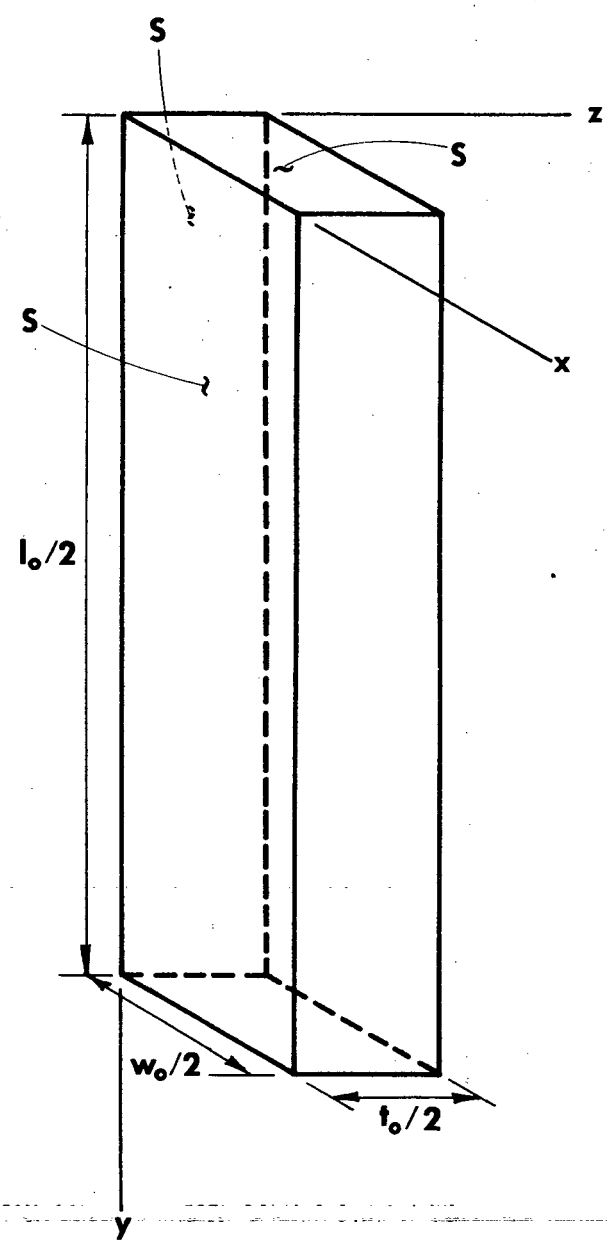

S: symmetry plane

Neck development in flat bars is observed to be dramatically dependent upon initial bar geometry. Nadai [2] reports that for thin bars ($w_o/t_o > 10$) necking takes the form of local thinning in oblique bands parallel to the x-y plane of Figure (13). For thicker bars ($w_o/t_o < 7$), however, necking appears as a symmetric reduction in width in an x-z plane of that figure. In bars of intermediate aspect ratio ($7 < w_o/t_o < 10$) complex combinations of these necking modes are observed.

Experimental investigation of the necking instability phenomenon has not provided a sufficient basis for identification of criteria for either necking initiation or location of the necking region in an initially prismatic bar. Criteria for attainment of maximum load*, such as those employed in verifying the FIPDEF program (Appendix IV), provide only a lower bound for necking initiation. Experimental and very limited analytical results indicate, however, that necking occurs somewhat later than maximum load. The additional extension required is dependent upon the properties of the material tested and possibly upon initial bar geometry.

Presuming the existence of a stress- and/or strain-based

*The earliest prediction of maximum load criteria was provided by Considere [24] who considered simple extension of incompressible materials.

necking initiation criterion neck location might be determined by the distribution of small imperfections in geometry or material properties in seemingly perfect bars. Satisfaction of the necking criteria in the vicinity of one such flaw, or in a region of high flaw density, will cause additional prescribed bar extension to concentrate in the flaw region, thereby developing a neck. It has been shown that the intentional introduction of geometric flaws can be used to control neck location. Standard test procedures (ASTM [25] standard E-8) for flat bar specimens allow a local reduction of area of up to 10 percent for this purpose. It must be noted, however, that the above interpretation of necking initiation has not to date yielded complete understanding of the mechanics of the problem.

The present investigation is limited to consideration of symmetric necking in flat bars of elasto-plastic material. In lieu of analysis in three spatial dimensions, the present effort is restricted to consideration of the limiting cases of plane stress and plane strain deformation in the x-y plane of Figure (13). Neck location is controlled by considering an initial geometric flaw in the form of an 0.5 percent area reduction in the plane y = 0, which becomes the root plane of the neck. The

The analysis is further simplified by assuming the transverse tractions on the ends of the bar ($y = \pm \ell/2$) to be zero.

V.2 Previous Analyses

Tensile bar necking has been analyzed by a variety of techniques. The utility of these analyses has been limited largely by their consideration of idealized models of material behavior as well as, in some cases, an inability to predict both deformed geometry and internal stress and strain fields throughout the necking bar. A number of these analyses are described below to indicate the range of previous efforts as well as to provide a basis for comparison with the results of the present analysis.

Bridgeman [1] developed a solution for the stress distributions in the root planes of necks in round and flat tensile bars. The analyses consider a material obeying a Mises yield criterion and neglect elastic deformation. An assumption of uniform strain in the root plane is made in both cases. The assumption is corroborated for the axisymmetric case by the experimental work of Bridgeman himself as well as that of Davidenkov and Spiridonova [26]. No experimental evidence exists to support the uniform strain assumption in the planar case. The solutions, while physically plausible, are of limited use since *a priori* knowledge of neck geometry is required and no relationship is established between overall bar extension and development of the neck.

Full field solutions for tensile necking in flat bars have been obtained by a number of investigators through analysis of plane strain extension for rigid-plastic materials. The perfectly plastic case has been considered by Richmond [27] and Onat and Prager [28] and hardening plastic by Cowper and Onat [6].

These solutions may also be distinguished by the manner in which necking deformation is introduced. Richmond considers the prismatic bar as the limit of a V-notched bar and thereby has in effect introduced an initial imperfection. Onat and Prager explicitly consider initial shallow longitudinal grooves. Cowper and Onat, on the other hand, develop admissible solutions corresponding to incipient necking by demonstrating bifurcation of the solution to the homogeneous extension problem for a hardening material.

Neck geometries are predicted by all three analyses. Richmond predicts a boundary profile which is convex at the root plane and tends to a linear profile away from the neck region. Qualitative agreement with limited experimental data is demonstrated. The Richmond profile, while differing drastically with the V shaped neck predicted by Onat and Prager, is qualitatively similar to that shown to be admissible for hardening

material by Cowper and Onat. This similarity perhaps indicates that analysis of necking employing slight initial geometric imperfections provides results indicative of behavior of perfect bars.

Analysis of necking has recently been extended to include consideration of elasto-plastic (work-hardening) material behavior by Chen [29] and Needleman [30]. Both investigators have developed numerical solutions for the axisymmetric case. The two studies are significant in the context of the present effort not only by virtue of their consideration of elastic deformation but also because both analyses indicate that necking initiation is distinct from attainment of maximum load. The observation is of increased significance since Chen considers an initially imperfect bar while Needleman establishes necking deformation using a bifurcation technique.

V.3 The Numerical Problem

Two numerical analyses have been performed, one in plane stress, the other in plane strain. Initial geometry, material properties and in plane boundary conditions were identical in both analyses.

The undeformed bar of Figure (13) is represented in two dimensions by the finite element model of Figure (14). The model employs 600 finite elements defined by the positions of 341 nodes. The finite element model is bounded by symmetry lines at $x = 0$ and $y = 0$ and represents one quarter of a complete bar. An initial geometric imperfection is introduced by reducing the cross section at $y = 0$ by 0.5 percent. The amplitude of the imperfection is shown greatly magnified in Figure (14).

The bar is taken to be of isotropic homogeneous material whose inelastic deformation is described by the constitutive formulation of Section I.2. Elastic deformation is characterized by the constants

$$E = 10 \times 10^6 \quad \text{lb/in}^2$$

$$\nu = 0.3$$

Work hardening plastic deformation is controlled by the effective stress-effective plastic strain relation plotted on both linear and logarithmic scales in Figure (15). Initial yield occurs for

$$\sigma_{ef} = \sigma_Y = 35 \times 10^3 \quad \text{lb/in}^2$$

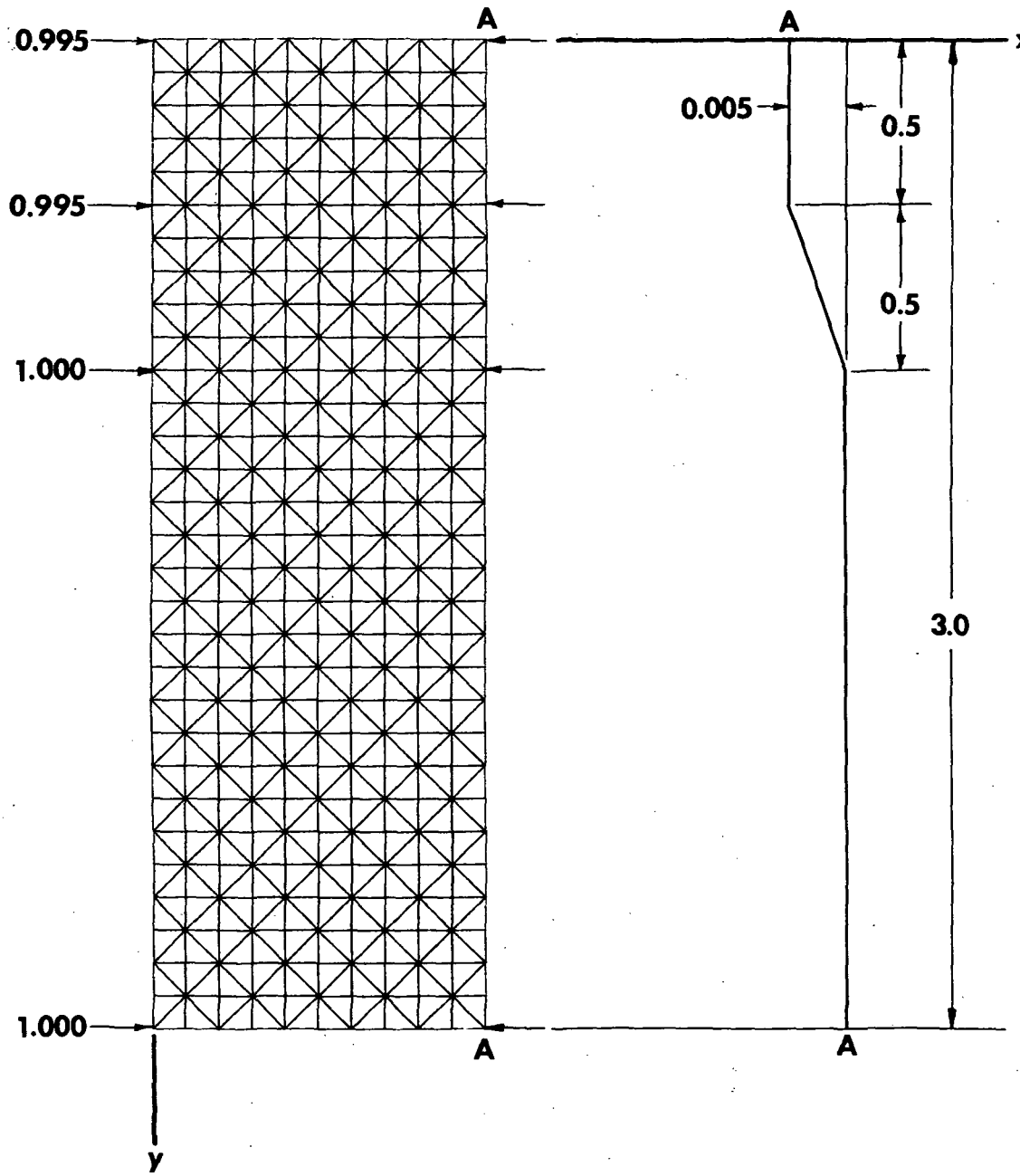

Figure 14 Flat Tensile Bar: Finite Element Model

Figure 15 Effective Plastic Stress-Strain Curve

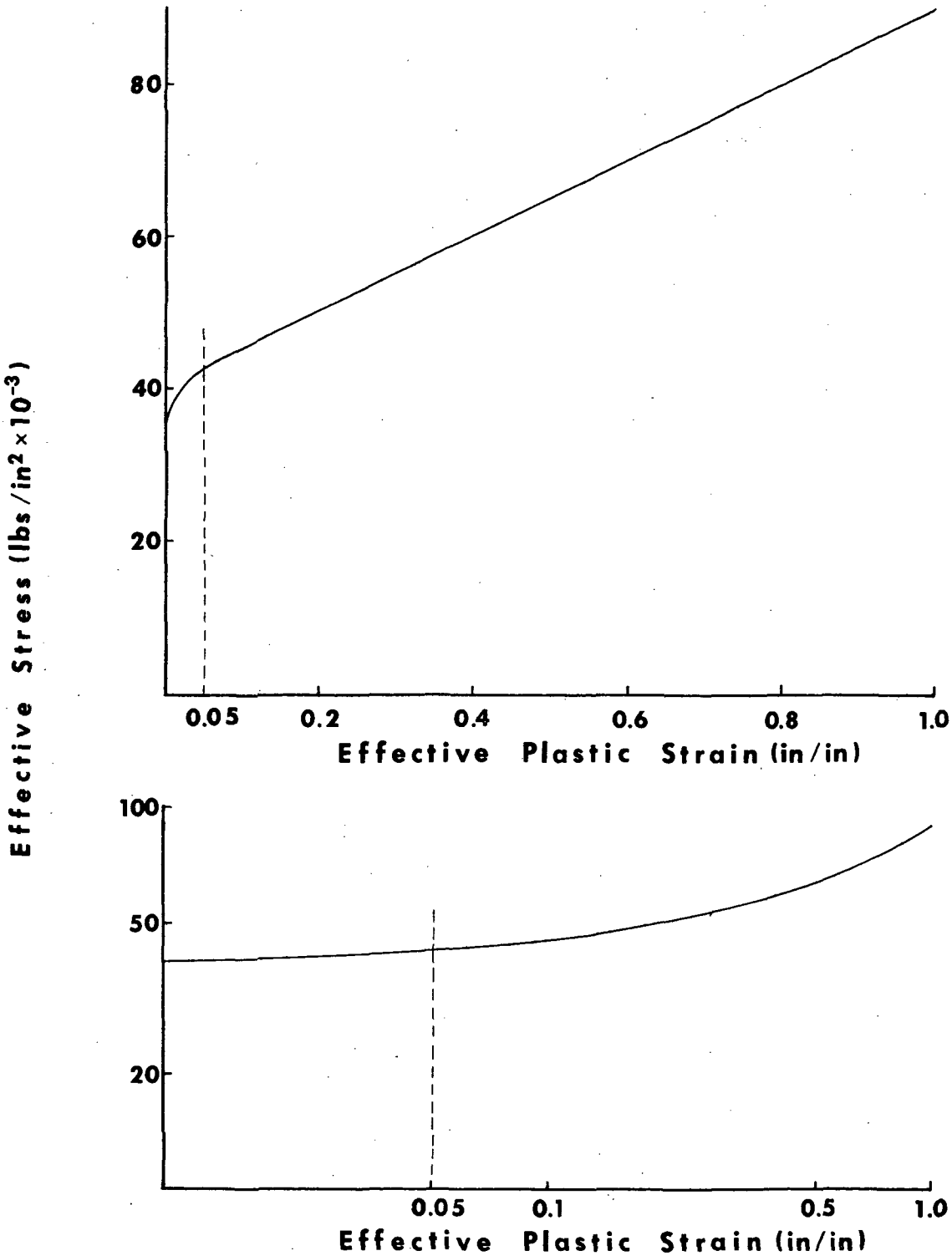

Thereafter the stress-strain relation is

$$\varepsilon_{ef}^{(p)} = \begin{cases} A[(\sigma_{ef}/\sigma_Y)-1]^N & 0 < \varepsilon_{ef}^{(p)} < 0.05 \\ (\sigma_{ef} - K)/\beta & \varepsilon_{ef}^{(p)} > 0.05 \end{cases} \qquad (111)$$

where

$A = 5.0814$ $\qquad$ $K = 40 \times 10^3$ lb/in^2

$N = 3.0$ $\qquad$ $\beta = 50 \times 10^3$ lb/in^2

The effective modulus ratio $E/(d\sigma_{ef}/d\varepsilon_{ef}^{(p)})$ therefore varies smoothly from zero at the yield point to a constant value of 200 for effective plastic strains in excess of 0.05. The plastic stress-strain curve is input to the analysis in the form of data points corresponding to (111). The spacing of these points in strain varies from $\delta\varepsilon_{ef}^{(p)} = 10^{-5}$ at initial yield to $\delta\varepsilon_{ef}^{(p)} = 0.05$ in the linear portion of the curve.

The initial stress-free configuration of the two dimensional quarter symmetry model of the bar is shown in Figure (14). The initial length to width ratio is 3:1. The model is deformed by prescribing the history of incremental boundary conditions. Within each increment these boundary conditions are as follows:

1. Normal displacements and tangential traction are zero on the symmetry boundaries $x = 0$ and $y = 0$.

2. The lateral boundary initially at $x = w_o/2$ is traction free throughout the analysis.

3. Extension is imposed by prescription of uniform positive normal displacement of the boundary initially at $y = \ell_o/2$. Tangential traction on the boundary is zero.

The magnitude of the incremental extensions was varied over the extension history. Initially small steps ($\delta\ell/\ell_o \simeq 10^{-3}$) were taken to establish plastic flow over the entire bar. Incremental extensions were then gradually increased according to the algorithm $\delta\ell/(\ell-\ell_o) = 0.05$ until necking initiated. Subsequent incremental extensions were maintained at approximately 0.5 percent of the length of that portion of the bar which continued to deform plastically. The final overall stretch ratio ℓ/ℓ_o considered was 1.43 in plane stress and 1.62 in plane strain.

Approximately 130 loading increments were employed in each case, each increment requiring an average of one minute of computing time on a Univac 1108. The analyses were terminated when deformations were developed which were judged sufficient to permit reasonable assessment of the necking process. The results do not suggest any breakdown in the analysis. There is no reason to suspect that the analysis could not have been extended indefinitely although in the absence of quantitative criteria for prediction of tensile fracture such effort was not warranted.

The analyses provide full histories of deformation and stress associated with the process of extension and necking in plane stress and plane strain. The deformation is given explicitly by the deformed configuration of the finite element model. The stress field is represented in terms of its component values at the centroid of each finite element.

V.4 Necking in Plane Stress and Plane Strain

Overall tensile bar behavior may be characterized in terms of relationships between extension and applied load provided by the numerical analysis. These relationships are discussed below and compared with the results of homogeneous analysis in which necking is not considered. Inspection of neck geometry and internal stress field histories provides some insight into differences between load-extension relations predicted for plane stress and plane strain extension.

Load-Extension Response: Numerically established relationships between applied load and extension or engineering strain $\bar{e} = \delta\ell/\ell_o$, are given in Figure (16) for both plane stress and plane strain. Results are shown from the inhomogeneous analysis of Section V.3 as well as from homogeneous analysis in which necking is disallowed. The inhomogeneous and homogeneous numerical analyses are distinguished only by the use in the latter case of a two member finite element model of an initially prismatic bar. The homogeneous approach provides what might be termed fundamental solutions for finite elasto-plastic extension which provide a convenient reference in discussion of the necking process.

A maximum load phenomenon is evident in all cases shown in Figure (16). The critical extension $\bar{e}_c$ at which maximum

Figure 16 Load-Extension Data;
Plane Stress and Plane Strain

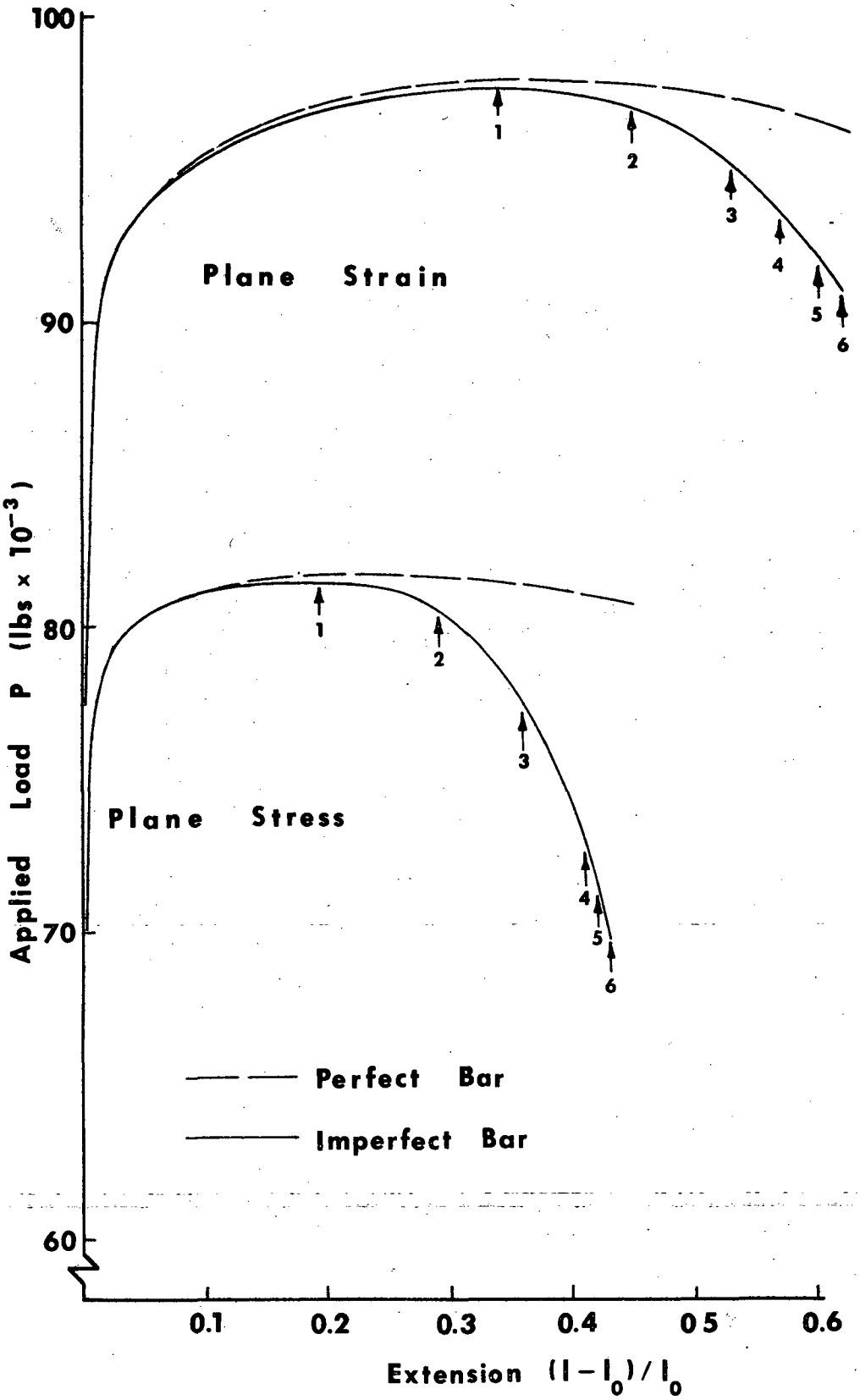

load occurs is significantly larger in plane strain than in plane stress. In both cases $\bar{e}_c$ for the perfect bar is slightly larger than that for the initially imperfect bar.

These differences in critical extension may be explained qualitatively and in an approximate sense quantitatively on the bases of the Considere [24] criterion for attainment of maximum load. By solving the equation

$$dP_y/d\bar{\lambda}_y = 0 \tag{112}$$

for an incompressible material it may be inferred that at maximum load

$$\sigma_y = \beta_y \equiv d\sigma_y/d\bar{\varepsilon}_y \tag{113}$$

The overscript bar denotes deformation measures averaged over the entire bar as opposed to local values. In (112, 113) P_y is the tensile load, $\bar{\lambda}_y = 1 + \bar{e}_y = \ell/\ell_o$ is the uniform stretch of the bar, σ_y is the so-called true stress (load divided by current area) and $\bar{\varepsilon}_y = \ell n\bar{\lambda}_y$ is the logarithmic or natural strain. The assumption of incompressibility, which is not made in the numerical analyses, is later shown to be a reasonable approximation for some purposes. Noting the linear nature of the stress-strain curve for large plastic strains, Figure (15), it may be predicted

using (113) that the maximum load natural strain in plane strain is approximately 1.7 times the corresponding strain in plane stress. The data of Figure (16) show the numerically established ratios to be 1.57 and 1.6 for the perfect and imperfect bars, respectively. The deviation between the above prediction and the numerical results is a consequence of the elastic dilatation considered in the numerical analysis.

The difference in critical extension between the perfect and imperfect bars is qualitatively explained by the presence of the initial imperfection. In the imperfect bar the stress at the location of the initial area reduction will be somewhat higher than that existing in the perfect bar for the same overall extension. Hence (113) is satisfied for a slightly smaller (~10%) extension of the initially flawed bar. The difference in initial minimum cross-sectional area similarly explains the development of lower loads in the imperfect bar than in the initially prismatic bar prior to attainment of maximum load.

Post-maximum load behavior in both plane stress and plane strain is characterized by a more rapid reduction in applied load than that demonstrated by the fundamental solutions of Figure (16). The load reduction in plane stress is noticeably greater than the reduction in plane strain. Six stages in the load reduction process

are noted in Figure (16) for convenient reference in discussing the associated necking deformation. The first stage is the maximum load point.

The difference between plane stress and plane strain load reduction is more readily apparent in Figure (17a) in which post-maximum load response is plotted normalized to the critical values, maximum load P_c and critical overall stretch $\bar{\lambda}_c$. The fundamental solution is also shown for an incompressible material. This solution, identical for plane stress and plane strain, is found as

$$P/P_c = (\bar{\lambda}_c/\bar{\lambda}) \, [\ell n(\bar{\lambda}/\bar{\lambda}_c) + 1] \tag{114}$$

A more rapid deterioration of applied load in the case of plane stress extension is apparent in Figure (17a). This observation is consistent with the more rapid concentration of stretch at the root plane of the neck in plane stress as shown in Figure (17b). The figure shows $\tilde{\lambda}$, the average root plane stretch, as a function of $\bar{\lambda}$, the stretch of the entire bar. The data are again normalized to their values at the maximum load point, stage 1. The root plane stretch $\tilde{\lambda}$ is computed from the numerical results as (assuming incompressibility)

$$\tilde{\lambda} = A_o/A \tag{115}$$

Figure 17 The Influence of Necking

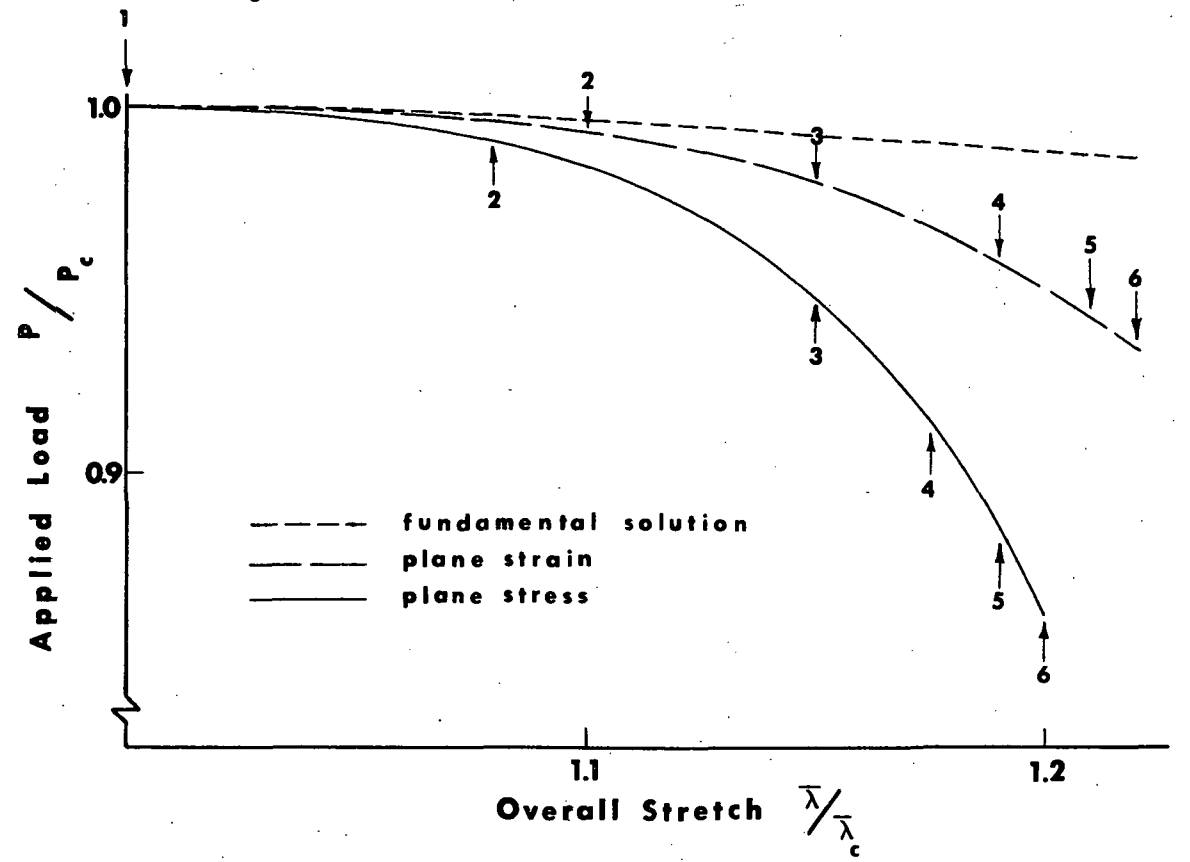

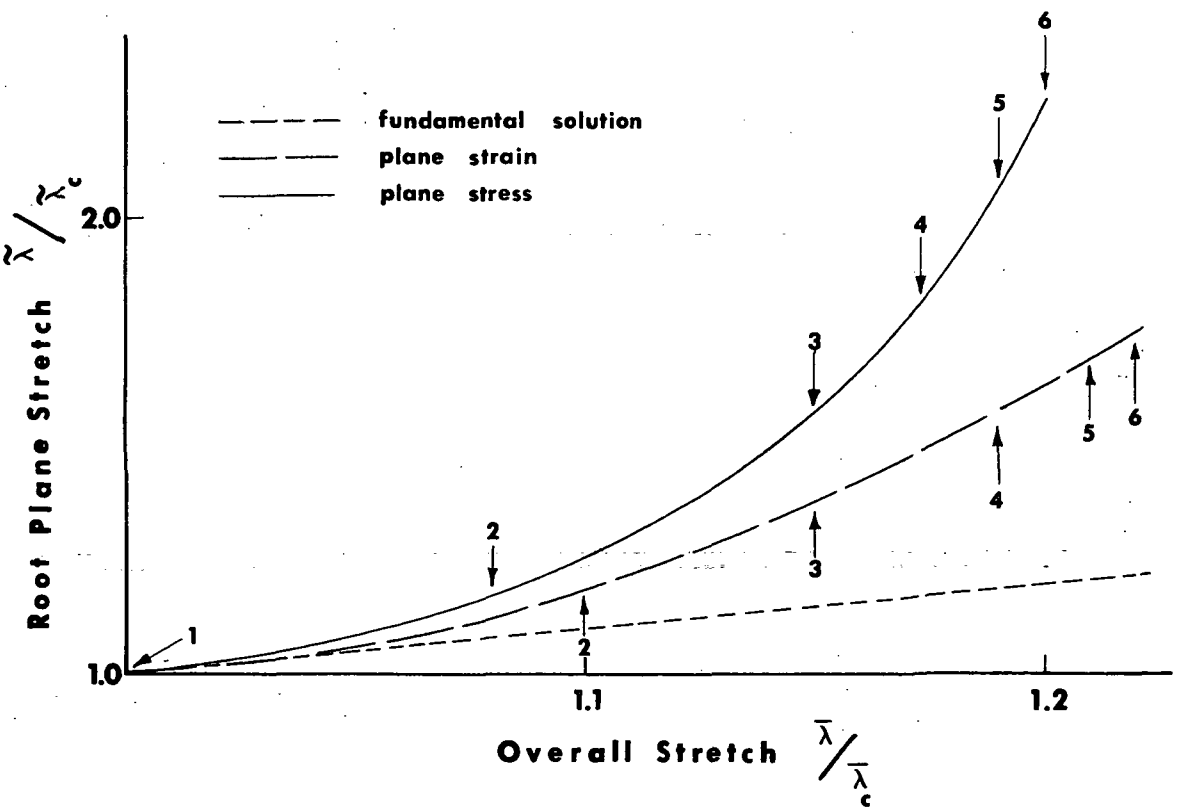

where A_o (A) is the original (current) root plane area.

The data of Figures (16, 17) also suggest that necking does not initiate until somewhat after maximum load is attained. This observation has also been made by Chen [29] and Needleman [30] based on analyses of the elasto-plastic axisymmetric case. The present results also indicate that necking initiation, signified by the occurrence of elastic unloading away from the root plane, occurs somewhat later in plane strain than in plane stress. The normalized overall stretch ratio $\bar{\lambda}/\bar{\lambda}_c$ at necking initiation is approximately 1.03 in plane stress and 1.06 in plane strain for the material and initial geometry considered in the present analyses.

Necking Deformation: The physical character of the necking process is illustrated by the deformation histories depicted in Figure (18). Configurations of the finite element model are shown which correspond to the undeformed state and the six stages in the necking process previously identified in Figure (16). Results are shown for both plane stress and plane strain.

The geometric imperfection present in the undeformed state appears slightly amplified in the maximum load configuration, stage 1. Shortly thereafter necking initiates and subsequent

Figure 18

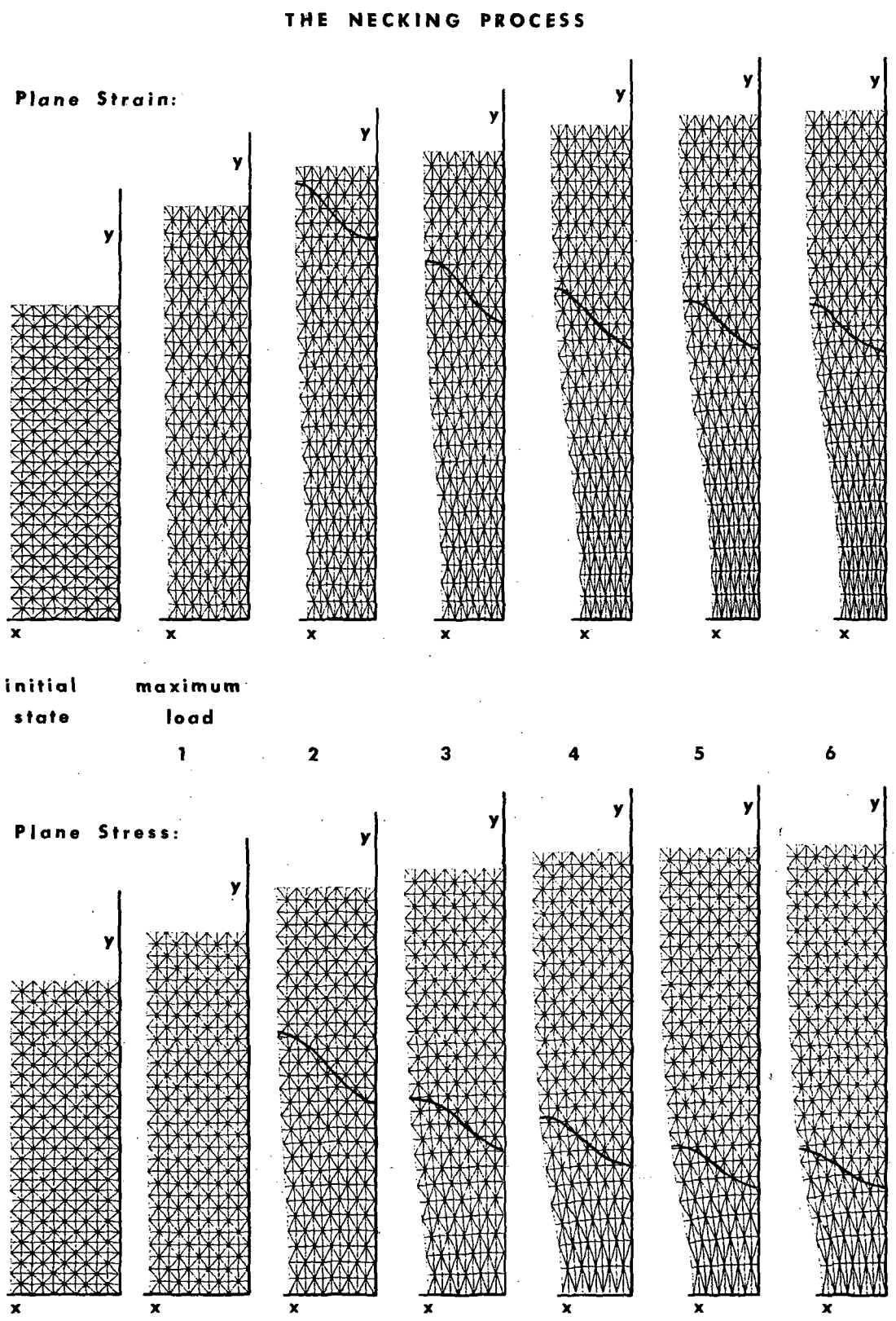
THE NECKING PROCESS
Plane Strain:
y
x
initial state
maximum load
1
2
3
4
5
6
Plane Stress:

prescribed bar extension is increasingly concentrated in the vicinity of the initial area reduction, stages 2-6. Simultaneously the existance of decreasing load in combination with little or no reduction in area produces elastic unloading in regions removed from the neck. Unloading first appears in the center ($x = 0$) of the bar at the furthest boundary ($y = \ell/2$) from the initial flaw and thereafter spreads down the bar. The elastic-plastic boundary is shown in Figure (18) as an oblique solid line. As bar extension proceeds this boundary moves down the bar, closer to the center, material above the boundary recovering elastically, material below it continuing to deform plastically. The position of the boundary throughout the necking process qualitatively corroborates Bridgeman's [1] experimental observation that plastic deformation in necking bars is confined to the region between the inflection points of the neck boundary profile.

The neck profiles shown in Figure (18) for necking in plane strain are in qualitative agreement with results obtained by Richmond [27] and Cowper and Onat [6] for rigid-perfectly plastic and hardening plastic materials, respectively.

While the profile histories of Figure (18) provide a complete picture of neck development in plane strain this is not the case for plane stress. While the plane stress analysis proceeds in

the x-y plane of that figure it admits and indeed, in a thickness average sense, reflects the effect of out of plane deformation. The nature of this deformation is shown in Figure (19) where boundary profile histories in the three symmetry planes (x,y,z = 0) are shown. It is apparent that the necking process in plane stress is properly considered as a problem in three spatial dimensions since a three dimensional neck develops.

In plotting the profiles of Figure (19) the bar has been assumed to have an initial thickness of unity over its entire length. Thus the symmetry model for which results are shown is bounded by a symmetry plane at z = 0 and a traction free surface initially at z = 0.5. Note that the initial imperfection involved a reduction only in width at y = 0 not in thickness.

The analysis does not predict the portion of the boundary profile at y = 0 (the root plane) which is nominally parallel to the z axis. The absence of shear in this plane and the symmetry condition at z = 0 suggest the profile shown. Merchant [31] has observed profiles of this nature in thin plate steel tensile specimens.

The prediction of a three dimensional neck in plane stress is consistent with the more rapid load reduction and root plane stretch concentration previously noted, Figure (17), in this case as opposed

Figure 19 Plane Stress Boundary Profiles

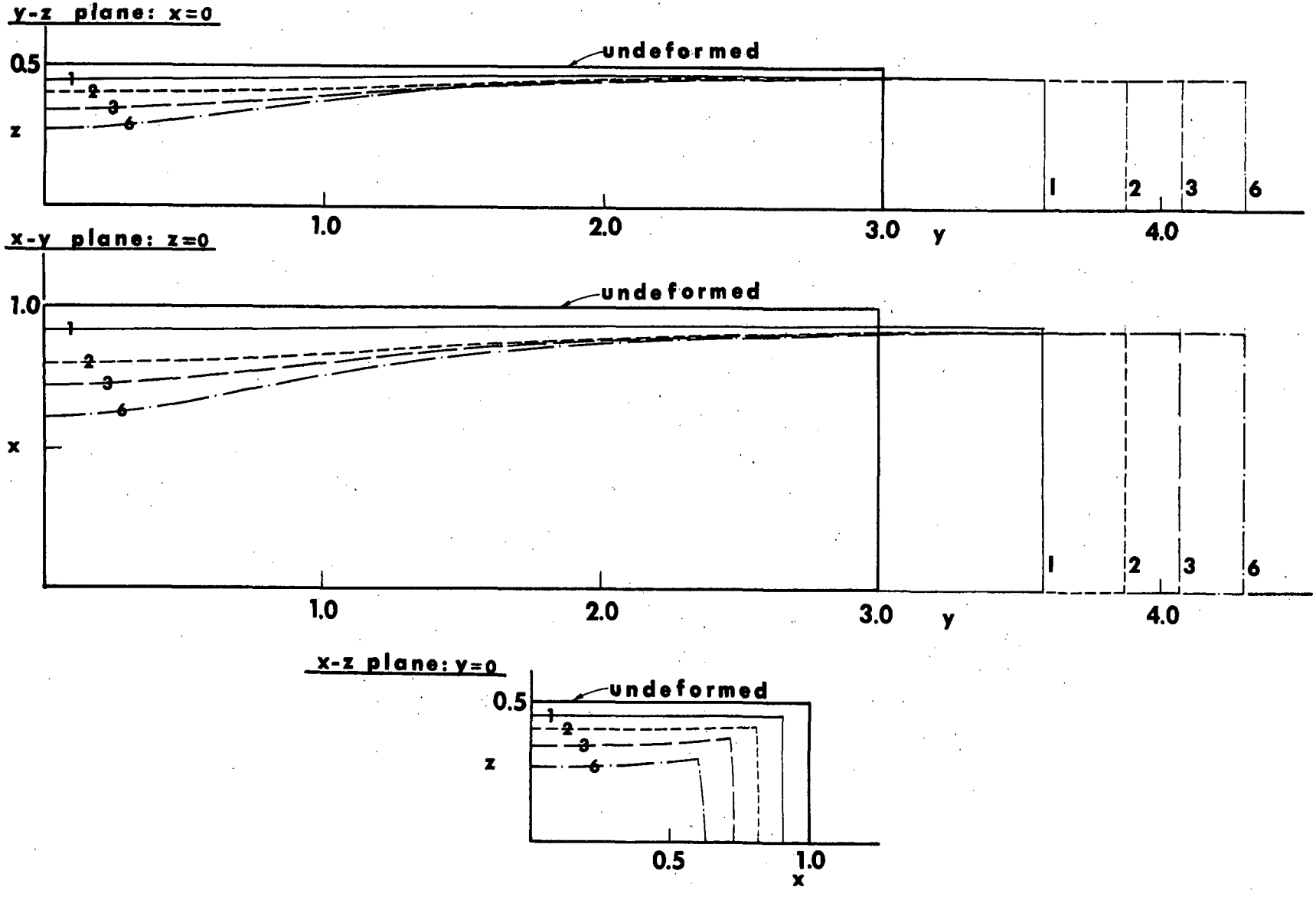

to that of plane strain. The result also exemplifies the limited utility of plane stress analysis which by definition neglects stress field three dimensionality which must follow from the deformed profiles of Figure (19).

The Field Solution: The numerical results provide full histories of stress and deformation over the two dimensional domain of the analysis. The essential characteristics of these results are discussed below in terms of distributions of field quantities along the symmetry lines at x,y = 0. The numerical analysis provides stress component values at finite element centroids. The data plotted below represent averages of results for pairs of adjacent elements and are plotted at the centroid positions. No extrapolation has been performed. Thus results reported at x,y = 0 are actually values obtained at centroid positions slightly removed from these symmetry lines.

Figures (20, 21) show histories of stress distributions at x = 0 in plane stress and plane strain, respectively. Distributions are given at maximum load, stage 1, as well as at stages 2, 3, and 6 of the subsequent necking process. Associated x-y plane boundary profiles and elastic-plastic boundary locations are also provided for convenient reference. The plane stress and plane strain results are similar in form and variation during the necking process.

Figure 20 Axial Stress Distribution:
Plane Stress

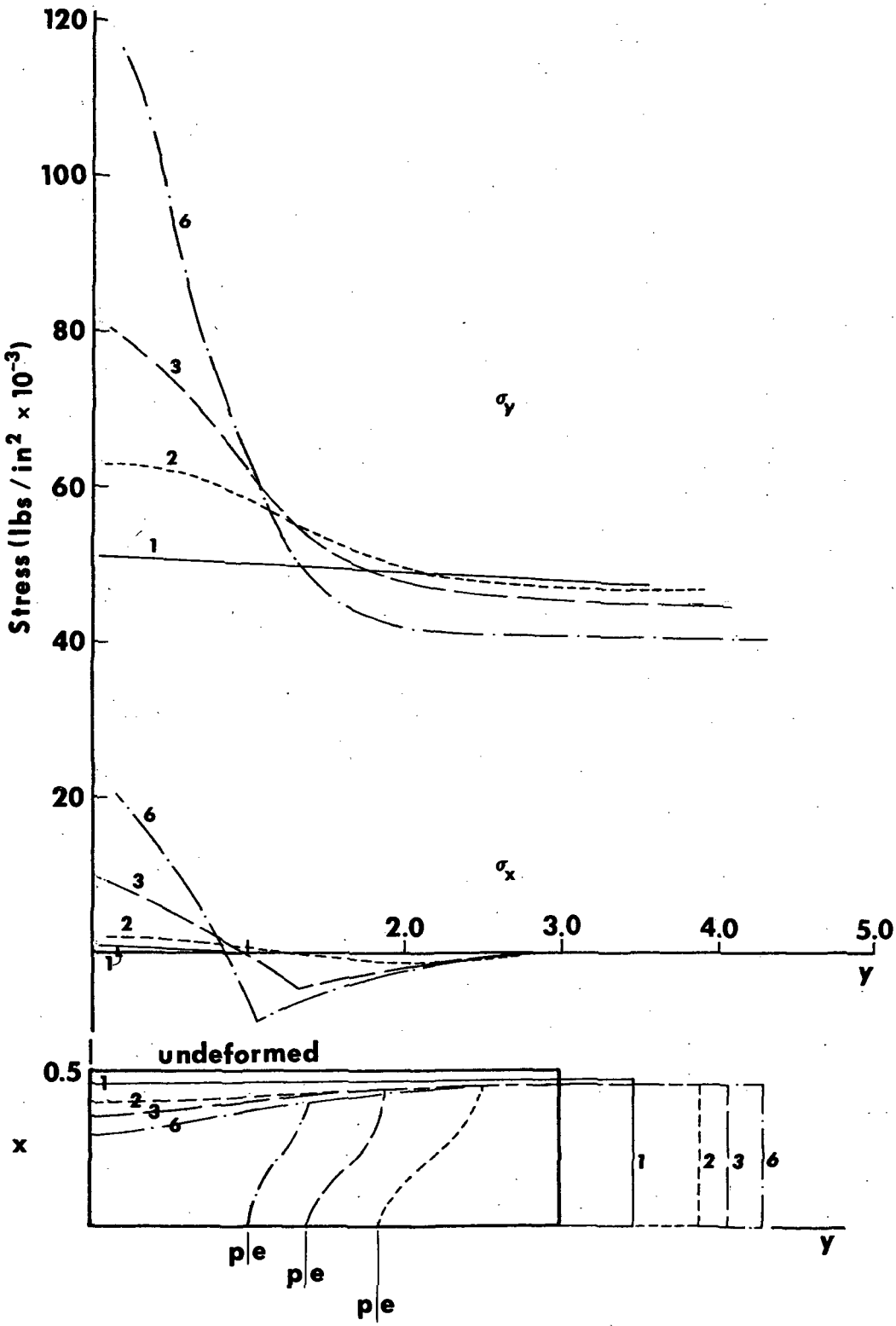

Figure 21 Axial Stress Distribution:
Plane Strain

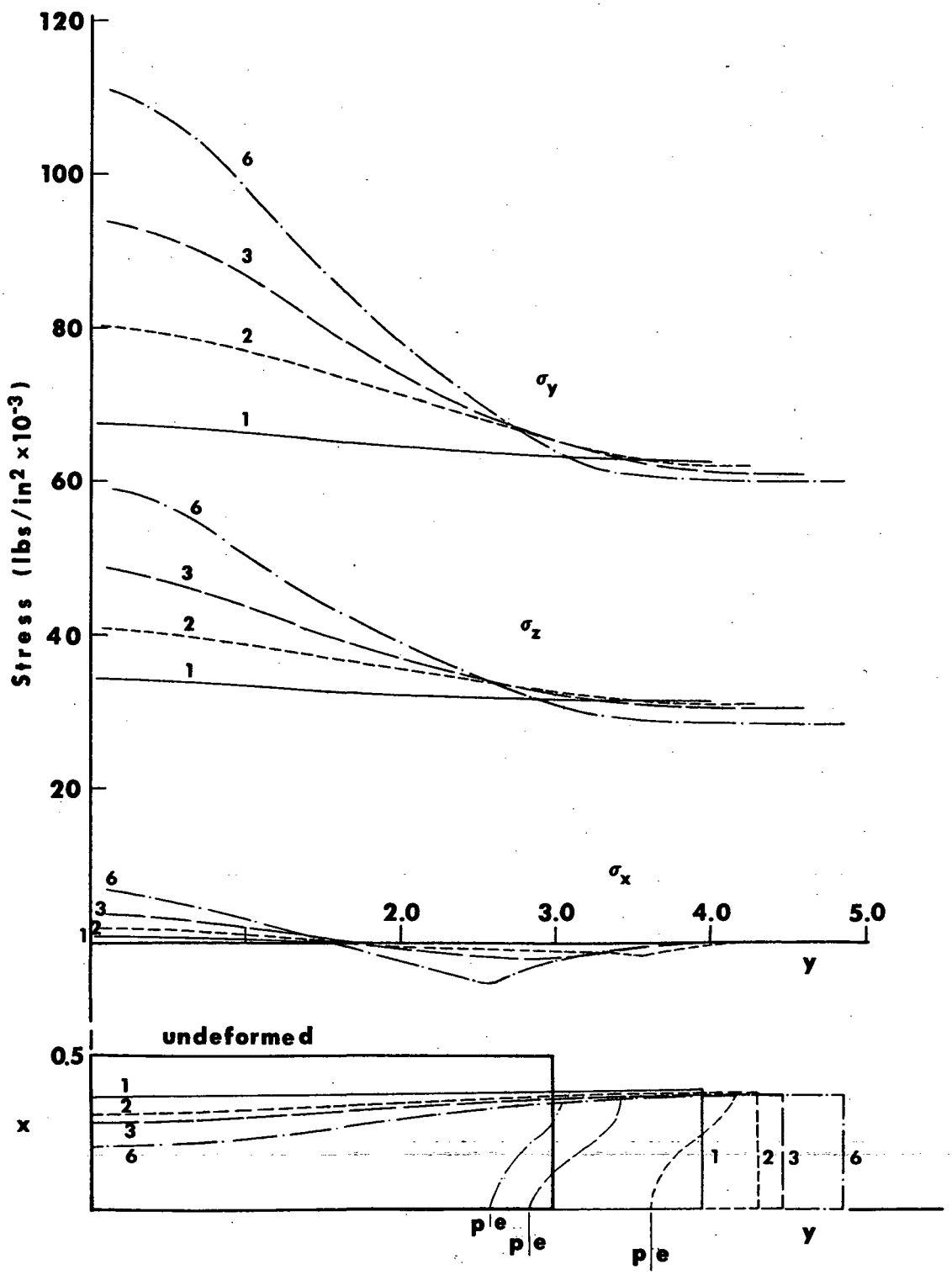

They are distinguished by the previously noted greater localization of the necked region in plane stress and the presence of a non-zero σ_z component in plane strain. A number of observations may be made which are equally applicable to both cases:

1. The effect of the initial imperfection is apparent at maximum load, stage 1. Noticeable although small amplification of its effect upon the axial stress distribution has occurred. Recall that the initial local area reduction at y = 0 was 0.5 percent while at maximum load the loading direction normal stress σ_y varies by 5 percent over the half length of the bar. The transverse stress σ_x is non-zero only in the vicinity of the initial flaw and attains a maximum value of approximately 2 percent of σ_y.
2. At subsequent stages (2, 3, 6) of the necking process explicit correlation may be established between the axial stress distribution and neck geometry. All stress components respond dramatically to neck development. At stage 6 the root plane (y = 0) value of σ_y (and in in plane strain σ_z as well) is nearly twice that found at the opposite end of the bar. This distribution is directly related to the variation in cross-sectional area along the length of the bar. The root plane transverse

stress σ_x, responding to boundary curvature in the necked region, rises to 20 percent and 7 percent of σ_y in plane stress and plane strain, respectively. Furthermore the sign of σ_x in both cases correlates with the sign of the boundary curvature, positive when the boundary is concave and negative when it is convex.

3. The presence of elastic unloading behind (for greater y) the elastic-plastic boundary is clearly evidenced by the cusp in the σ_x distribution occurring at the boundary location. The boundary position is also reflected in the relative magnitudes of the stress components σ_y, σ_z at the various stages in the necking process. For example, in plane stress σ_y at stage 6 exceeds σ_y at stage 3 in the plastic region ($y \lesssim 1.0$) while the converse holds in the elastic region ($y \gtrsim 1.0$). The progress of the elastic-plastic boundary through the bar may be followed by inspection of the axial stress distributions in the manner described above.

The distribution of stress and deformation in the root plane of the neck is of particular interest since material property relations inferred from tensile data reflect average material behavior in this plane. Distributions of stress and loading direction stretch at several stages of necking are given in

Figures (22) for plane stress and (23) for plane strain. The field quantities are plotted as functions of x/x_m where x_m is the minimum width of the necked region.

The distributions at maximum load, stage 1, again reflect the presence of the initial imperfection. In both cases variations in σ_y across the width is small ($\lesssim$ 2 percent) while σ_x is no greater than 1 percent of σ_y at any point. As bar extension proceeds, however, the difference between necking in plane stress and plane strain is quite apparent. In plane stress the variation of stress and stretch across the root plane is significantly greater.

The stress distribution in plane stress is the result of both diminishing thickness toward $x/x_m = 0$, see Figure (19), and the presence of hydrostatic tension derived from the in plane boundary profile through the development of $\sigma_x > 0$ in the root plane. The σ_y variation is approximately 17 percent at stage 6. Note that the variation in stretch is noticeably less, about 10%, since it is the result of thickness variation only, plastic flow being independent of hydrostatic tension.

In plane strain, on the other hand, variation of field quantities across the root plane results only from in plane neck geometry. This circumstance apparently provides sufficient

Figure 22 Root Plane Data: Plane Stress

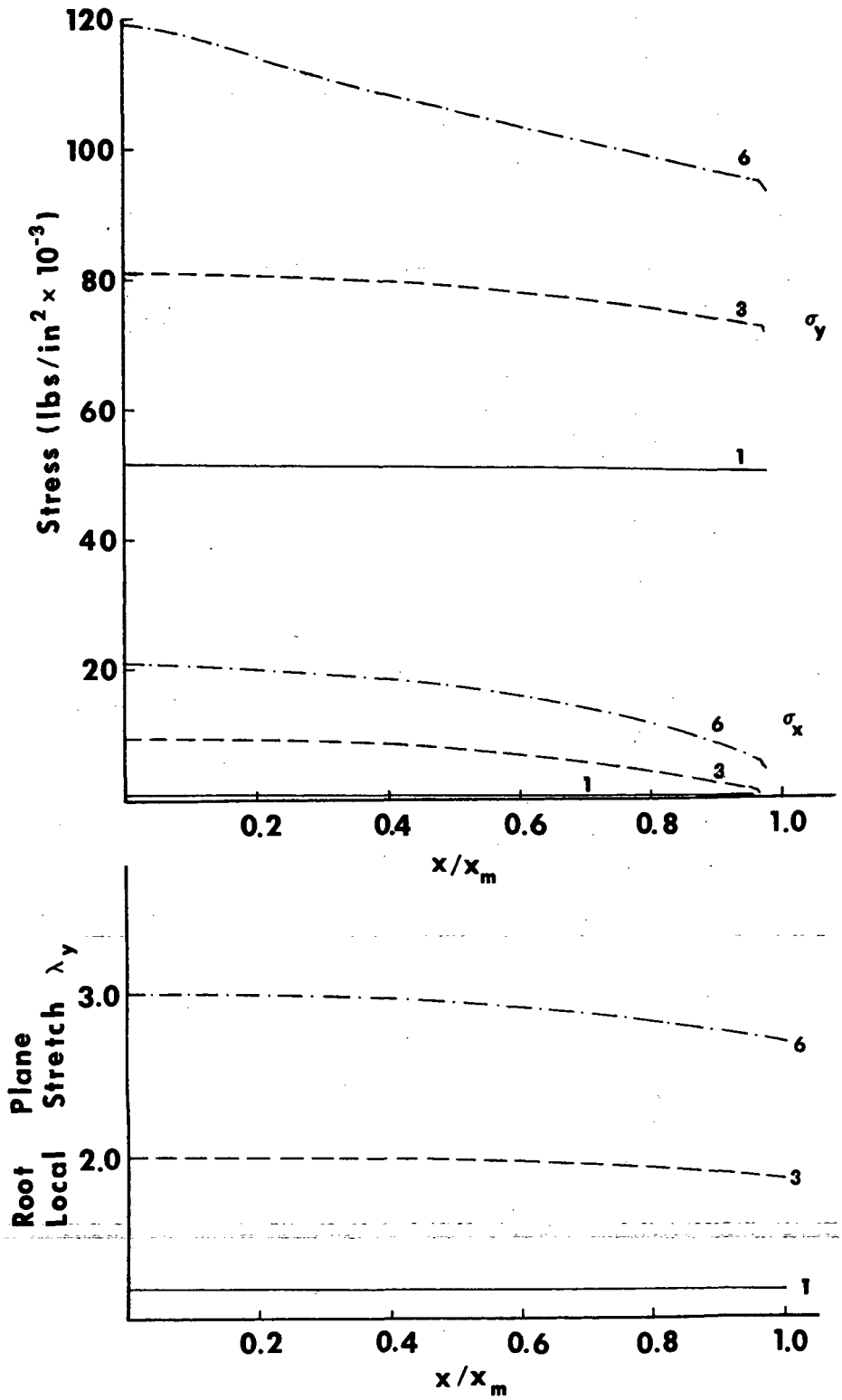

Figure 23 Root Plane Data: Plane Strain

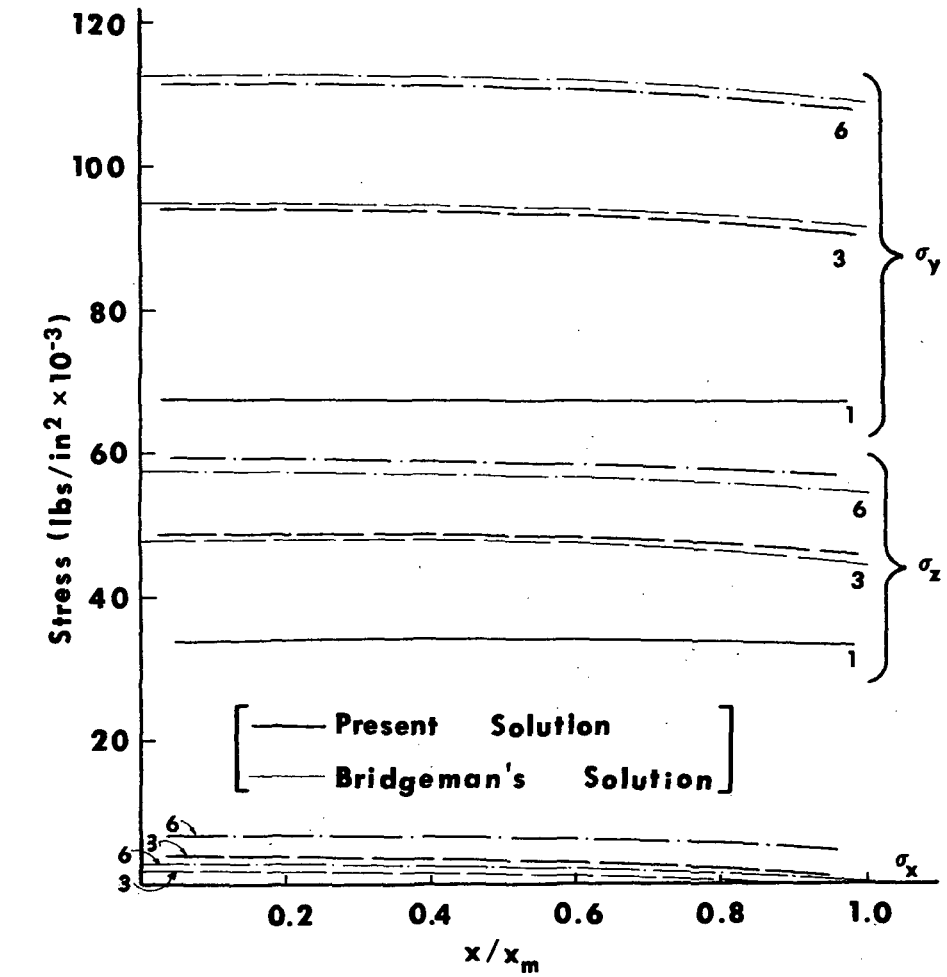

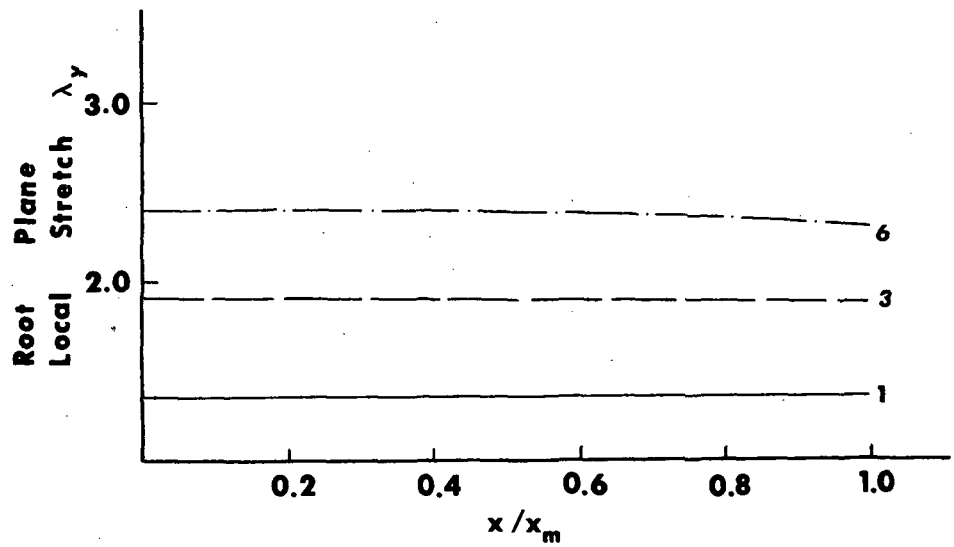

"stiffening" in the plane strain neck that boundary curvature remains much larger than in plane stress despite significant reduction in area at the root plane, 55 percent at stage 6. Variation in stress 5 percent, and stretch, 12 percent, at stage 6 are much smaller than in plane stress.

Figure (23) also provides a comparison of root plane stress distributions in plane strain predicted by equations due to Bridgeman [1] and by the present numerical analysis. Boundary profile data required as input to the Bridgeman analysis are extracted from the numerical results. Bridgeman's equations are seen to overpredict σ_y while underpredicting both σ_z and σ_x. While the absolute differences between the results are not large in the present case the trend of the comparison over the necking history considered suggests that for smaller root plane boundary profile radii the Bridgeman analysis may significantly underpredict hydrostatic tension.* The present results do not indicate under what circumstances such profiles might develop.

*Needleman [30] draws a similar conclusion for the axisymmetric case.

VI. INFERENCE OF STRESS-STRAIN RELATIONS

The numerical data of Section V provide a basis for inference of stress-strain relations utilizing procedures similar to those employed for reduction of tensile data obtained experimentally. This exercise provides a basis for assessment of the validity of these relations since the actual stress-strain curve (111) for the material tested (analyzed) is known. Comparison of inferred and actual stress-strain behavior is undertaken over the full range of deformation from initial yield through development of a significant neck, stage 6 of the plane stress and plane strain necking processes of Section V.

The comparison is performed in terms of effective stress and effective plastic strain. Procedures employed for the inference of these quantities from tensile data of Section V are described below.

Plane Stress: In plane stress the effective stress is found as

$$\sigma_{ef} = \bar{\sigma}_y = P_y/A_y \tag{116}$$

where P_y is the axial load and A_y the corresponding minimum cross-sectional area of the tensile bar. The overscript bar in (116) denotes a cross-section average value.

Prior to initiation of necking the average plastic strain in the bar may found in terms of overall bar extension as described in Appendix I. Thereafter, however, the overall extension is not indicative of minimum section, root plane, plastic strain. Alternatively, therefore, average minimum section plastic strain is computed directly from the minimum section area. The effective plastic strain $\bar{\varepsilon}_{ef}^{(p)}$ is given by

$$\bar{\varepsilon}_{ef}^{(p)} = \ell n \bar{\lambda}_y^{(p)} = \ell n (A_o / A_y^{(p)}) \tag{117}$$

in which incompressibility of plastic deformation has been noted. In (117) A_o is the undeformed area and $A_y^{(p)}$ is the deformed area corrected for elastic deformation. The corrected area $A_y^{(p)}$ is that which would exist should the applied load be removed and elastic recovery occur. In plane stress

$$A_y^{(p)} \simeq A_y [1 + \nu \bar{\sigma}_y / E]^2 \tag{118}$$

where A_y is the deformed area under load.

It is apparent that for metals ($\bar{\sigma}_y / E << 1$) the elastic area correction (118) will be small and of diminishing significance as plastic deformation increases. The data in hand confirm that for plastic strains in excess of several percent the elastic correction (118) is negligible thus permitting the use of $A_y^{(p)} \simeq A_y$ in (117).

Plane Strain: Procedures similar to those described above are employed in plane strain. They are, however, complicated by the impossibility of inferring the plane strain (z) direction component of plastic strain from experimental data. Recall that in-plane strain

$$d_z = d_z^{(e)} + d_z^{(p)} \equiv 0 \tag{119}$$

where the elastic and plastic deformation rate components are not individually zero. To facilitate data reduction, however, we assume $\bar{\varepsilon}_z^{(p)} = \int d_z^{(p)} dt$ to be zero. The results below demonstrate this approximation to be of increasing accuracy as in-plane plastic deformation becomes large. The average effective plastic strain is thereby found as

$$\bar{\varepsilon}_{ef}^{(p)} = 1.157\ \ell n \bar{\lambda}_y^{(p)} = 1.157\ \ell n(A_o/A_y^{(p)}) \tag{120}$$

The elastically corrected area $A_y^{(p)}$ is found from

$$A_y^{(p)} = A_y\ [1 + (\nu(1+\nu)/E)\ \bar{\sigma}_y] \tag{121}$$

which reflects the influence of the plane strain condition upon elastic recovery. As for plane stress the assumption $A_y^{(p)} \simeq A_y$ is demonstrated to be a reasonable approximation for large plastic strains.

Computation of the effective stress is similarly impeded by lack of precise knowledge of σ_z. The ratio σ_z/σ_y is given by Poisson's ratio ν at the yield point and tends toward 0.5 for large plastic strains. Its variation with increasing deformation, however, cannot be ascertained experimentally. In lieu of such information we consider both limiting cases and find

$$\begin{aligned} \bar{\sigma}_{ef}|_{\nu} &= 0.890\ \bar{\sigma}_y \quad \text{for } \sigma_z/\sigma_y = \nu = 0.3 \\ \bar{\sigma}_{ef}|_{0.5} &= 0.866\ \bar{\sigma}_y \quad \text{for } \sigma_z/\sigma_y = 0.5 \end{aligned} \tag{122}$$

The present numerical results are within these bounds prior to necking initiation.

Effective stress-plastic strain data inferred from the plane stress and plane strain results of Section V are given in Figure (24). The actual stress-strain relation (111) employed in the numerical analysis is also shown.

Comparison of the inferred data points and the actual property curve for small plastic strains (<0.01) indicates, not unexpectedly, that noticeably more accurate prediction results when the data are corrected for elastic deformation. The corrected data for plane stress are quite accurate. Stress-strain data inferred from the plane strain results, however, are significantly in error

Figure 24 Inferred Stress-Strain Data

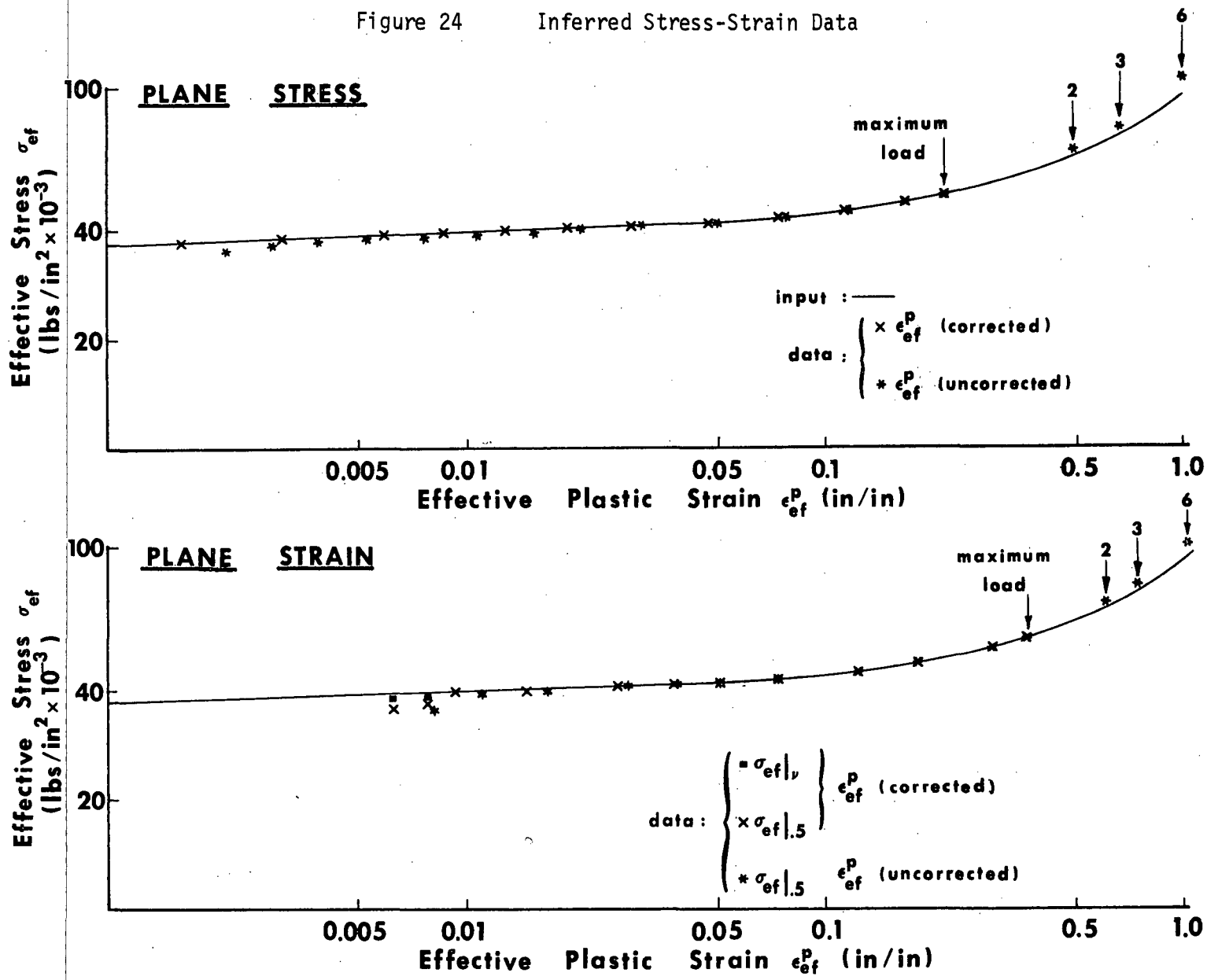

for effective plastic strains less than one percent. The error results from the assumption of zero plastic strain in the plane strain direction. This observation indicates that the inference of stress-strain data utilizing results of tensile testing of flat bars is not appropriate unless specimen dimensions ensure deformation under conditions closely approximating plane stress.

For effective plastic strains exceeding two percent the results shown in Figure (24) clearly suggest that flat bar tensile data provide an adequate basis for inference of stress-strain data. The transition from the power law portion to the linear portion of the actual stress-strain curve, occurring for $\varepsilon_{ef}^{(p)} = 0.05$, is accurately detected in both plane stress and plane strain. Furthermore it is evident that for plastic strains in excess of several percent the data need not be corrected for elastic deformation. The results also suggest that in the absence of necking the data reduction procedures employed are adequate for the inference of stress-strain data so long as the deformation is predominantly plastic.

The effect of necking is evident in Figure (24). For effective plastic strains exceeding those corresponding to maximum load the effective stress is increasingly over-predicted in both plane stress and plane strain. At stage 6 of the necking

processes the error is approximately 10 percent in both cases, being slightly larger in plane stress. It is also clear, however, that the maximum load point does not provide a strict upper bound upon the utility of inferred stress-strain relations. This observation is consistent with the previously noted fact that necking does not initiate until somewhat after maximum load is attained. The data of Figure (24) indicate that reasonable prediction of material behavior may be obtained for effective plastic strains up to 50 percent higher than those existing at maximum load.

The foregoing observations are, of course, strictly pertinent to testing of materials whose behavior may be characterized by stress-strain curves of the modified linear form (111). In particular it should be noted that in the above analyses the effective plastic modulus ($d\sigma_{ef}/d_{ef}^{(p)}$) is constant throughout the necking process. Consideration of a variable modulus would quantitatively affect the quality of stress-strain relations inferred from post-instability data.

In order to demonstrate the effect of a variable modulus the preceding plane stress and plane strain analyses have been repeated for the power law stress-strain curve of Figure (25). This curve is identical to the previously considered modified

Figure 25 Linear and Power Law Hardening

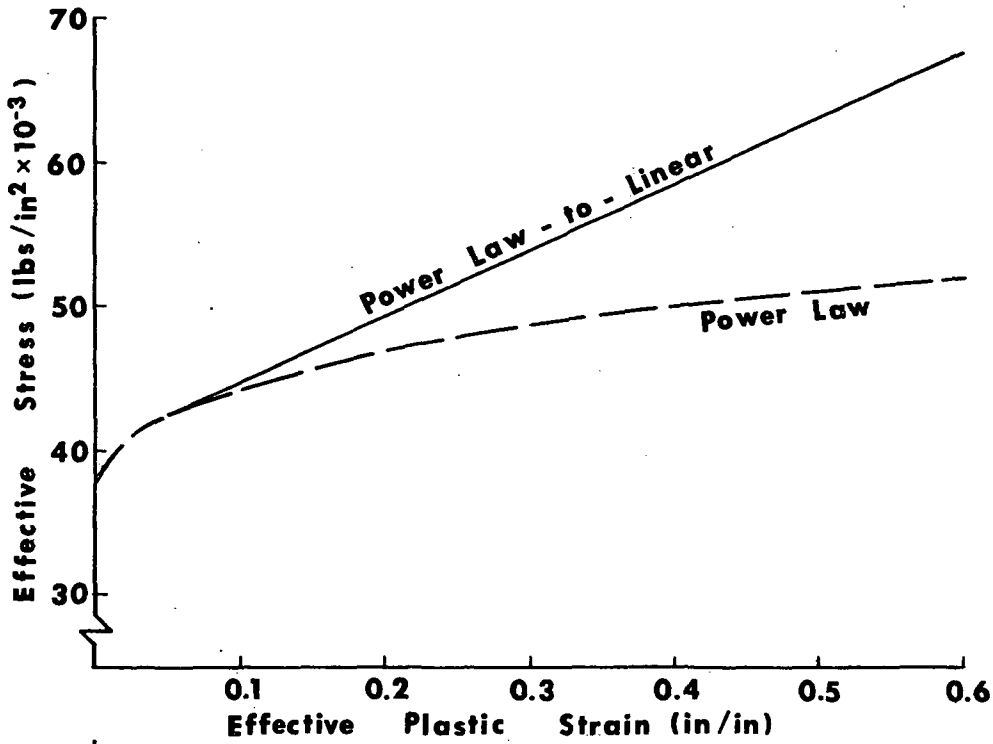

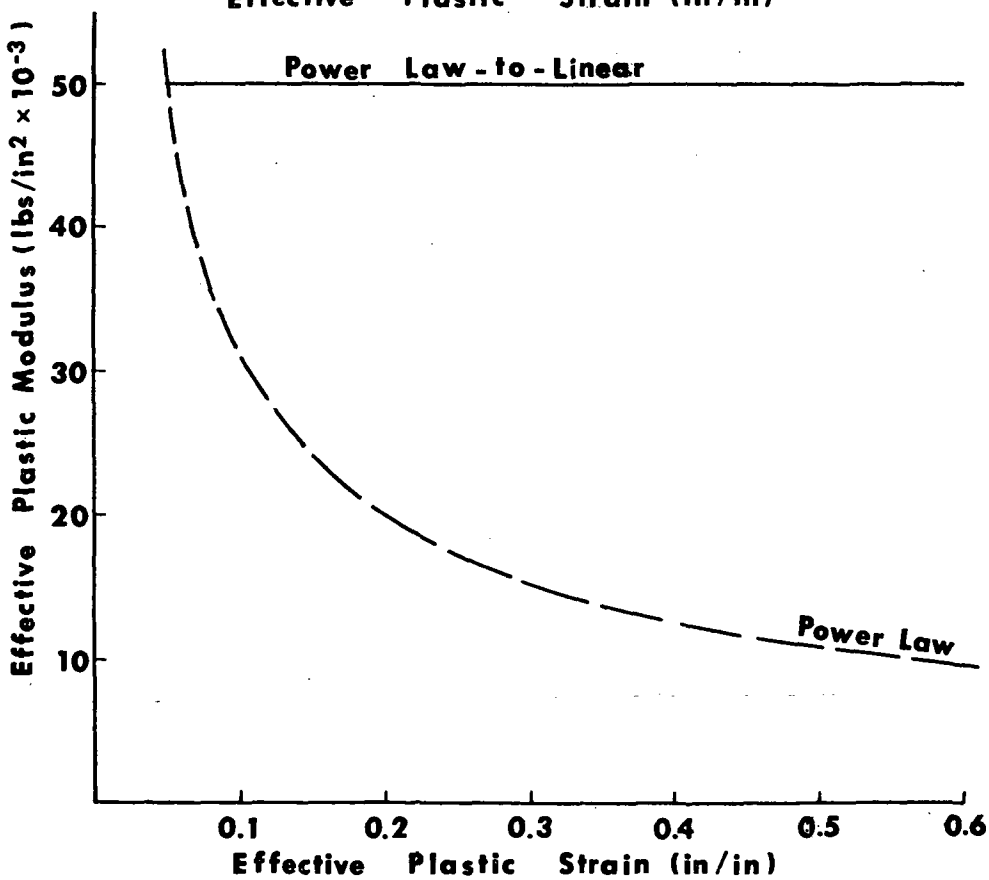

linear relation for $0 \leq \varepsilon_{ef}^{(p)} < 0.05$. For $\varepsilon_{ef}^{(p)} \geq 0.05$ the plastic modulus associated with the power law curve diminishes rapidly. Figure (25) provides a comparison of the two stress-strain curves as well as their associated plastic moduli.

Effective stress-strain data inferred from the post-instability results of plane stress and plane strain analyses are compared with the power law input relation in Figure (26). Two significant effects of the variable and diminishing modulus are immediately apparent. Maximum load is attained at an effective plastic strain much lower than that found in the case of a constant plastic modulus. Furthermore, the error in stress-strain curve prediction subsequent to attainment of maximum load develops more rapidly for the power law material than is observed in Figure (24) for a linear hardening material.

The observed effects of a variable plastic modulus are qualitatively consistent with the nature of the equations governing the finite deformation process. Inspection of the velocity equilibrium equations (67) reveals that the nature of the deformation process is controlled by the relative magnitude of the existing stresses and the material stiffness. In the present case of a continuously diminishing modulus the governing equations are dominated by the effect of existing stress for smaller total deformation than would be the case for a constant modulus. Thus

Figure 26 Inferred Stress Strain Data:
Power Law Input

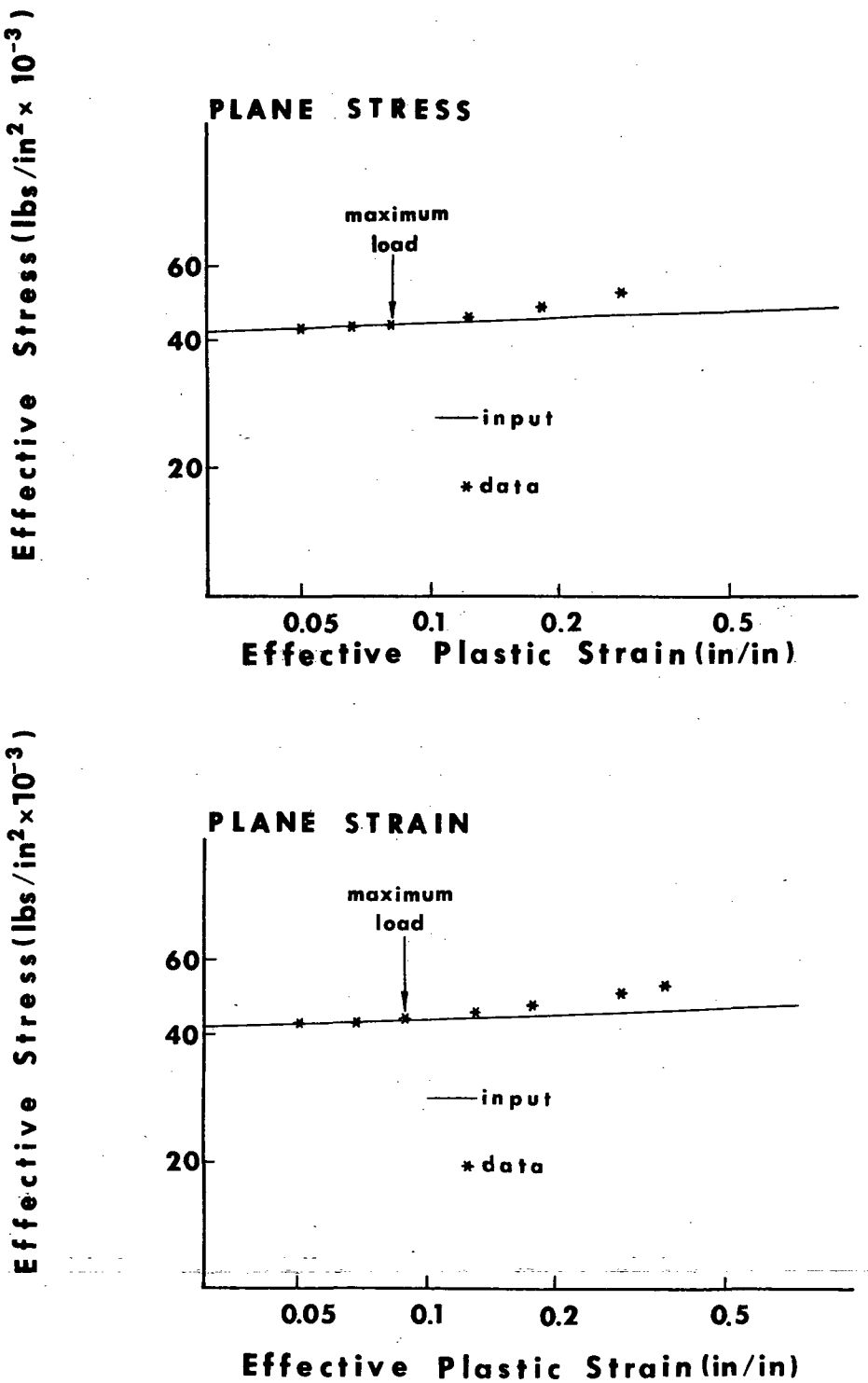

maximum load is attained for smaller uniform bar extension as observed in the numerical results and predicted by the Considere criterion (113). Subsequent to necking initiation the plastic modulus of material in the necking region diminishes with increasing overall bar extension. Thus a more localized neck, and consequently higher root plane hydrostatic tension, will develop accounting for a larger error in inferred effective stress for the power law material.

The preceding results suggest that stress-strain relations inferred from flat bar tensile data are highly accurate only for a bounded, material dependent range of plastic strain. This range excludes both the vicinity of initial yield, wherein non-proportional loading renders the inferred effective quantities indeterminate, as well as the large strains associated with tensile necking.

Of equal significance, however, is the demonstration of the utility of finite deformation analysis capability in assessing the validity of stress-strain relations developed from test data. The present solution capability admits consideration not only of functional relations such as those considered above but also of numerical relations provided directly by experimental data.

The analysis might profitably be employed for evaluation of more sophisticated property inference procedures as well as for the prediction of experimental load-deformation data on the basis of inferred stress-strain relations. The latter approach provides a direct means of assessing the validity of stress-strain relations subsequently to be employed in design analysis.

VII. CONCLUDING REMARKS

A theoretical basis has been established for analysis of finite deformation of metals. The observation that finite deformation of such elasto-plastic materials may be viewed as a process rather than an event has led to the derivation of a complete initial- and boundary-value problem distinguished by its quasi-linear nature. This feature of the formulation motivates the adoption of an incremental approach to numerical problem solving.

Efficient numerical solution capability has been developed for problems of two dimensional deformation under conditions of either plane stress or plane strain. The validity of the numerical analysis has been evaluated by considering a variety of elastic and elasto-plastic finite deformation problems whose homogeneous nature renders analytic solution possible. It is demonstrated that accurate solutions may be obtained for problems involving extremely large displacements and rotations.

The numerical analysis has been employed for the investigation of necking in flat metal tensile bars. The results of this investigation provide not only the first full numerical solutions for tensile necking of metals in plane stress and plane strain

but also an appraisal of the validity of stress-strain relations inferred from tensile test data. It is demonstrated that such relations inferred from the behavior of flat tensile bars are erroneous for both very small and very large (post-instability) plastic strains. The post-instability error is shown to be significantly dependent upon material behavior and in particular upon variation of the plastic modulus.

It is evident from the results obtained that present knowledge of the mechanics of tensile testing is insufficient to enable precise characterization of material behavior from tensile data over the full range of a test. The theory and numerical analysis which have been developed provide the means for necessary further study of tensile testing mechanics and procedures. Such investigations might consider, for example, the effects of material properties and tensile bar geometry upon the necking process. The possibility exists of developing procedures for correcting tensile test data to account for root plane hydrostatic tension and thereby to provide a basis for inference of accurate stress-strain relations from post-instability test results. The existence of such a material independent correction procedure is suggested by the experimental work of Bridgeman [1].

The availability of analysis capability for finite elasto-plastic

deformation also provides the basis for evaluation of alternative material property tests. Two obvious candidates present themselves, compression testing and indentation testing. Both of these are attractive since neither involves an instability phenomenon. Since full solutions for stress and deformation may be obtained the inhomogeneous character of the indentation or hardness test would not necessarily obstruct inference of effective stress-strain data. The utility of these alternative procedures might be assessed not only by analysis of the individual tests but also by comparison of stress-strain data inferred from the results of analysis of several test methods.

The present analysis of necking in flat tensile bars, as well as the possible avenues of research identified above, suggest the primary significance of the finite deformation solution capability which has been developed. Precise characterization of inelastic material behavior can be extracted from the results of mechanical testing only if the mechanics of each test employed is understood and, in particular, only if quantitative distinction can be made between the effects of material and geometric nonlinearity. The availability of an analysis incorporating treatment of both forms of nonlinearity provides the means of distinguishing their effects.

REFERENCES

1. Bridgeman, P. W., *Studies in Large Plastic Flow and Fracture*, McGraw-Hill, New York, 1952.
2. Nadai, A., *Theory of Flow and Fracture of Solids*, McGraw-Hill, New York, 1950.
3. Oden, J. T., *Finite Elements of Nonlinear Continua*, McGraw-Hill, New York, 1972.
4. Marcal, P. V., "Finite Element Analysis of Combined Problems of Nonlinear Material and Geometric Behavior", Presented at joint ASME Computer Conference *Computational Approaches in Applied Mechanics*, Chicago, June 1969.
5. Stricklin, J. A., W. E. Haisler and W. A. Von Riesemann, "Formulation, Computation, and Solution Procedures for Material and/or Geometric Nonlinear Structural Analysis by the Finite Element Method", Sandia Corporation, Albuquerque, New Mexico, Report SC-CR-72-3102, July 1972.
6. Cowper, G. R. and E. T. Onat, "The Initiation of Necking and Buckling in Plane Plastic Flow", *Proceedings* Fourth U. S. National Congress of Applied Mechanics, 1962.
7. Swedlow, J. L., "Character of the Equations of Elasto-Plastic Flow in Three Independent Variables", *Int. J. Non-Linear Mechanics*, Vol. 3, pp. 325-336, 1968.

8. Eringen, A. C., *Nonlinear Theory of Continuous Media*, McGraw-Hill, New York, 1962.

9. Truesdell, C. A. and R. A. Toupin, "The Classical Field Theories", in *Handbuch der Physik*, Vol. 3, S. Flugge (ed.), Springer Verlag, Berlin, 1954.

10. Jaumann, G., "Grundlagen der Bewegungslehre", Leipzig, 1905.

11. Truesdell, C. A., "The Simplest Rate Theory of Pure Elasticity", *Comm. Pure Appl. Math.*, Vol. 8, pp. 123-132, 1955.

12. Oldroyd, J. G., "On the Formulation of Rheological Equations of State", *Proc. Roy. Soc. (London)*, Vol. (A)200, pp. 523-541, 1950.

13. Prager, W., *Introduction to Mechanics of Continua*, Ginn and Co., Boston, 1961.

14. Fung, Y. C., *Foundations of Solid Mechanics*, Prentice-Hall, Englewood Cliffs (New Jersey), 1965.

15. Green, A. E. and P. M. Naghdi, "A General Theory of an Elastic-Plastic Continuum", *Arch. Rat. Mech. Anal.*, Vol. 18, No. 4, pp. 251-281, 1965.

16. Drucker, D. C., "A More Fundamental Approach to Plastic Stress-Strain Relations", *Proceedings* First U. S. National Congress of Applied Mechanics, 1951.

17. Naghdi, P. M., "Stress-Strain Relations in Plasticity and Thermoplasticity", in *Plasticity*, Proceedings of the Second Symposium on Naval Structural Mechanics (eds: E. H. Lee and P. S. Symonds), Pergamon Press, New York, 1960.

18. Hill, R., *The Mathematical Theory of Plasticity*, Oxford Univ. Press, London, 1950.

19. Rice, J. R., "A Note on the 'Small Strain' Formulation for Elastic-Plastic Problems", Brown Univ., Div. of Eng., Providence (R. I.), April 1970.

20. Kantorovich, L. V. and V. I. Krylov, *Approximate Methods of Higher Analysis*, C. D. Benster (trans.), Interscience, New York, 1964.

21. Zienkiewicz, O. C. and Y. K. Cheung, *The Finite Element Method in Structural and Continuum Mechanics*, McGraw-Hill, London, 1967.

22. Reissner, E., "On a Variational Theorem in Elasticity", *J. Math. and Phys.*, Vol. 29, pp. 90-95, 1950.

23. Rektorys, K., *Survey of Applicable Mathematics*, M. I. T. Press, Cambridge, 1969.

24. Considere, M., *Annals du Ponts et Chaussees*, Series 6, Vol. 9, 1885.

25. *1972 Annual Book of ASTM Standards*, Standard E-8, American Society for Testing and Materials, Philadelphia, 1972.

26. Davidenkov, N. N. and N. I. Spiridonova, "Analysis of the State of Stress in the Neck of a Tension Test Specimen", *Proc. ASTM*, Vol. 40, pp. 1147-1158, 1940.

27. Richmond, O., "Plane Strain Necking of V-Notched and Unnotched Tensile Bars", *J. Mech. Phys. Solids*, Vol. 17, pp. 83-90, 1969.

28. Onat, E. T. and W. Prager, "The Necking of a Tension Specimen in Plane Plastic Flow", *J. Appl. Phys.*, Vol. 25, No. 4, pp. 491-493, 1954.

29. Chen, W., "Necking in a Bar", Harvard Univ., Div. of Eng. and Appl. Phys., Report ARPA-40, March 1970.

30. Needleman, A., "A Numerical Study of Necking in Circular Cylindrical Bars", *J. Mech. Phys. Solids*, Vol. 20, pp. 111-127, 1972.

31. Merchant, R., personal communication, 1971.

32. MacGregor, C. W., "The Tensile Test", *Proc. ASTM*, Vol. 40, pp. 508-534, 1940.

33. Swedlow, J. L., "A Procedure for Solving Problems of Elasto-Plastic Flow", SM-73, Dep. Mech. Eng., Carnegie-Mellon Univ., Sept. 1971.

APPENDIX I

Operational Form of the Elasto-Plastic Constitutive Equations

In order to utilize the elasto-plastic flow equations (50) and the inverse equations (53) we must choose a specific form for the yield function $\phi = \tau_{eq}$ of (39) and operationally define the equivalent plastic modulus $\mu_{eq}^{(p)}$ of (46). Means must be provided for the evaluation of $\mu_{eq}^{(p)}$ from test data for particular materials.

In the present analysis ϕ is taken as the octahedral shear stress τ_o

$$\phi = \tau_{eq} = \tau_o \equiv [(2/3)\, J_2]^{1/2} \tag{I-1}$$

where J_2 is the second invariant of the deviatoric stresses s_{ij}

$$J_2 = (1/2)\, s^{ij}\, s_{ij} \tag{I-2}$$

An equivalent plastic strain rate $d_{eq}^{(p)}$ is defined (43) by requiring the rate of plastic work $\dot{W}^{(p)}$ to be given as

$$\dot{W}^{(p)} = \tau_o\, d_{eq}^{(p)} \tag{I-3}$$

from which we find

$$d_{eq}^{(p)} = 3 d_o^{(p)} \tag{I-4}$$

In (I-4) $d_o^{(p)}$ is the rate of octahedral plastic shear strain

$$d_o^{(p)} = [(1/3)\, d_{ij}^{(p)}\, d^{ij(p)}]^{1/2} \tag{I-5}$$

Integration of (I-4) with respect to time defines the equivalent plastic strain $\varepsilon_{eq}^{(p)}$ in terms of the octahedral plastic strain $\gamma_o^{(p)}$.

$$\gamma_o \equiv \int d_o^{(p)}\, dt$$
$$\varepsilon_{eq}^{(p)} \equiv \int d_{eq}^{(p)}\, dt = 3\int d_o^{(p)}\, dt = 3\gamma_o^{(p)} \tag{I-6}$$

The equivalent plastic modulus $\mu_{eq}^{(p)}$ may now be expressed in terms of an octahedral plastic shear modulus $\mu_o^{(p)}$.

$$\mu_{eq}^{(p)} \equiv (1/2)\, d\tau_{eq}/d\varepsilon_{eq}^{(p)} = (1/3)\, \mu_o^{(p)} \tag{I-7}$$

$$\mu_o^{(p)} \equiv (1/2)\, d\tau_o/d\gamma_o^{(p)} \tag{I-8}$$

The octahedral plastic shear modulus may be evaluated for particular materials utilizing data obtained by quasi-static testing under simple loading conditions. In the case of uniaxial tension* we have a single non-zero stress component $\sigma_x(t) > 0$ and from (I-1) we find the octahedral shear stress

$$\tau_o = (\sqrt{2}/3)\, \sigma_x \tag{I-9}$$

*The discussion is restricted to tensile data obtained prior to initiation of necking.

Note that σ_x is defined as applied load divided by actual specimen cross-sectional area as discussed in detail by MacGregor [32]. As σ_x increases with time the tensile specimen deforms in simple extension. For an isotropic material this homogeneous elasto-plastic flow process is described by the cartesian deformation rate components

$$\begin{aligned} d_x &= d_x^{(p)} + d_x^{(e)} > 0 \\ d_y &= d_y^{(p)} + d_y^{(e)} < 0 \\ d_z &= d_z^{(p)} + d_z^{(e)} < 0 \\ d_y &= d_z \end{aligned} \tag{I-10}$$

Noting the incompressibility of plastic flow we find

$$d_y^{(p)} = d_z^{(p)} = -(1/2)\, d_x^{(p)} \tag{I-11}$$

The plastic strain rate in the loading direction is given by

$$d_x^{(p)} = (\dot{\ell}/\ell) - \dot{\sigma}_x/E \tag{I-12}$$

where ℓ is the instantaneous x dimension of the tensile specimen gage length and E is the elastic Young's modulus. Substituting (I-12) into (I-5) and integrating with respect to time the octahedral

plastic strain is found as

$$\gamma_o^{(p)} = (1/\sqrt{2}) \left[\ell n \lambda_x - \sigma_x/E\right] \tag{I-13}$$

where $\lambda_x = \ell/\ell_o$ and ℓ_o is the original (undeformed) gage length.*

The octahedral property relation $\tau_o(\gamma_o^{(p)})$ provided by (I-9) and (I-13) may be approximated by a monotonic function or retained in the numerical form provided by the experimental data. The FIPDEF program utilizes the octahedral data directly and employs a finite difference technique to re-evaluate $\mu_o^{(p)}$ in each finite element at the beginning of each time step. The value of τ_o for which $\gamma_o^{(p)}$ tends to zero defines the initial proportional limit for the material. Elastic analysis is performed until the octahedral stress exceeds this value.

It is occasionally convenient to utilize material property variables which reduce to the principal uniaxial quantities in the case of simple extension under uniaxial loading. For this purpose we define

$$\begin{aligned} \sigma_{ef} &\equiv [3\, J_2]^{1/2} \\ d_{ef}^{(p)} &= [(2/3)\, d_{ij}^{(p)}\, d^{ij(p)}]^{1/2} \\ \varepsilon_{ef}^{(p)} &= \int d_{ef}^{(p)}\, dt \end{aligned} \tag{I-14}$$

*Under the assumption of infinitesimal elastic strains (<<1) the undeformed length defines an appropriate reference state for the entire plastic deformation process.

In the case of uniaxial tension these reduce to

$$\sigma_{ef} = \sigma_x$$
$$d_{ef}^{(p)} = d_x^{(p)} \tag{I-15}$$

These effective quantities (I-13) are related to the octahedral variables as

$$\tau_o = (\sqrt{2}/3)\ \sigma_{ef}$$
$$d_o^{(p)} = (1/\sqrt{2})\ d_{ef}^{(p)} \tag{I-16}$$
$$\mu_o^{(p)} = (1/3)\ \ d\sigma_{ef}/d\varepsilon_{ef}^{(p)}$$

The elasto-plastic flow equations (50) and inverse equations (53) may be written in terms of the octahedral quantities as

$$2\mu d^i{}_j = \hat{\sigma}^i{}_j - (\nu/1+\nu)\ \hat{\sigma}^k{}_k\ \delta i_j + (\mu/\mu_o^{(p)})(3\tau_o{}^2)^{-1} s^i{}_j\ s^{kl}\hat{\sigma}_{kl} \tag{I-17}$$

$$\hat{\sigma}^i{}_j = \lambda d^k{}_k\ \delta^i{}_j + 2\mu d^i{}_j - 2\mu[3\tau_o{}^2(1+\mu_o^{(p)}/\mu)]^{-1}\ s^i{}_j\ s^{kl}\ d_{kl} \tag{I-18}$$

where λ,μ are the Lame constants of linear elasticity.

APPENDIX II

Elasto-Plastic Constitutive Equations for Plane Stress and Plane Strain

The general elasto-plastic constitutive equations of Section I.2 are specialized in Appendix I for analysis of materials in which plastic yielding is controlled by the octahedral stress. These equations (I-17, 18) are expanded below for analysis of elasto-plastic flow under conditions of either plane stress or plane strain.

It is convenient to develop the equations in matrix form. For this purpose we define matrix vectors consisting of the in plane cartesian components of the Jaumann stress rate $\hat{\sigma}_{ij}$ and deformation rate d_{ij}.

$$\hat{\sigma}^{\zeta} \equiv \begin{bmatrix} \hat{\sigma}_x \\ \hat{\sigma}_y \\ \hat{\sigma}_{xy} \end{bmatrix} \tag{II-1}$$

$$D^{\zeta} \equiv \begin{bmatrix} d_x \\ d_y \\ 2d_{xy} \end{bmatrix} \tag{II-2}$$

For either plane stress or plane strain the elasto-plastic flow equations may be written

$$D^{\zeta} = B^{\zeta\xi}\,\hat{\sigma}^{\xi} \quad ; \quad \zeta, \xi = 1, 2, 3 \tag{II-3}$$

and the inverse equations as

$$\hat{\sigma}^{\xi} = P^{\xi\zeta}\,D^{\zeta} \quad ; \quad \zeta, \xi = 1, 2, 3 \tag{II-4}$$

The constitutive matrices $B^{\zeta\xi}$ and $P^{\zeta\xi}$ are full and symmetric. Specific forms of these matrices are developed below. The notation employed is similar to that utilized by Swedlow [33].

Plane Stress: It is assumed that

$$\sigma_z = \sigma_{xz} = \sigma_{yz} = 0 \tag{II-5}$$

Under these conditions the constitutive matrices are found as

$$B^{\zeta\xi} = (1/E) \begin{bmatrix} 1 + s_x^2/s_o^2 & -\nu + s_x s_y/s_o^2 & 2s_x\,\sigma_{xy}/s_o^2 \\ & 1 + s_y^2/s_o^2 & 2s_y\,\sigma_{xy}/s_o^2 \\ \text{(sym)} & & 2(1+\nu+2\sigma_{xy}^2/s_o^2) \end{bmatrix} \tag{II-6}$$

$$P^{\zeta\xi} = E/(1-\nu^2)$$

$$\begin{bmatrix} 1-P(s_x+\nu s_y)^2/s_o^2 & \nu-P(s_x+\nu s_y)(s_y+\nu s_x)/s_o^2 & (\nu-1)P(s_x+\nu s_y)\sigma_{xy}/s_o^2 \\ & 1-P(s_y+\nu s_x)^2/s_o^2 & (\nu-1)P(s_y+\nu s_x)\sigma_{xy}/s_o^2 \\ (sym) & & [(1-\nu)/2]-(1-\nu^2)P\sigma_{xy}/s_o^2 \end{bmatrix} \quad \text{(II-7)}$$

where

$$s_o^2 = 6\tau_o^2 \mu_o^{(p)}/E \quad \text{(II-8)}$$

$$1/P = 1-\nu^2+[s_x^2+2\nu s_x s_y+s_y^2 + 2(1-\nu)\sigma_{xy}^2]/s_o^2 \quad \text{(II-9)}$$

In plane stress the octahedral stress is found from (I-1) and $\mu_o^{(p)}$ is the octahedral plastic shear modulus (I-8).

$$\tau_o^2 = (2/9)\ (\sigma_x^2 - \sigma_x\sigma_y + \sigma_y^2 + 3\ \tau_{xy}^2) \quad \text{(II-10)}$$

The deviatoric stresses are

$$\begin{aligned} s_x &= (2\sigma_x - \sigma_y)\ /\ 3 \\ s_y &= (2\sigma_y - \sigma_x)\ /\ 3 \\ s_z &= -(\sigma_x + \sigma_y)\ /\ 3 \end{aligned} \quad \text{(II-11)}$$

The constitutive equations (I-17) also provide the auxiliary relation

$$d_z = (1/E)\,[(-\nu+s_z s_x/s_o^2)\hat{\sigma}_x + (-\nu+s_z s_y/s_o^2)\hat{\sigma}_y + 2(s_z\sigma_{xy}/s_o^2\hat{\sigma}_{xy})] \qquad \text{(II-12)}$$

Plane Strain: It is assumed that $\partial/\partial z$ is a null operator and that

$$d_z = d_{xz} = d_{yz} = 0 \qquad \text{(II-13)}$$

Under these conditions the constitutive matrices become

$$B^{\zeta\xi} = \frac{1}{E(1+s_z^2/s_o^2)}$$

$$\begin{bmatrix} 1-\nu^2+(s_x^2+2\nu s_x s_z+s_z^2)s_o^2 & -\nu(1+\nu)+(s_x s_y-2\nu s_z^2)/s_o^2 & 2[(s_x+\nu s_z)\sigma_{xy}/s_o^2 \\ & 1-\nu^2+(s_y^2+2\nu s_y s_z+s_z^2)/s_o^2 & 2[(s_y+\nu s_z)\sigma_{xy}/s_o^2 \\ \text{(sym)} & & 2\{(1+\nu)+2[\sigma_{xy}^2+(1+\nu)s_z^2/s_o^2\} \end{bmatrix} \qquad \text{(II-14)}$$

$$P^{\zeta\xi} = 1/(1+\nu)$$

$$\begin{bmatrix} 3\kappa(1-\nu) - Q\,s_x^2/s_o^2 & 3\kappa\nu - Q\,s_x s_y/s_o^2 & -Q\,s_x\sigma_{xy}/s_o^2 \\ & 3\kappa(1-\nu) - Q\,s_y^2/s_o^2 & -Q\,s_y\sigma_{xy}/\sigma_o^2 \\ & & -Q\sigma_{xy}^2/s_o^2 \end{bmatrix} \qquad \text{(II-15)}$$

where s_o^2 is defined by (II-8) and

$$\begin{aligned} s_x &= (2\sigma_x - \sigma_y - \sigma_z) / 3 \\ s_y &= (2\sigma_y - \sigma_z - \sigma_x) / 3 \\ s_z &= (2\sigma_z - \sigma_x - \sigma_y) / 3 \\ \tau_o^2 &= (2/9)(\sigma_x^2+\sigma_y^2+\sigma_z^2-\sigma_y\sigma_z-\sigma_x\sigma_z-\sigma_x\sigma_y + 3\sigma_{xy}^2) \end{aligned} \tag{II-16}$$

In (II-15)

$$Q = 2\mu/(1 + \mu/\mu_o(p)) \tag{II-17}$$

and κ is the elastic bulk modulus.

$$\kappa = E/ 3(1-2\nu) \tag{II-18}$$

Note that boundedness of κ and thereby $P^{\zeta\xi}$ in (II-15) requires $\nu < 1/2$. Hence plane strain analysis of elastically incompressible materials is not possible. Approximate analysis of such materials may be accomplished by setting $\kappa/E >> 1$.

In addition to (II-14, 15) we have the auxiliary relation

$$\begin{aligned} \hat{\sigma}_z = \dot{\sigma}_z = 1/(1+\nu)\{&[3\kappa\nu - Qs_z s_x/s_o^2]d_x + [3\kappa\nu - Qs_z s_y/s_o^2]d_y \\ &- [2Q\, s_z\sigma_{xy}/s_o^2]d_{xy}\} \end{aligned} \tag{II-19}$$

APPENDIX III

The Rate Stiffness Matrix for Planar Analysis

The rate stiffness equations are specialized below for analysis of planar problems under conditions of either plane stress or plane strain. A triangular finite element is employed with the assumption that the velocity field varies linearly within the element.

The Linear Velocity Element: Consider the triangular finite element of Figure (III-1). The instantaneous configuration of the element is defined by the coordinates of its vertices or nodes. These nodal coordinates are represented in matrix form as X^{α}

$$X^{\alpha} \equiv \begin{bmatrix} X_1 \\ Y_1 \\ X_2 \\ Y_2 \\ X_3 \\ Y_3 \end{bmatrix} \qquad \text{(III-1)}$$

where X_1 (Y_1) is the x (y) coordinate of node 1, etc.

Figure III-1 Linear Velocity Finite Element

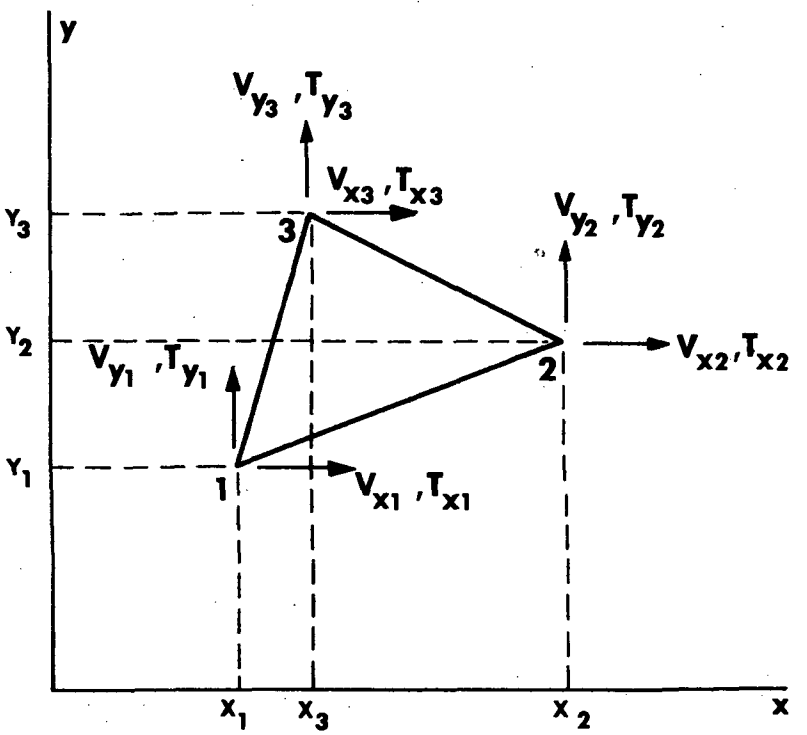

Vectors of nodal velocity components V^{α} and nodal loading rate components T^{α} are similarly defined.

$$V^{\alpha} \equiv \begin{bmatrix} V_{x1} \\ V_{y1} \\ V_{x2} \\ V_{y2} \\ V_{x3} \\ V_{y3} \end{bmatrix} \qquad \text{(III-2)}$$

$$T^{\alpha} \equiv \begin{bmatrix} T_{x1} \\ T_{y1} \\ T_{x2} \\ T_{y2} \\ T_{x3} \\ T_{y3} \end{bmatrix} \qquad \text{(III-3)}$$

The velocity field components within the element are approximated as

$$v_x = A^\alpha \; {}^T\phi_x{}^\alpha \; (x,y)$$

$$v_y = A^\alpha \; {}^T\phi_y{}^\alpha \; (x,y) \qquad \alpha = 1,\ldots,6 \qquad \text{(III-4)}$$

where the vector functions ϕ^α possess the components

α	${}^T\phi_x{}^\alpha$	${}^T\phi_y{}^\alpha$
1	1	0
2	0	1
3	x	0
4	0	x
5	y	0
6	0	y

(III-5)

Hence the velocity field approximation (III-4) is expanded as

$$v_x \; (x,y) = A_1 + A_3 x + A_5 y$$

$$v_y \; (x,y) = A_2 + A_4 x + A_6 y \qquad \text{(III-6)}$$

Evaluation of the velocity field approximation (III-6) at the nodal positions (III-1) must yield the nodal velocities (III-2).

Substituting (III-1) into (III-6) and solving the resulting equations for A^{α} obtains

$$A^{\alpha} = \Gamma^{\alpha\beta} V^{\beta} \qquad \alpha, \beta = 1,\ldots,6 \qquad \text{(III-7)}$$

$$\Gamma^{\alpha\beta} = (1/2A)$$

$$\begin{bmatrix} (X_2Y_3-Y_2X_3) & 0 & (X_3Y_1-Y_3X_1) & 0 & (X_1Y_2-Y_1X_2) & 0 \\ 0 & (X_2Y_3-Y_2X_3) & 0 & (X_3Y_1-Y_3X_1) & 0 & (X_1Y_2-Y_1X_2) \\ (Y_2-Y_3) & 0 & (Y_3-Y_1) & 0 & (Y_1-Y_2) & 0 \\ 0 & (Y_2-Y_3) & 0 & (Y_3-Y_1) & 0 & (Y_1-Y_2) \\ (X_3-X_2) & 0 & (X_1-X_3) & 0 & (X_2-X_1) & 0 \\ 0 & (X_3-X_2) & 0 & (X_1-X_3) & 0 & (X_2-X_1) \end{bmatrix} \qquad \text{(III-8)}$$

and A is the area of the element.

$$A = (1/2)\,[X_2(Y_3-Y_1) + X_1(Y_2-Y_3) + X_3(Y_1-Y_2)] \qquad \text{(III-9)}$$

Substituting (III-7) into (III-4) yields the velocity field representation (III-10) corresponding to the general form (74) of Section III.1.

The element deformation rate and Jaumann stress rate fields in the x-y plane are given by the matrix vectors $\hat{\sigma}^{\zeta}$ and D^{ζ}, respectively ($\zeta = 1,\ldots,3$)

$$\hat{\sigma}^{\zeta} = \begin{bmatrix} \hat{\sigma}_x \\ \hat{\sigma}_y \\ \hat{\sigma}_{xy} \end{bmatrix} \qquad D^{\zeta} = \begin{bmatrix} d_x \\ d_y \\ 2d_{xy} \end{bmatrix} \qquad \text{(III-10)}$$

These in-plane rates are related by the constitutive equations of Appendix II

$$\hat{\sigma}^{\zeta} = P^{\zeta\xi} D^{\xi} \quad ; \quad \alpha, \beta = 1,\ldots,3 \qquad \text{(III-11)}$$

where $P^{\zeta\xi} = P^{\xi\zeta}$ takes a form appropriate for either plane stress (II-7) or plane strain (II-15).

The Planar Rate Stiffness Matrix: The preceding formulation of the rate behavior of the linear velocity element provides the basis for specialization of the element rate stiffness matrix $K^{\alpha\beta}$ of (79) to a form appropriate for two dimensional analysis. The general form of this matrix is given below employing cartesian tensor notation*. The matrix is decomposed into three components to facilitate the ensuing two dimensional specialization.

*The notation of Section III is employed here. The distinction between covariant and contravariant tensor components need not be made in cartesian coordinates.

$$K^{\alpha\beta} = K_1^{\alpha\beta} + K_2^{\alpha\beta} + K_3^{\alpha\beta} \qquad \alpha, \beta = 1,\ldots,6 \qquad \text{(III-12)}$$

$$K_1^{\alpha\beta} = \int_{B_m} \{\Gamma^{\alpha\eta}\phi^{\eta}_{ij} \; P_{ijkl} \; \phi^{T_\delta}_{kl} \; \Gamma^{\delta\beta}\} dV$$

$$K_2^{\alpha\beta} = \int_{B_m} \{\Gamma^{\alpha\eta}[\phi^{\eta}_{j,i} \; \sigma_{ip} \; \phi^{T_\delta}_{j,p} - 2\phi^{\eta}_{ij} \; \sigma_{jm} \; \phi^{T_\delta}_{im}] \Gamma^{\delta\beta}\} dV$$

$$K_3^{\alpha\beta} = \int_{B_m} \{\Gamma^{\alpha\eta}\phi^{\eta}_{i,p} \; \sigma_{ip} \; \phi^{T_\delta}_{j,j} \Gamma^{\delta\beta}\} dV$$

In (III-12) matrices $K_1^{\alpha\beta}$ and $K_2^{\alpha\beta}$ are symmetric while $K_3^{\alpha\beta}$ is not. Latin indices take the values 1, 2, 3.

Expansion of (III-12) for analysis of plane stress and plane strain deformation procedes on the basis of the following observations.

1. Since all quantities present in (III-12) are uniform in a single element the requisite volume integration over B_m reduces to multiplication by V_m the volume of the element.

$$V_m = \ell_m A \qquad \text{(III-13)}$$

In (III-13) A is given by (III-9) and ℓ_m, the element thickness in the z direction is computed by noting that in plane stress

$$d_z = \dot{\ell}_m / \ell_m \qquad \text{(III-14)}$$

where d_z is given by (II-12), while in plane strain

$$\ell_m = 1 \tag{III-15}$$

2. Substituting for $\phi_{ij}{}^{\alpha}$ in $K_1{}^{\alpha\beta}$ the matrix may be written as

$$K_1{}^{\alpha\beta} = \int_{B_m} \overset{T}{\Gamma}{}^{\alpha\xi} P^{\xi\zeta} \overline{\Gamma}^{\zeta\beta} \, dV \qquad \begin{matrix} \alpha,\beta = 1,\ldots,6 \\ \xi,\zeta = 1, 2, 3 \end{matrix} \tag{III-16}$$

where $P^{\xi\zeta}$ is the constitutive matrix in (III-11) and

$$\overline{\Gamma}^{\alpha\xi} = (1/2A) \begin{bmatrix} (Y_2-Y_3) & 0 & (Y_3-Y_1) & 0 & (Y_1-Y_2) & 0 \\ 0 & (X_3-X_2) & 0 & (X_1-X_3) & 0 & (X_2-X_1) \\ (X_3-X_2) & (Y_2-Y_3) & (X_1-X_3) & (Y_3-Y_1) & (X_2-X_1) & (Y_1-Y_2) \end{bmatrix} \tag{III-17}$$

3. Reduction of $K_2{}^{\alpha\beta}$ to proper form for planar analysis is accomplished by considering Latin indices to take the values 1, 2, corresponding to the x and y coordinate directions.

4. The matrix $K_3{}^{\alpha\beta}$ contains a factor $\overset{T}{\phi}_{j,j}$ associated with the dilatation rate $v_{j,j}$, i.e.,

$$\overset{T}{\phi}_{j,j}{}^{\delta} \Gamma^{\delta\alpha} V^{\alpha} \tilde{=} v_{j,j} = d_x + d_y + d_z \tag{III-18}$$

In plane strain $v_{j,j}$ is completely defined by the in-plane deformation rate components d_x and d_y ($d_z = 0$) and $K_3^{\alpha\beta}$ may be employed as written in (III-12) for i,j,p = 1, 2. In plane stress, however, $d_z \neq 0$ and is given by (II-12). To accommodate both of the above cases the matrix is written as

$$K_3^{\alpha\beta} = \int_{B_m} \{\Gamma^{\alpha\eta}\, \phi_{i,p}^{\eta}\, P^{\delta}\, \Gamma^{\delta\beta}\} dV \tag{III-19}$$

where

$$P^{\delta} \equiv (1/3\kappa) \begin{bmatrix} 0 \\ 0 \\ E_{11} + E_{13} \\ E_{13} + E_{23} \\ E_{13} + E_{23} \\ E_{12} + E_{22} \end{bmatrix} \tag{III-20}$$

For analysis of plane stress $E_{\xi\zeta}$ in (III-20) are the $P^{\xi\zeta}$ of the constitutive equations (III-11); for plane strain we take

$$E_{11} = E_{22} = 3\kappa$$

$$E_{12} = E_{13} = E_{23} = 0$$

and in both cases κ is the elastic bulk modulus $\kappa = E/3(1-2\nu)$.

In summary the rate stiffness matrix for planar problems is written as

$$K^{\alpha\beta} = K_1{}^{\alpha\beta} + K_2{}^{\alpha\beta} + K_3{}^{\alpha\beta} \qquad \text{(III-21)}$$

where

$$K_1{}^{\alpha\beta} = (\ell_m A)\ \{\overset{T}{\Gamma}{}^{\alpha\xi}\ P^{\xi\zeta}\ \Gamma^{\zeta\beta}\}$$

$$K_2{}^{\alpha\beta} = (\ell_m A)\ \{\overset{T}{\Gamma}{}^{\alpha\eta}[\phi^{\eta}_{j,i}\ \overset{T}{\sigma}_{ip}\phi^{\delta}_{j,p} - 2\phi^{\eta}_{ij}\ \overset{T}{\sigma}_{jm}\phi^{\delta}_{im}]\Gamma^{\delta\beta}\}$$

$$K_3{}^{\alpha\beta} = (\ell_m A)\ \{\overset{T}{\Gamma}{}^{\alpha\eta}\phi^{\eta}_{i,p}\ \overset{T}{P}{}^{\delta}\ \Gamma^{\delta\beta}\}$$

In (III-20) Latin indices take the values 1, 2 while of the Greek indices; ξ,ζ take the values 1, 2, 3, while the remainder vary over 1,...,6. Analysis of either plane stress or plane strain procedes by choosing appropriate forms for $P^{\xi\zeta}$ and P^{δ} and setting the value of ℓ_m according to either of (III-14) or (III-15).

APPENDIX IV

Solution of Verification Problems

Homogeneous Finite Deformation

Problems of homogeneous finite deformation may be defined by specification of velocity fields $v_i(x^j,t)$ whose gradients are spatially uniform, that is,

$$v_{i;j} = f_{ij}(t) \tag{IV-1}$$

The time dependent stress fields corresponding to velocity fields of the form (IV-1) are likewise spatially uniform. Consequently the velocity equilibrium equations (67) are satisfied identically by any velocity field corresponding to homogeneous deformation.

Complete solutions to such problems are developed by time integration of the velocity field to define the deformed configuration of a body and of the constitutive equations (53) to define the stress field in the body. Solutions are developed below for problems of finite homogeneous extension and simple shear. Except as noted the solutions are developed in a fixed cartesian coordinate system (x,y,z).

A-IV.1 Finite Extension

Consider the problem of extension of an isotropic material in the x-y plane as defined by the cartesian velocity components

$$v_x = \alpha x$$
$$v_y = k\alpha y \qquad \text{(IV-2)}$$

where α is a constant and k is an unknown function of the material properties and possibly the state of stress. We may consider cases of plane strain for which

$$v_z = 0 \qquad \text{(IV-3)}$$

and of plane stress for which we expect

$$v_z = k\alpha z \qquad \text{(IV-4)}$$

The deformation rate components for this velocity field are

$$d_x = \alpha$$
$$d_y = k\alpha$$
$$d_z = \begin{cases} 0 & \text{plane strain} \\ k\alpha & \text{plane stress} \end{cases} \qquad \text{(IV-5)}$$
$$d_{xy} = d_{xz} = d_{yz} = 0$$

Integrating (IV-5) with respect to time the total deformation may be described by the logarithmic strain components

$$\varepsilon_x = \ell n\, \lambda_x = \alpha t$$

$$\varepsilon_y = \ell n\, \lambda_y = K \ell n\, \lambda_x \qquad \text{(IV-6)}$$

$$\varepsilon_z = \ell n\, \lambda_z = \begin{cases} 0 & \text{plane strain} \\ K \ell n\, \lambda_x & \text{plane stress} \end{cases}$$

In (IV-6) $(\lambda_x, \lambda_y, \lambda_z)$ are coordinate direction stretch ratios and K is expected to be a function of material properties and possibly the state of stress.

Non-zero stress components σ_x, σ_y and in plane strain σ_z are found by substituting the deformation rate (IV-5) into the constitutive equations (53) and integrating with respect to time. The Jaumann stress rate $\hat{\sigma}_{ij}$ in (53) reduces to a material derivative $\dot{\sigma}_{ij}$ since no rotation occurs.

In plane applied loads are found by integrating the tractions t_x and t_y over x and y coordinate faces of the body, respectively. That is, for a body which is initially a unit cube, as in Section IV, we find

$$P_x = \sigma_x A_x \quad \text{on x faces}$$

$$P_y = \sigma_y A_y \quad \text{on y faces} \qquad \text{(IV-7)}$$

where

$$A_x = \lambda_y \lambda_z$$

$$A_y = \lambda_x \lambda_z \qquad \text{(IV-8)}$$

Elastic Material: Substituting the deformation rate components (IV-5) into the constitutive equations (53) for $\mu/\mu_{eq}^{(p)} = 0$ yields

$$\begin{aligned}
\dot{\sigma}_x &= (\lambda+2\mu)\, d_x + \lambda(d_y+d_z) \\
\dot{\sigma}_y &= (\lambda+2\mu)\, d_y + \lambda(d_x+d_z) \\
\dot{\sigma}_z &= (\lambda+2\mu)\, d_z + \lambda(d_x+d_y) \\
\dot{\sigma}_{xz} &= \dot{\sigma}_{xy} = \dot{\sigma}_{yz} = 0
\end{aligned} \qquad \text{(IV-9)}$$

Integrating (IV-9) with respect to time for an initially stress free material obtains

$$\begin{aligned}
\sigma_x &= (\lambda+2\mu)\, \varepsilon_x + \lambda(\varepsilon_y+\varepsilon_z) \\
\sigma_y &= (\lambda+2\mu)\, \varepsilon_y + \lambda(\varepsilon_x+\varepsilon_z) \\
\sigma_z &= (\lambda+2\mu)\, \varepsilon_z + \lambda(\varepsilon_x+\varepsilon_y) \\
\sigma_{xz} &= \sigma_{xy} = \sigma_{yz} = 0
\end{aligned} \qquad \text{(IV-10)}$$

where the strains $(\varepsilon_x, \varepsilon_y, \varepsilon_z)$ are given by (IV-6).

Solutions to problems of plane stress and plane strain extension may be given in terms of a prescribed stretch ratio in the x direction $\lambda_x = \tilde{\lambda}$.

Plane Stress

$$\sigma_x = E\, \ell n\, \tilde{\lambda}$$

$$\sigma_y = \sigma_z = 0$$

$$\lambda_y = \lambda_z = \tilde{\lambda}^{-\nu}$$

$$A_x = \lambda_y \lambda_z = \tilde{\lambda}^{-2\nu} \qquad \text{(IV-11)}$$

$$A_y = \lambda_x \lambda_z = \tilde{\lambda}^{1-\nu}$$

$$P_x = \sigma_x A_x = E\, \tilde{\lambda}^{-2\nu}\, \ell n \tilde{\lambda}$$

$$P_y = \sigma_y A_y = 0$$

Plane Strain

$$\sigma_x = [E/(1-\nu^2)]\ \ell n\, \tilde{\lambda}$$

$$\sigma_z = [\, E/(1-\nu^2)]\, \ell n\, \tilde{\lambda}$$

$$\sigma_y = 0 \qquad \text{(IV-12)}$$

$$\lambda_y = \tilde{\lambda}[\nu/(\nu-1)]$$

$$\lambda_z = 1$$

$$A_x = \lambda_y\lambda_z = \tilde{\lambda}^{[\nu/(\nu-1)]}$$

$$A_y = \lambda_x\lambda_z = \tilde{\lambda}$$

$$P_x = \sigma_x A_x = [E/(1-\nu^2)]\,\tilde{\lambda}^{[\nu/(\nu-1)]}\ell n\,\tilde{\lambda} \qquad \text{(IV-12)}$$

$$P_y = \sigma_y A_y = 0$$

Elasto-Plastic Material: Development of solutions for elasto-plastic materials is facilitated by considering the flow equations (51) rather than the inverse equations (53). Substituting the deformation rates (IV-5) into these equations and noting that the shear stresses are zero yields

$$d_x = (1/E)[\dot{\sigma}_x-\nu(\dot{\sigma}_y+\dot{\sigma}_z)]+(3/2)(\dot{\sigma}_{ef}/\beta\sigma_{ef})[\sigma_x-(1/3)(\sigma_x+\sigma_y+\sigma_z)]$$

$$d_y = (1/E)[\dot{\sigma}_y-\nu(\dot{\sigma}_y+\dot{\sigma}_z)]+(3/2)(\dot{\sigma}_{ef}/\beta\sigma_{ef})[\sigma_y-(1/3)(\sigma_x+\sigma_y+\sigma_z)] \qquad \text{(IV-13)}$$

$$d_z = (1/E)[\dot{\sigma}_z-\nu(\dot{\sigma}_y+\dot{\sigma}_z)]+(3/2)(\dot{\sigma}_{ef}/\beta\sigma_{ef})[\sigma_z-(1/3)(\sigma_x+\sigma_y+\sigma_z)]$$

$$d_{xz} = d_{yz} = d_{xy} = 0$$

where σ_{ef} is defined by I-14 and in the present case is given as

$$\sigma_{ef}^2 = (1/2)[(\sigma_x-\sigma_y)^2 + (\sigma_y-\sigma_z)^2 + (\sigma_z-\sigma_x)^2]$$

In (IV-13) we have

$$1/\beta = 0 \qquad \text{for } \sigma_{ef} < \sigma_y \text{ ; elastic flow}$$

$$\beta = d\sigma_{ef}/d\varepsilon_{ef}^{(p)} > 0 \text{ for } \sigma_{ef} \geq \sigma_y \text{ ; elasto-plastic flow}$$

where σ_y is the initial yield stress of the material.

Immediate integration of (IV-13) is not possible due to the presence of the stress components in the equations. To facilitate integration of these equations we assume proportional loading, i.e.,

$$\sigma_{ij} = q(t)\ \sigma_{ij}^{\circ} \tag{IV-14}$$

where σ_{ij}° is a constant reference stress state defining stress component proportionality. The time varying loading level is controlled by the scalar q(t). Integration of (IV-13) subject to (IV-14) provides equations relating total stresses and logarithmic strains (IV-6). This simplified formulation, termed deformation theory, is correct to the extent that the constraint (IV-14) is valid for particular problems. For plane stress extension the stresses have the form (IV-14). In plane strain, however, the proportionality between the in plane stress components (σ_x,σ_y) and out of plane component σ_z changes at the

yield point. Hence the deformation theory is in a strict sense not appropriate for plane strain elasto-plastic analysis. For the extension problem considered here the quantitative error in deformation theory results is small and the availability of those results in analytic form facilitates comparison with FIPDEF numerical results. For more general problems, however, the general flow theory of Section I.2 must be employed.

For $\sigma_{ef} < \sigma_y$ the solutions for plane stress and plane strain are given by (IV-11) and (IV-12), respectively. In each case a yield point value of $\tilde{\lambda}$, $\tilde{\lambda}=\lambda_y$, may be found corresponding to $\sigma_{ef}=\sigma_y$. For $\sigma_{ef} > \sigma_y$ the solutions are as follows.

Plane Stress

$$\begin{aligned} \tilde{\lambda} &\geq \tilde{\lambda}_y = e^{\gamma\eta} \\ \sigma_x &= [\beta/(1+\eta)][\ell n\tilde{\lambda}+\gamma] \\ \sigma_y &= \sigma_z = 0 \\ P_x &= \{[\beta/(1+\eta)[\ell n\tilde{\lambda}+\gamma]/\tilde{\lambda}\}\, e^{\Gamma_o} \\ P_y &= 0 \end{aligned} \qquad \text{(IV-15)}$$

where e is the natural base.

In (IV-15)

$$\eta = \beta/\varepsilon$$

$$\gamma = \sigma_y/\beta$$

$$\Gamma_o = [\eta(1-2\nu)\ (\ell n\tilde{\lambda}+\gamma)]/(1+\eta)$$

Plane Strain

$$\tilde{\lambda} > \lambda_y = e^{\phi\gamma\eta(1-\nu^2)}$$

$$\ell n\ \lambda_y = H_1\ \sigma_x + H_2$$

$$\sigma_x = H_3\ \ell n\ \tilde{\lambda} + H_y \qquad \text{(IV-16)}$$

$$\sigma_y = 0$$

$$\sigma_z = \sigma_x[1+2\nu\eta)/2(1+\eta)] + \sigma_y\phi[(2\nu-1)/2(1+\eta)]$$

$$P_x = H_3\lambda_y\ \ell n\ \tilde{\lambda} + H_4\ \lambda_y$$

where e, η, γ are as defined previously and

$$H_1 = -(1+2\nu\eta)\ [3+2\eta(1+\nu)]\ /\ [4(1+\eta)\beta\ ]$$

$$H_2 = [\gamma\phi/4(1+\eta)]\ [4\nu\eta+2\eta+3+4\eta\nu^2]$$

$$H_3 = 4\beta(1+\eta)\ /\ [3+4\eta(2-\nu)+4\eta^2(1-\nu^2)]$$

$$H_4 = (\sigma_y/\phi)\ (4\eta+3\phi^2)\ /\ [3+4\eta(2-\nu) + 4\eta^2\ (1-\nu^2)]$$

$$1/\phi^2 = 1-\nu + \nu^2$$

Maximum Load Phenomenon: The applied load in the direction of extension may be written as

$$P_x = \sigma_x A_x = f(\tilde{\lambda}) \qquad \text{(IV-17)}$$

This relationship $P_x(\tilde{\lambda})$ is characterized in all cases considered here by a maximum value P_c occurring at some critical stretch λ_c. The critical stretch may be found by solving

$$d/d\tilde{\lambda}\ (P_x) = 0 \qquad \text{(IV-18)}$$

where $P_x(\tilde{\lambda})$ is given by any of (IV-11, 12, 15, 16). The maximum load is evaluated by substituting $\tilde{\lambda} = \lambda_c$ in the appropriate load equation.

Expressions for P_c, λ_c are given in Table (IV-1) for each of the four extension problems solved in this section.

TABLE (IV-1)

CRITICAL VALUES OF LOAD AND STRETCH: HOMOGENEOUS EXTENSION

	ELASTIC		ELASTO-PLASTIC	
	P_c	$\ell n\,(\lambda_c)$	P_c	$\ell n\,(\lambda_c)$
Plane Stress	$E/2\nu e$	$1/2\nu$	$[\beta/(1+2\nu\eta)]e^{\gamma-1}$	$\Gamma - \gamma$
Plane Strain	$E/[\nu(1+\nu)e]$	$(1-\nu)/\nu$	$[\beta/(1+2\nu\eta)][4\Gamma/(1+2\Gamma)]e^{\gamma\phi\Gamma_1-1}$	$\Gamma_2-(\gamma/\phi)\Gamma_3$

Notation:

$E \equiv$ Young's Modulus
$\nu \equiv$ Poisson's Ratio
$\beta \equiv d\sigma_c/d\varepsilon_e(p) =$ constant
$\sigma_y \equiv$ uniaxial yield stress
$e \equiv$ natural base

$\eta = \beta$
$\gamma = \sigma_y/\beta$
$\Gamma = (1+\eta)/(1+2\nu\eta)$
$1/\phi^2 = 1-\nu+\nu^2$

$\Gamma_1 = 1+\eta\nu^2-(1+2\nu\eta)^2/4(1+\eta)$

$\Gamma_2 = [3+4\eta(2-\nu)+4\eta^2(1-\nu^2)]/\{(1+2\nu\eta)[3+2\eta(1+\nu)]\}$

$\Gamma_3 = (4\eta+3\phi^2)/[4(1+\eta)]$

A-IV.2 Unidirectional Extension

Consider the homogeneous deformation corresponding to the velocity field components

$$v_{x'} = \alpha x'$$

$$v_{y'} = 0 \qquad \text{(IV-19)}$$

$$v_{z'} = 0$$

where (x', y', z') is the rotating coordinate system of Figure (10b). The deformation rate components in the rotating system are

$$d_{x'} = \alpha$$

$$d_{y'} = d_{z'} = d_{x'y'} = d_{x'z'} = d_{y'z'} = 0 \qquad \text{(IV-20)}$$

and the total deformation is described by the single non-zero strain component

$$\varepsilon_{x'} = \ell n\, \lambda_{x'} \qquad \text{(IV-21)}$$

For an elastic material the stress field in the prime system is found by writing (IV-10) in that system and setting all strains to zero except $\varepsilon_{x'}$. The complete solution of the problem in (x', y', z') is

$$\lambda_{x'} = \tilde{\lambda}$$

$$\sigma_{y'} = \lambda_{z'} = 1$$

$$\sigma_{x'} = \{(1-\nu)\, E/[(1+\nu)\ (1-2\nu)]\}\ \ell n\ \tilde{\lambda} \qquad \text{(IV-22)}$$

$$\sigma_{y'} = \sigma_{z'} = (\nu/1-\nu)\ \sigma_x$$

$$P_{x'} = \sigma_{x'} A_{x'} = \sigma_{x'} \lambda_{y'} \lambda_{z'} = 1$$

$$P_{y'} = \sigma_{y'} A_{y'} = \sigma_{y'} \tilde{\lambda} = (\nu/1-\nu)\ \tilde{\lambda}\ \sigma_{x'}$$

where the initial configuration has been taken as a stress free unit cube.

A-IV.3 Simple Shear

The velocity field (IV-23) is imposed upon an initially stress free elastic continuum.

$$v_x = 2ky$$
$$v_y = v_z = 0 \qquad \text{(IV-23)}$$
$$k = \text{constant}$$

Corresponding to (IV-23) are the non-zero deformation rate components

$$d_{xy} = d_{yx} = k \qquad \text{(IV-24)}$$

and non-zero spin components

$$\omega_{xy} = -\omega_{yx} = k \qquad \text{(IV-25)}$$

Recalling the definition of the Jaumann stress rate, $\hat{\sigma}^k_{\ l}$

$$\hat{\sigma}^k_{\ l} = \dot{\sigma}^k_{\ l} + \sigma^k_{\ m}\,\omega^m_{\ l} - \sigma^m_{\ l}\,\omega^k_{\ m} \qquad \text{(IV-26)}$$

The constitutive equations, (53) for $\mu/\mu_{eq}^{(p)} = 0$, may be written

$$d/d\tau(\sigma_x) = \sigma_{xy}$$

$$d/d\tau(\sigma_y) = -\sigma_{xy} \qquad \text{(IV-27)}$$

$$d/d\tau(\sigma_{xy}) = \mu + (1/2)\ (\sigma_y - \sigma_x)$$

where:

$$2\mu = E/(1+\nu)$$

$$\tau = 2kt$$

Integrating (IV-27) subject to initial conditions of zero stress obtains the solution

$$\sigma_{xy} = \mu \sin \tau$$

$$\sigma_x = \mu\ (1-\cos \tau) \qquad \text{(IV-28)}$$

$$\sigma_y = \mu\ (\cos \tau - 1)$$

Page Intentionally Left Blank

"The aeronautical and space activities of the United States shall be conducted so as to contribute . . . to the expansion of human knowledge of phenomena in the atmosphere and space. The Administration shall provide for the widest practicable and appropriate dissemination of information concerning its activities and the results thereof."

—NATIONAL AERONAUTICS AND SPACE ACT OF 1958

NASA SCIENTIFIC AND TECHNICAL PUBLICATIONS

TECHNICAL REPORTS: Scientific and technical information considered important, complete, and a lasting contribution to existing knowledge.

TECHNICAL NOTES: Information less broad in scope but nevertheless of importance as a contribution to existing knowledge.

TECHNICAL MEMORANDUMS: Information receiving limited distribution because of preliminary data, security classification, or other reasons. Also includes conference proceedings with either limited or unlimited distribution.

CONTRACTOR REPORTS: Scientific and technical information generated under a NASA contract or grant and considered an important contribution to existing knowledge.

TECHNICAL TRANSLATIONS: Information published in a foreign language considered to merit NASA distribution in English.

SPECIAL PUBLICATIONS: Information derived from or of value to NASA activities. Publications include final reports of major projects, monographs, data compilations, handbooks, sourcebooks, and special bibliographies.

TECHNOLOGY UTILIZATION PUBLICATIONS: Information on technology used by NASA that may be of particular interest in commercial and other non-aerospace applications. Publications include Tech Briefs, Technology Utilization Reports and Technology Surveys.

Details on the availability of these publications may be obtained from:

SCIENTIFIC AND TECHNICAL INFORMATION OFFICE

NATIONAL AERONAUTICS AND SPACE ADMINISTRATION

Washington, D.C. 20546